SPAM: Solar Spectrum Prediction for Applications and Modeling

Vera Nikolaeva[1] and Evgeny I. Gordeev[2]

[1]Arctic and Antarctic Research Institute
[2]Saint Petersburg State University

November 22, 2022

Abstract

Solar Spectrum Prediction for Applications and Modeling (SPAM) – a new empirical model of solar X-Ray, EUV and FUV radiation flux at the top of the Earth's atmosphere. The model is based on 14 years of daily averaged TIMED spacecraft measurements from 2002 to 2016 when the SEE sensors were regularly calibrated. We used a second-order parametrization of the irradiance spectrum by a single parameter – the F10.7 index, which is a reliable and consistently observed measure of solar activity. The SPAM model consists of two submodels for general and specific use. The first is the Solar-SPAM model of the photon energy flux in the first 190 1nm spectral bands, which can be used for a wide range of applications in different fields of research. The second model, Aero-SPAM, is designed specifically for aeronomic research and provides a photon flux for 37 specific wavelength intervals (20 wave bands and 16 separate spectral lines within the range of 5 –105 nm and an additional 121.5 nm Ly-alpha line), that play a major role in the photoionization of atmospheric gas particles. We provide the full set of parameterization coefficients that allows for immediate implementation of the model for research and applications. In addition, we used the Aero-SPAM model to build a ready-to-use numerical application for calculating the photoionization rates of the main atmospheric components N2, O2, O, N and NO with known absorption and ionization cross sections.

SPAM: Solar Spectrum Prediction for Applications and Modeling

Vera Nikolaeva[1,2] and Evgeny Gordeev[3]

[1]Arctic and Antarctic Research Institute, St. Petersburg, 199397 Russia.

[2]Pushkov Institute of Terrestrial Magnetism, Ionosphere, and Radio Wave Propagation, Russian Academy of Sciences, Moscow, 142191 Russia.

[3]St. Petersburg State University, St. Petersburg, 199034 Russia.

Corresponding authors: Vera Nikolaeva (nikolaeva.vera@gmail.com) and Evgeny Gordeev (evgeny.i.gordeev@spbu.ru)

Key Points:

- SPAM - empirical model of solar shortwave radiation at the top of the atmosphere, parametrized by single ground-based F10.7 index.
- SPAM consists of two sub-models: Solar-SPAM for general use and Aero-SPAM for aeronomy.
- SPAM is specially designed with the ability to make solar spectrum forecast, enabling to monitor and forecast ionospheric photochemistry.

Abstract

Solar Spectrum Prediction for Applications and Modeling (SPAM) – a new empirical model of solar X-Ray, EUV and FUV radiation flux at the top of the Earth's atmosphere. The model is based on 14 years of daily averaged TIMED spacecraft measurements from 2002 to 2016 when the SEE sensors were regularly calibrated. We used a second-order parametrization of the irradiance spectrum by a single parameter – the $F_{10.7}$ index, which is a reliable and consistently observed measure of solar activity. The SPAM model consists of two submodels for general and specific use. The first is the Solar-SPAM model of the photon energy flux in the first 190 1nm spectral bands, which can be used for a wide range of applications in different fields of research. The second model, Aero-SPAM, is designed specifically for aeronomic research and provides a photon flux for 37 specific wavelength intervals (20 wave bands and 16 separate spectral lines within the range of 5 –105 nm and an additional 121.5 nm Ly-alpha line), that play a major role in the photoionization of atmospheric gas particles. We provide the full set of parameterization coefficients that allows for immediate implementation of the model for research and applications. In addition, we used the Aero-SPAM model to build a ready-to-use numerical application for calculating the photoionization rates of the main atmospheric components N_2, O_2, O, N and NO with known absorption and ionization cross sections.

Plain Language Summary

The small part of the solar radiation spectrum in the range of 0–190 nm makes a decisive contribution to the chemistry and dynamics of the Earth's thermosphere and ionosphere, becoming one of the governing parameters for space weather and global climate dynamics. Variability of shortwave radiation flux in specific spectral ranges can exceed 50% during 27-day solar rotation, order of magnitude in the course of the solar cycle, and several orders of magnitude during solar flares. Solar radiation in this wavelength range is completely absorbed by the upper atmosphere, providing a need for model development as an alternative to direct satellite measurements. For the needs of space weather monitoring and forecasting, and many other applications, we present the simple but accurate empirical model of the solar shortwave radiation spectrum - SPAM (Solar **S**pectrum **P**rediction for **A**pplications and **M**odeling), parameterized by a single ground-based $F_{10.7}$ solar activity index. The model is based on 14 years of spacecraft measurements and divided into two submodels: the Solar-SPAM model of the photon energy flux in the wavelength range 0–190 nm, intended for general use, and the Aero-SPAM model of photon flux in 37 specific wavelength intervals, intended to aeronomic calculations.

1 Introduction

Operating at low Earth orbit, TIMED spacecraft provide measurements of the solar radiation spectrum in the shortwave range 0–190 nm (Woodraska et al., 2004). Exactly this radiation range is the main source of ion production at 80–200 km altitudes in the sunlit atmosphere (e.g., Woods et al., 2000). The small part of the solar radiation spectrum from 0–190 nm, measured by the TIMED spacecraft, makes a decisive contribution to the chemistry and dynamics of the Earth's thermosphere and ionosphere (Lean et al., 2011; Vourlidas et al., 2018), becoming one of the governing parameters for space weather (Lilensten et al., 2008) and global climate dynamics including ozone variability (Rozanov et al., 2006; Gray et al., 2010; Fuller-Rowell et al., 2004).

In the D-region and the lower part of the E-region of ionosphere the EUV band including Ly-alpha continuum (centered on 121.5 nm) usually plays a major role in the photoionization process with minor contributions from the X-ray (0–10 nm) and FUV (122–190 nm) irradiance. However, during solar flares, the X-ray flux can increase by several orders of magnitude, which leads to a significant increase in the photoionization of the D-region (Pacini and Raulin, 2006; Kaufmann and Paes de Barros, 1969). The UV radiation from 100–190 nm induces the molecular oxygen dissociation in mesosphere, contributing to the ozone layer formation (Brasseur and Solomon, 2005). The EUV range of the radiation spectrum is absorbed by the upper atmosphere, creating the ionosphere regular E and F1 layers (Chapman, 1931; Nusinov et al., 2000; Nikolaeva et al., 2021b), which plays a crucial role in the propagation of HF radio waves (Cervera et al., 2021; Gao et al., 2006).

Shortwave irradiance permanently changes together with changing Sun (solar cycle, solar rotation, solar flares), which in turn leads to congruent variation of the chemical composition in the upper atmosphere (Byram et al., 1956; Lean, 1987; Vaishnav et al, 2018; Ward et al., 2021; Qian and Solomon, 2012; Svalgaard, 2013).Variability of shortwave radiation flux in specific spectral ranges can exceed 50% during 27-day solar rotation, 200% in the course of the solar cycle, and several orders of magnitude during solar flares (Lean et al., 2001).

Solar X-rays and UV irradiance is completely absorbed by the upper atmosphere, so spacecraft measurements remain the only reliable source of information on the shortwave radiation flux (Schmidtke, 2015; Kretzschmar et al., 2008; Del Zanna and Mason, 2018). Spacecraft lifetime limits, their possible planned and unplanned outages, sensor degradation and other reasons lead to the need of empirical modeling and spectrum reconstruction used for many applications. This task is far from new, but given the strong variability of the shortwave spectrum, the limited possibilities of its measurement and its strong influence on the chemistry of the upper atmosphere, the problem of the solar spectrum modeling remains relevant (Tobiska, 1996; Woods, 2008; Lean, 1990; Tobiska and Eparvier, 1998).

There are a number of EUV models specially designed for atmospheric studies. The publicly available EUVAC empirical model (Richards et al., 1994) is based on the Atmosphere Explorer E spacecraft measurements from 1977 to 1981, and is widely used for aeronomy research as a source of EUV radiation covering the wavelength range from 5 to 105 nm. The model is parameterized by function $P_{10.7}= (F_{10.7}A + F_{10.7})/2$, where $F_{10.7}$ is the daily solar activity index, and $F_{10.7}A$ is the 81-day average around the day of calculation. This formulation significantly narrows the applicability of the model, making it impossible to use for the real-time observations and forecasts. Moreover, (Nikolaeva et al., 2021a) revealed a significant systematic deviation of the EUVAC results. The discrepancy between the simulated and measured total EUV radiation is 20–40% depending on the solar activity level (Nikolaeva et al., 2022b).

With the launch of the TIMED spacecraft, the EUVAC model was further upgraded to the HEUVAC version using measurements from 2003 to 2010, but its parametrization remained the same as in EUVAC (Richards et al., 2006). However (Girazian and Withers, 2015) found that during the solar minimum the HEUVAC soft X-ray irradiance is ∼65% larger and Ly-alpha continuum flux is ∼30% smaller than spacecraft measurements. They suggested their own model, but parameterized by the same function $P_{10.7}$, which again led to the inability of real-time calculations and forecasts.

Flare irradiance spectral model (FISM) and the improved version FISM2 consider both the quiet Sun variation and the solar flare component of irradiance spectrum (Chamberlin et al., 2007; Chamberlin et al., 2008; Chamberlin et al., 2020). FISM is based on modification of the solar minimum reference spectrum by summarizing irradiance variability from the solar cycle, solar rotation and two solar flare components due to gradual and impulsive phase variations. All contributions are modeled independently taking into account various proxies: $F_{10.7}$, MgII core-to-wing ratio and Ly-alpha emission line, the 17.1 and 30.4 nm emission lines from SDO/EVE, as well as the GOES X-ray radiation flux and its time derivative. FISM2 is currently available through the LASP Interactive Solar Irradiance Data Center (https://lasp.colorado.edu/lisird/data/fism_p_ssi_earth/), but the online version has a two-year lag.

Nusinov et al. (2021) made a simple EUV and FUV spectrum model using TIMED satellite data and parameterized by radiation flux in the Ly-alpha line. They propose to use their model for the reconstruction of the shortwave radiation spectrum from the measurements of spaceborne spectral-selective photometers with reduced spectral resolution.

The complexity of parameterization, model inaccessibility and unavailability of control parameters in real time make it difficult to use solar irradiance models in aeronomic research and especially in real-time monitoring and forecasting. For the needs of aeronomy and other applications, we present the simple but accurate empirical model of the solar shortwave radiation spectrum SPAM (Solar **S**pectrum **P**rediction for **A**pplications and **M**odeling), parameterized by a single ground-based $F_{10.7}$ solar activity index. The model is based on 14 years of TIMED measurements and divided into two separate submodels: the Solar-SPAM model of the photon energy flux spectrum for the wavelength range 0–190 nm with an initial TIMED resolution of 1 nm; and the Aero-SPAM model of photon flux in 37 wavelength intervals including 20 wave bands and 16 separate spectral lines within the range of 5–105 nm with an additional Ly-alpha line 121.5 nm, intended to aeronomic calculations.

2 Data

2.1 $F_{10.7}$ index

The solar activity index $F_{10.7}$ is the radio emission at 10.7 cm (2800 MHz) measured by the ground-based receiver. The $F_{10.7}$ index has high correlation with sunspot numbers, ultraviolet and visible solar irradiance that make it an excellent measure of solar activity. The $F_{10.7}$ observational series is one of the longest among solar activity indices. Everyday measurements have been publicly available since 1947 (Tapping, 2013). Also, the reliable forecast of the $F_{10.7}$ index (Gaidash et al. 2017; Huang et al., 2009; Lei et al., 2019; Henney et al., 2012; Zhang et al., 2022) gives an opportunity to predict the upper atmosphere state up to 55 days.

In this study the daily solar $F_{10.7}$ index was taken from the OMNI database (https://omniweb.gsfc.nasa.gov/ow.html). The $F_{10.7}$ index traditionally measures in solar flux units (s.f.u.), one s.f.u. equals 10^{-22} W·m^{-2}·Hz^{-1}.

2.2 TIMED spacecraft data

The TIMED spacecraft (Thermosphere Ionosphere Mesosphere Energetics and Dynamics) was commissioned on December 7, 2001 and is still in operation. One of the scientific objectives of the TIMED mission is to study the mesosphere and lower thermosphere dynamics under the influence of solar shortwave irradiance.

The SEE device (Solar EUV Experiment) (Woodraska et al., 2004) was developed for the TIMED mission at the University of Colorado. The SEE data represent the solar spectrum from 0 to 190 nm covering X-ray (0–10 nm), EUV (10–122 nm) and FUV (122–190 nm) spectrum ranges with 1 nm spectral and 97-minute temporal resolution. The SEE device observes the Sun for about 3 minutes on each orbit, which gives 14–15 measurements per day. The SEE data is then processed to Level 3A by applying correction for atmospheric absorption and sensor degradation and averaging over each 3-minute observational interval. Here we use the Level 3A SEE data (http://lasp.colorado.edu/home/see/data) to develop the empirical model of solar shortwave irradiance SPAM.

The SEE data represents the total energy flux in each 1 nm wide spectral interval. In the following, we will use the center point to define a specific interval, e.g., speaking of the spectral channel 11.5 nm, we mean the same as the spectral band 11–12 nm.

Several sounding rocket launches were undertaken during the mission to detect degradation trends and calibrate the SEE detector. The last suborbital calibration flight was carried out on June 1, 2016. Analyzing the spacecraft data, we found suspicious behavior of the radiation flux in some of the SEE spectral channels beginning from December 2016, soon after the last sensor calibration (more details in the Discussion section). Although the TIMED spacecraft is still in operation, we limit the SEE data used in development of the SPAM model to the interval from 22.01.2002 to 24.11.2016.

3 **Solar-SPAM: shortwave energy spectrum model**

The model is based on the long time series of X-Ray, EUV and FUV solar irradiance received by the TIMED SEE instrument from 22.01.2002 to 24.11.2016. The histogram in Figure 1 shows the distribution of 5368 daily averaged spectra samples against the SPAM control parameter $F_{10.7}$. Since the number of samples clearly decreases with increasing solar activity, we set the limits on the data used in the SPAM model development to $65<F_{10.7}<200$ s.f.u., which includes 95% of all measured data. These limits can also be considered as the limits of applicability of the model.

Figure 2a shows the average energy spectrum based on TIMED measurements from 2002 to 2016. The vertical bars denote the standard deviation in each spectral channel from 0 to 190 nm. The average spectrum has a complex structure with sharp changes in the energy flux by an order of magnitude even in neighboring channels.

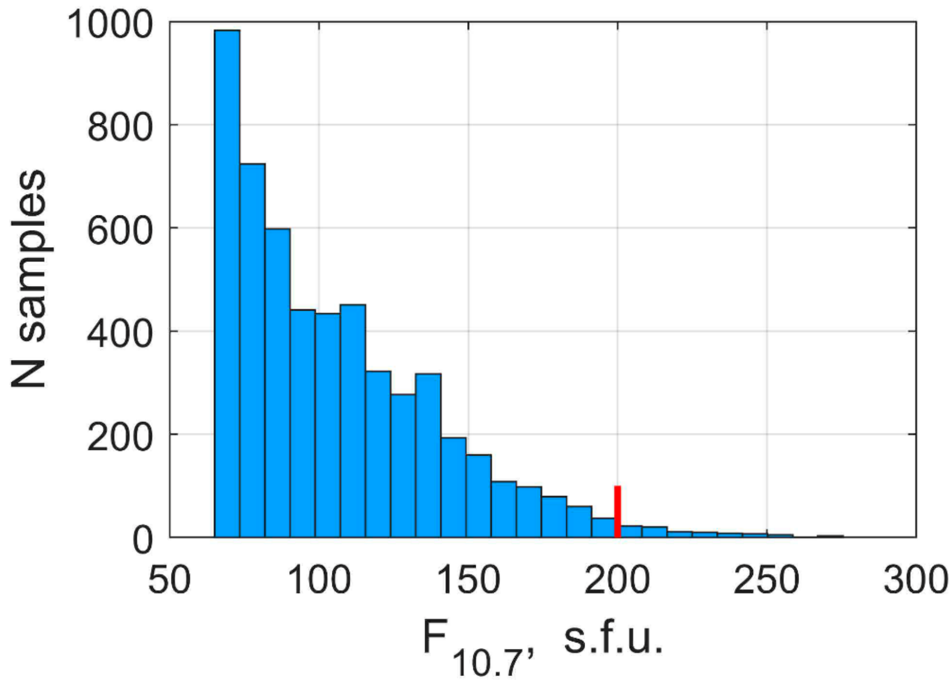

Figure 1. Distribution of TIMED data, used to develop the SPAM model against F10.7 solar activity index.

It is worth noting how strongly the level of variability changes with increasing wavelength. If the values of the X-ray energy flux vary more than an order of magnitude, then for the EUV range the energy flux changes only several times, and even less changes at the edge of the measured FUV range — within a few tens of percent (see examples in Figure 3 and Supplementary Material for the full set of scatterplots). To illustrate the level of irradiance variability more specifically, we show the relative standard deviation of the measured energy flux as a function of wavelength (Figure 2b). The standard deviation value drops exponentially from 100% to 2% with increasing wavelength from 0 to 190 nm.

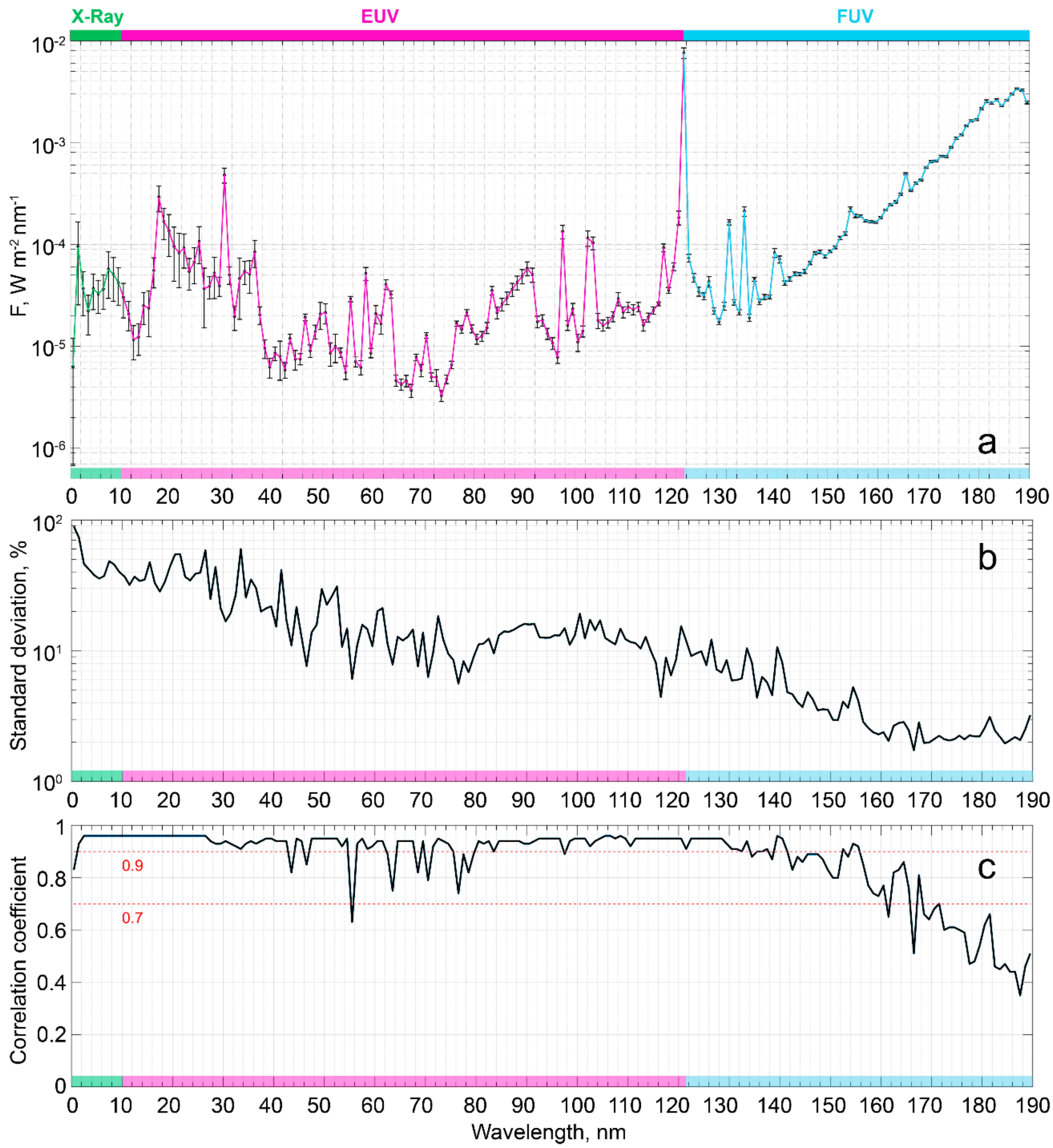

Figure 2. Panel a: Average energy spectrum in the range of 0–190 nm built on the TIMED SEE data. Standard deviation is shown as a vertical line in each 1 nm wide spectral channel; Panel b: Relative standard deviation, note the logarithmic scale; Panel c: correlation coefficient.

The naturally low variability of the FUV energy flux (Figure 3) in the course of the solar cycle leads also to low correlation coefficients in the spectral interval from 170 to 190 nm. The distribution of correlation coefficients over wavelengths is shown in Figure 2c. Most of the spectral bands demonstrate a high accuracy of the fitting procedure, and the value of the correlation coefficient exceed 0.7 for most and 0.9 for many spectral bands.

Continuous TIMED observation time series makes it possible to obtain a reliable functional dependence between the differential energy flux and solar activity index $F_{10.7}$. The second order polynomial suggested as a best fit function by (Bruevich and Yakunina, 2019) for parameterization of the flux intensity in separate spectral lines of HeII (30.4 nm), HeI (58.4 nm), CIII (97.8 nm) and FeXVIII (9.4 nm) in 24-th cycle by $F_{10.7}$ index. As a result of data analysis, we found that the second-order parameterization is also valid for the entire shortwave radiation spectrum measured by TIMED spacecraft, including X-Ray, EUV and FUV radiation. Thus, when developing the Solar-SPAM model, we used the parametrization of the energy flux F in each individual SEE spectral channel in the following form:

$$F = P_1 \cdot F_{10.7}^2 + P_2 \cdot F_{10.7} + P_3, \qquad (1)$$

where P_1, P_2 and P_3 are regression coefficients, $F_{10.7}$ is a daily averaged value of the index.

Figure 3 shows the scatterplots of energy flux measurements as a function of $F_{10.7}$ index and their quadratic fitting functions for several X-Ray, EUV and FUV spectral channels: 0.5, 2.5, 4.5, 58.5 (contains HeI 58.4 nm line), 97.5 (contains CIII 97.8 nm line), 102.5 (contains Ly-beta 102.6 nm line), 139.5, 150.5 and 189.5 nm.

The entire set of regression coefficients of the Solar-SPAM model (Eq. 1) is collected in Table A1 in Appendix A and can be instantly applied to reconstruct the model of the solar radiation spectrum. Table A1 also includes the correlation coefficients (R) and root mean square errors (RMSE) to demonstrate the level of confidence of the Solar-SPAM model.

The high variability of the shortwave solar radiation, especially in the X-ray and EUV range, naturally provides a wide range of possible ionospheric and thermospheric conditions and should be taken into account in aeronomic modeling and research. The next section is devoted to the development of a specific model intended for aeronomic studies.

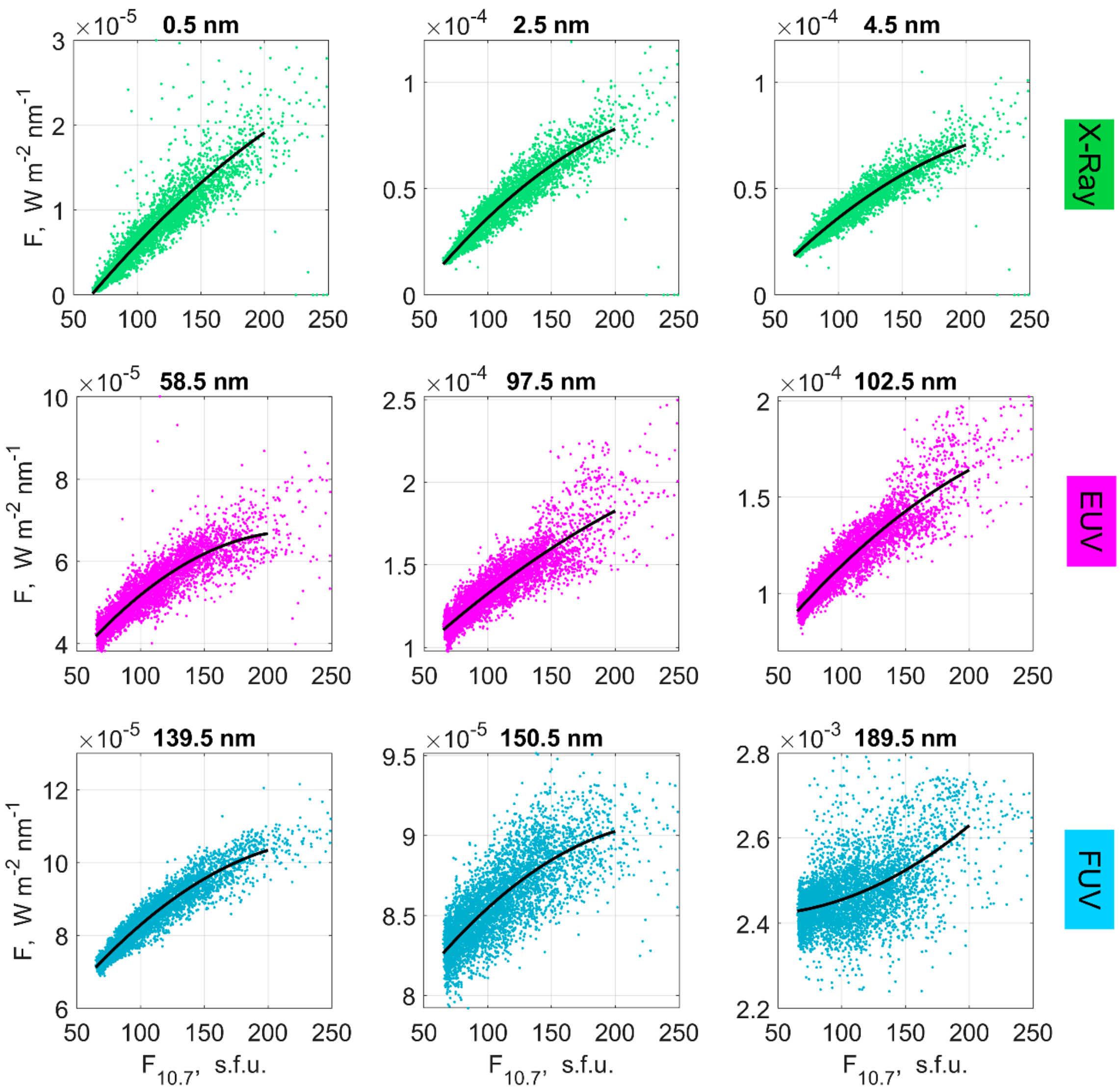

Figure 3. The scatterplots of TIMED energy flux measurements F versus F10.7 index for 0.5, 2.5, 4.5, 58.5, 97.5, 102.5, 139.5, 150.5, 189.5 nm. Black lines are the second order polynomial fitting functions.

4 Aero-SPAM: EUV photon flux model for aeronomic applications

Here we present the development of an empirical model of solar irradiance suitable for aeronomic studies, as well as its ready-to-use application for calculating photoionization rates in the vertical column of the atmosphere. There is a set of well-defined spectral bands and individual spectral lines responsible for the photoionization of the main atmospheric neutrals with known absorption and ionization cross sections (Torr and Torr, 1979; Banks and Kockarts, 1973; Ohshio et al., 1966). According to this set, we have reduced the TIMED data to 20 spectral intervals from 5 to 105 nm with a width of 5 nm each and 16 individual spectral lines, in correspondence to the EUVAC model (Richards et al., 1994). Additionally, we included to our model the strong spectral line Ly-alpha (λ = 121.5 nm) which is responsible for the nitric oxide ionization in the lower ionosphere. The radiation flux in each 5 nm interval is calculated by direct summation of the flux in the SEE channels that fall into this interval, while the flux in an individual spectral line is assumed to be equal to the flux in the corresponding 1 nm wide SEE channel.

For aeronomic applications, such as the calculation of photoionization rate in the upper atmosphere, solar irradiance is usually expressed in units of photon flux. Therefore, we converted the differential energy flux (F, $W \cdot m^{-2} \cdot nm^{-1}$) measured by TIMED SEE device into a differential photon flux (I, $m^{-2} \cdot s^{-1} \cdot nm^{-1}$) by dividing the original flux by the photon energy, corresponding to each spectral channel: $I = F/(hc/\lambda)$, where h – is Planck's constant, c – is the speed of light, and λ – is the central wavelength of each 1-nm SEE channel.

Further development of the model is fully consistent with the procedure used in the previous chapter. We use daily averaged data and a second-order polynomial fit to formulate the Aero-SPAM model:

$$I = P_1 \cdot F_{10.7}^2 + P_2 \cdot F_{10.7} + P_3, \qquad (2)$$

where P_1, P_2 and P_3 are regression coefficients, $F_{10.7}$ is a daily averaged value of the index. The photon flux I is calculated in 20 spectral intervals and 17 individual spectral lines listed in Table A2 in Appendix A, together with model coefficients, R and RMSE values.

Photoionization of the atmosphere by solar EUV is a main source of the regular ionospheric layers E and F_1 formation. The Aero-SPAM model is specifically developed for the calculation of photoionization rates in the Earth's upper atmosphere and can be used in many aeronomic applications and research. As an example, it is already integrated into the AIM-E numerical model of the ionosphere (Nikolaeva et al., 2021b; Nikolaeva et al., 2022a) as a part of the photoionization module. Below we provide a description, as well as a ready-to-use numerical module for calculating the photoionization rates of atmospheric gases using the Aero-SPAM model.

The photoionization rate $q_j(z)$ of the neutral gas j-th component at the altitude z is the number of photoionization acts per unit volume per unit time. Here we determine the photoionization rates for N, O, NO, N_2 and O_2 using expression (Shunk and Nagy, 1980):

$$q_j(z) = n_j \sum_\lambda \sigma_{j\lambda}^i I_\lambda^\infty \exp\left(-\sum_n \sigma_{n\lambda}^a \int_z^\infty \mathrm{C}h(\chi) n_n dz\right), \qquad (3)$$

where n_j – concentration of the j-th component of atmospheric gas, $\sigma_{j\lambda}^i$ – its photoionization cross section at wavelength λ, $\sigma_{j\lambda}^a$ – its photoabsorption cross section at wavelength λ, Ch(χ) – the extended Chapman function (Chapman, 1931; Smith and Smith, 1972) and I_λ^∞ – photon flux at wavelength λ at the top of the atmosphere, provided by Aero-SPAM model.

To illustrate the aeronomic application of the Aero-SPAM model we reconstruct the solar irradiance spectrum and calculate the vertical profiles of the photoionization rates (Eq. 3) during solar activity minimum 2009 June 20, and maximum 2015 June 18 (Fig. 4). The neutral atmosphere composition and temperature, required for the calculations, were taken from the NRLMSISE-00 model (Picone et al., 2002) hosted at the Community Coordinated Modeling Center (https://ccmc.gsfc.nasa.gov/), while the nitric oxide density, which is not represented in the MSISE model, was obtained from the E Region Auroral Ionosphere Model (AIM-E) (Nikolaeva et al., 2021b).

The values of $F_{10.7}$ solar activity index for the selected days 2009 June 20 and 2015 June 18 are 65 s.f.u. and 155 s.f.u., correspondingly. The differential photon flux changes significantly between minimum and maximum of the solar cycle (Fig. 4a). It is worth noting that the ratio of variation is not the same for different bands and spectral lines. For example, as it shown in Figure 4a, the change of the photon flux in the 25.6 nm line $\Delta I_{25.6}$ ~ 700%, whereas in the Ly-alpha line $\Delta I_{121.6}$ ~ 50%. Such a notable change in the spectrum of solar radiation leads to significant changes in atmospheric photochemistry and in the overall dynamics of the ionosphere.

Figure 4 (b, c) shows the vertical distribution of photoionization rates *q* between 90 and 250 km above the subauroral station Gorkovskaya (60.27°N, 29.38°E) at 12h MLT for the molecular oxygen and nitrogen (O_2 and N_2), atomic oxygen (O) and nitric oxide (NO). The altitude distribution of the total photoionization rate has two peaks at ~100 km and ~160 km. The first peak (~100 km) of the photoionization rate leads to the formation of the ionospheric regular layer E approximately in the same altitudes. The photoionization here is totally dominated by *qO2*, and changes more than 50% in the course of the solar activity cycle. The second peak (~160 km) of the photoionization rate is one of the main sources of formation of the regular layer F_1, together with the vertical plasma drift. It is formed mainly due to the qN_2 component which differs by about 70% for the minimum and maximum of the considered solar cycle. While the *qNO* value is several times lower than the photoionization rates of other components, the difference between the *qNO* profiles shown in Fig. 4 (b, c) is huge: ~250% for the E layer heights and ~400% for the F layer heights. Despite the low photoionization rate, *qNO* has a significant effect on the electron concentration in the ionosphere due to the relatively high density of neutral NO content in the upper atmosphere.

For the chemical models of the ionosphere (e.g., Verronen et al., 2016; Nikolaeva et al., 2021b; Lanchester et al, 2001), it is extremely important to take into account the changes in the shape of the solar radiation spectrum and the corresponding change in the vertical distribution of photoionization rates. Our Solar-SPAM and Aero-SPAM models accurately track these changes over the course of the changing Sun. Both models, as well as the photoionization rate module, are available on GitHub as ready-to-use Matlab scripts (https://github.com/magnetophys/SPAM).

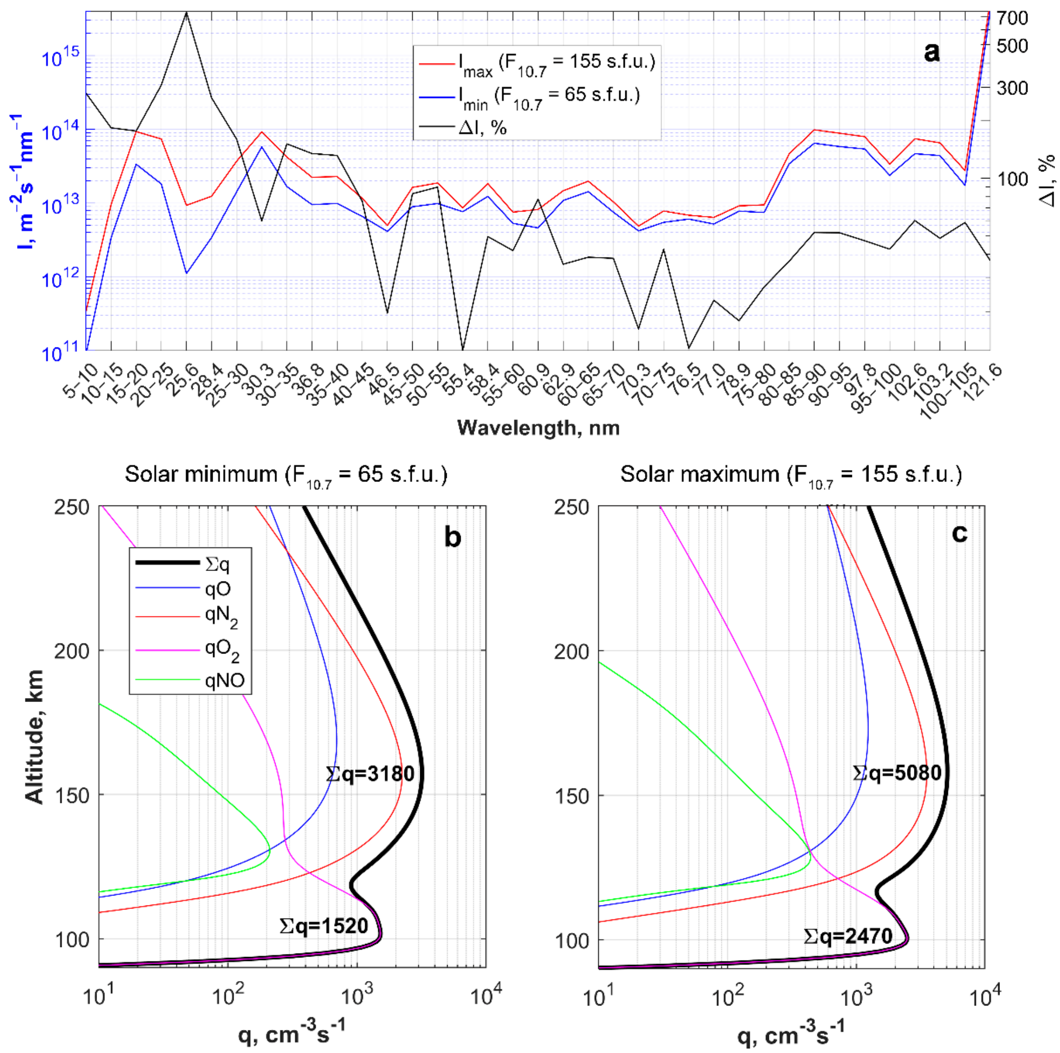

Figure 4. Panel **a**: simulated differential photon flux using Aero-SPAM model during the solar activity minimum at 2009 June 20 (blue line) and during solar activity maximum at 2015 June 18 (red line) and their relative difference (black line). Panels **b** and **c**: vertical distribution of the photoionization rates between 90 and 250 km above the Gorkovskaya station (60.27°N, 29.38°E) during the minimum and maximum of the solar activity cycle. The calculations were carried out for the photoionization rates of molecular oxygen O_2 (magenta), molecular nitrogen N_2 (red), atomic oxygen O (blue), nitric oxide NO (green) and total ionization rate (black) for the local noon during summer solstices.

5 Discussion

One of the main requirements for building a good empirical model is the reliability of the measurements, which becomes especially important in case of solar shortwave irradiance. The point is that the Earth's atmosphere completely absorbs solar irradiance in the range 0–190 nm, so measurements can only be carried out on board the spacecraft, which makes it difficult to continuously control the quality of received data. The sensitivity of the photosensors may suffer during prolonged operation of instruments in space, leading to systematic errors and false trends in observations (Dudok de Wit, 2022). To build an accurate model, it is necessary to exclude data distorted due to sensor degradation.

One of the few ways to calibrate instruments onboard a spacecraft (e.g. Mauceri et al., 2020; Snow et al, 2010; Klimov et al., 2021) is to launch a sounding rocket (e.g., Didkovsky et al., 2009) with a copy of the instrument on board. This method was used for calibration of the TIMED SEE device.

There were nine SEE suborbital calibration flights during 2002–2013 years, and after them the last one was launched on June 1, 2016 (http://lasp.colorado.edu/data/timed_see/level3a/README_SEE_L3A_012.TXT). Thus, the TIMED SEE data from 2002 to 2016 can be considered well calibrated and reliable for model development.

We noticed non-typical trends in spacecraft measurements made after the last calibration rocket launch in 2016, apparently related to the SEE detector degradation, that are not indicated in the "Known Issues/Problems" section of the actual instrument's release notes (http://lasp.colorado.edu/data/timed_see/SEE_v12_releasenotes.txt).

Figure 5 shows several examples of the solar irradiance time series in different spectral lines. Panels a–d demonstrate the TIMED SEE measurements (red and green) for the entire period of spacecraft operation from 2002 to 2022 years, divided by the vertical blue line that denotes the date of the last calibration launch of a suborbital rocket on June 1, 2016. Half a year after the last calibration, artificial trends appeared in different spectral lines, which are easy to recognize by the abrupt shift in the measured values. Data obtained before sensor degradation is shown in red, and after – in green. The black curve denotes the Solar-SPAM calculations based on the daily averaged $F_{10.7}$ index.

Examples in Figure 5 demonstrate that different spectral lines of the detector were affected to varying degrees. Thus, for the 3.5 nm line (Fig. 5a) there is no visible jump in the measured radiation flux and there is a good agreement between the data and model calculations. This is generally true for the first 27 SEE channels covering the 0–28 nm spectral range. The situation changes dramatically in the case of all other SEE channels. For example, the sharp drop in the radiation flux can be seen in 53.5 and 159.5 nm lines shortly after the last calibration in 2016 (Fig. 5 b and d). At the same time, there is an unusual growth in the 97.5 nm line (more than 200% in comparison with the previous solar cycle) throughout the following years. We conclude the presence of anomaly in the TIMED SEE data after last calibration in 2016, which is not associated with the solar activity variations.

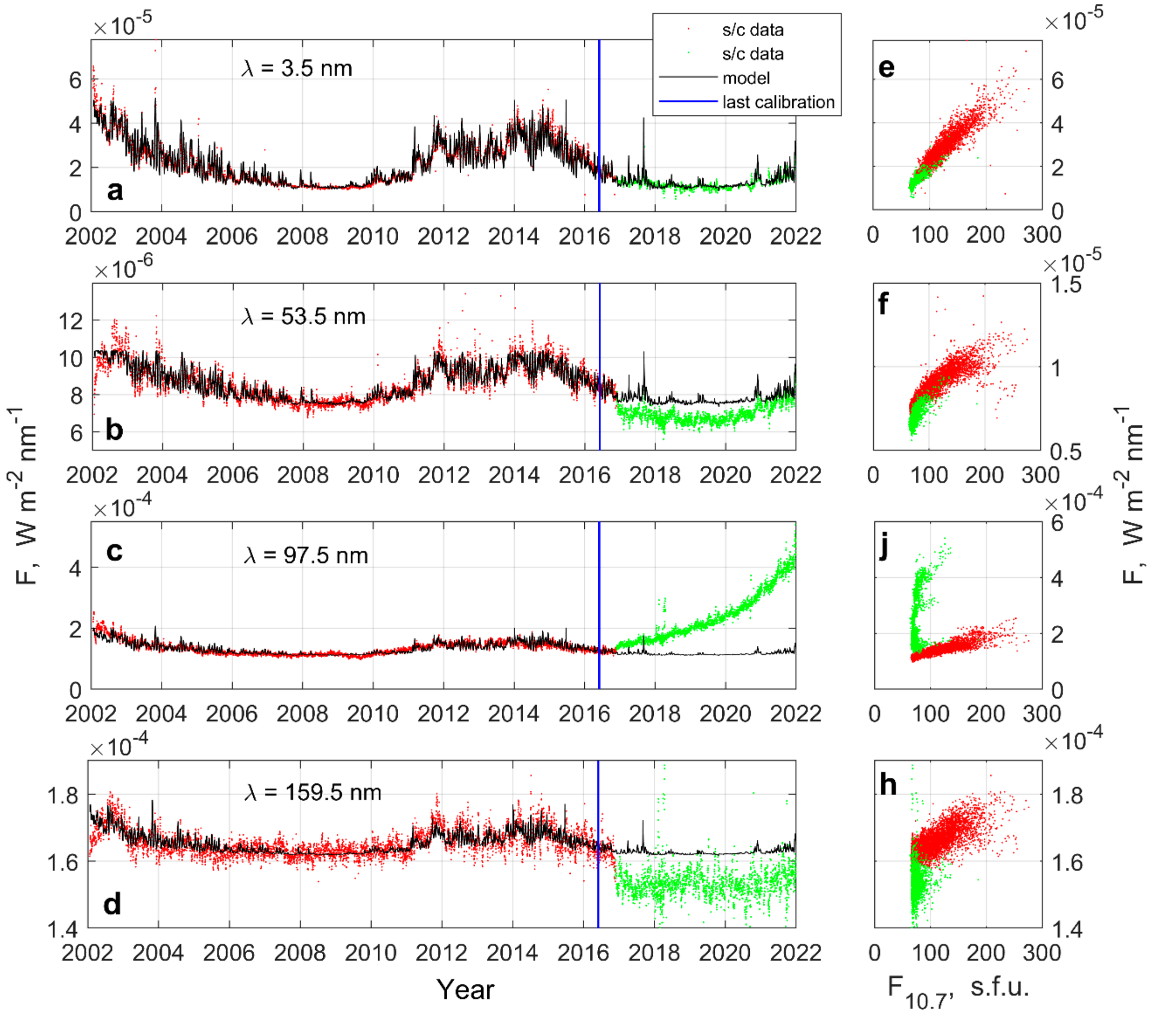

Figure 5. Solar irradiance time series in different spectral lines: **a** – 3.5 nm; **b** – 53.5 nm; **c** – 97.5 nm; **d** – 159.5 nm. TIMED SEE measurements shown in red (before) and in green (after sensor degradation); black curve is the Solar-SPAM calculations. Blue vertical line denotes the date of the last absolute detector calibration on June 1, 2016. Panels **e–h** show scatterplots of the radiation flux versus the F10.7 solar activity index.

All measurement time series for each individual SEE channel can be found in Supplementary Materials 1 in the same format as in Fig. 5.

6 Conclusions

SPAM – an empirical model for the solar irradiance spectrum has been developed using 14 years of TIMED spacecraft observations from 2002 to 2016. The model covers the X-Ray (0–10 nm), EUV (10–122 nm) and FUV (122–190 nm) spectral intervals with 1 nm resolution. The model is parametrized by single $F_{10.7}$ index – the solar radio flux at 10.7 cm, that gives a number of advantages:

1) The $F_{10.7}$ index is an excellent indicator of solar activity (Tapping, 2013) and may serve as a reliable proxy for the solar spectrum variations within the limits of the SPAM model applicability 65<$F_{10.7}$<200 s.f.u.

2) Since the atmosphere is transparent to radiation at a wavelength of 10.7 cm, the $F_{10.7}$ radio flux can be reliably measured from the Earth's surface in any weather. The time series of the daily $F_{10.7}$ has been available continuously since 1947 for seven solar cycles, so the SPAM model can be applied for a large-time-scale climatology studies requiring the solar irradiance variations.

3) The $F_{10.7}$ index is predictable, which allows SPAM to forecast the solar spectrum for various operational tasks. There are a number of services providing the forecast of the daily-averaged $F_{10.7}$ index, e.g., up to 55 days ahead (http://spaceweather.izmiran.ru/eng/forecasts.html), up to 27 days ahead open access forecast (https://www.swpc.noaa.gov/products/27-day-outlook-107-cm-radio-flux-and-geomagnetic-indices), up to 45 days ahead with 5-day resolution (https://www.swpc.noaa.gov/products/usaf-45-day-ap-and-f107cm-flux-forecast). Also, there is a long-term monthly average $F_{10.7}$ forecast up to 20 years including the next solar activity cycle that can be used for the future climate estimations (https://www.swpc.noaa.gov/products/predicted-sunspot-number-and-radio-flux).

4) The SPAM's single-variable parameterization is easy to implement. Despite the model simplicity, our results are in a good agreement with measurements.

Special part of the study is given to the aeronomy-oriented model Aero-SPAM. It provides photon flux values in 17 spectral lines and 20 bands, covering the 5–105 nm EUV range and additionally including the Ly-alpha 121.5 nm spectral line which is the main source of NO^+ formation. The Aero-SPAM model is used to calculate the ionization rates of the neutral atmosphere gasses (N_2, O_2, O, N and NO) with well-known absorption and ionization cross sections. The Aero-SPAM model for aeronomy calculations can be applied to monitor and forecast ionospheric regular E and F_1 regions.

Acknowledgments

SPAM development and results analysis was supported by the Russian Science Foundation grant 20-72-10023. Software development was carried out within the framework of Russian Science Foundation grant 19-77-10016. SPAM application for the upper atmosphere was supported by the Ministry of Science and Higher Education of the Russian Federation under agreement 075-15-2021-583.

APPENDIX A

Table A1: The Solar-SPAM model describing the solar irradiance spectrum (F, W·m^{-2}·nm^{-1}) depending on the daily $F_{10.7}$ index, $F = P_1 \cdot F_{10.7}^2 + P_2 \cdot F_{10.7} + P_3$. P_1, P_2 and P_3 are the regression coefficients for the X-Ray, EUV and FUV spectral intervals (λ) with 1 nm resolution. R is a correlation coefficient between $F_{10.7}$ index and measured photon energy flux, RMSE – root-mean-square error calculated for each wavelength λ.

λ, nm	P_1	P_2	P_3	R	RMSE
0.5	–2.58825263e–10	2.09144982e–07	–1.23612166e–05	0.83	3.14245291e–06
1.5	–4.94024181e–09	3.22175699e–06	–1.80553335e–04	0.93	2.67305197e–05
2.5	–1.51234762e–09	8.72873177e–07	–3.59300652e–05	0.96	4.64649582e–06

3.5	–8.19051896e–10	4.76131943e–07	–1.75069528e–05	0.96	2.57208191e–06
4.5	–1.25299002e–09	7.18966612e–07	–2.30913459e–05	0.96	3.78321360e–06
5.5	–1.05306909e–09	6.00386365e–07	–1.72945105e–05	0.96	3.13381799e–06
6.5	–1.24449248e–09	7.07626722e–07	–2.22302072e–05	0.96	3.69094684e–06
7.5	–2.59694610e–09	1.45374662e–06	–6.31698909e–05	0.96	7.43469515e–06
8.5	–2.16866639e–09	1.21455389e–06	–4.96505577e–05	0.96	6.21501074e–06
9.5	–1.52361462e–09	8.68533191e–07	–3.02456892e–05	0.96	4.53196359e–06
10.5	–1.01521500e–09	5.78430109e–07	–1.79161041e–05	0.96	3.02874105e–06
11.5	–5.92986152e–10	3.39846459e–07	–7.46323908e–06	0.96	1.86757596e–06
12.5	–3.91620799e–10	2.22633150e–07	–6.85281881e–06	0.96	1.16787269e–06
13.5	–3.68662392e–10	2.14384736e–07	–5.53046688e–06	0.96	1.20433914e–06
14.5	–8.15473279e–10	4.56904530e–07	–1.28641555e–05	0.96	2.34443139e–06
15.5	–1.05314223e–09	5.90337830e–07	–2.51992115e–05	0.96	3.02143819e–06
16.5	–1.71833912e–09	9.58528730e–07	–2.37694140e–05	0.96	4.91384954e–06
17.5	–7.84248508e–09	4.35156360e–06	–6.77832612e–05	0.96	2.24071577e–05
18.5	–5.35989584e–09	2.98171616e–06	–7.78638812e–05	0.96	1.53019138e–05
19.5	–5.64009182e–09	3.15119971e–06	–1.24435988e–04	0.96	1.61351843e–05
20.5	–4.90601610e–09	2.74377445e–06	–1.31174042e–04	0.96	1.40380060e–05
21.5	–4.26086127e–09	2.38514084e–06	–1.14409417e–04	0.96	1.22091037e–05
22.5	–3.19159017e–09	1.77982999e–06	–5.49342607e–05	0.96	9.12119600e–06
23.5	–1.75266637e–09	9.77475268e–07	–2.67796958e–05	0.96	5.01372608e–06
24.5	–2.43810818e–09	1.36192347e–06	–4.57043670e–05	0.96	6.97290978e–06
25.5	–3.98387625e–09	2.22551933e–06	–7.70072803e–05	0.96	1.13958300e–05
26.5	–2.00773403e–09	1.12849376e–06	–5.67602506e–05	0.96	5.77108499e–06
27.5	–1.19730867e–09	5.65394676e–07	–5.85964757e–06	0.94	3.19981683e–06
28.5	–1.46295195e–09	1.01404261e–06	–3.58365291e–05	0.93	8.68678105e–06
29.5	–8.15084563e–10	4.34467210e–07	3.65433670e–06	0.93	3.03848274e–06
30.5	–7.05077152e–09	4.04741769e–06	1.43586031e–04	0.94	2.75155631e–05
31.5	–7.77266741e–10	4.68802536e–07	1.08074811e–05	0.93	3.64885891e–06
32.5	–5.61602010e–10	2.83431306e–07	–3.27491491e–06	0.92	2.03502960e–06
33.5	6.11880133e–10	6.52060422e–07	–2.90103367e–05	0.91	1.14428500e–05
34.5	–2.13887412e–09	9.00810935e–07	–1.41575668e–05	0.93	5.08999204e–06
35.5	–2.29655541e–09	1.06445240e–06	–3.23960927e–05	0.94	6.31089521e–06
36.5	–1.69356060e–09	1.14642019e–06	–1.49427472e–05	0.93	9.15296502e–06
37.5	–4.44754965e–10	2.24144087e–07	2.29852502e–06	0.94	1.39955751e–06
38.5	–2.57264554e–10	1.20451838e–07	1.08315857e–07	0.95	6.47189724e–07
39.5	–1.90799471e–10	8.54129718e–08	–3.66570920e–07	0.95	4.29404481e–07
40.5	–1.63110170e–10	7.67917532e–08	2.48479107e–06	0.94	4.43317217e–07
41.5	–2.64676272e–10	1.61050402e–07	–5.64014188e–06	0.94	1.09306430e–06
42.5	–8.80727378e–11	5.09406819e–08	1.64104876e–06	0.94	3.40898878e–07
43.5	–1.29810569e–11	3.70763160e–08	8.20072441e–06	0.82	7.51972352e–07
44.5	–1.92736419e–10	9.35286333e–08	2.78944317e–08	0.95	5.03560346e–07
45.5	–1.07354187e–10	5.33853880e–08	3.23226206e–06	0.94	3.25167635e–07
46.5	7.14925370e–11	2.28505089e–08	1.60620921e–05	0.85	7.85818717e–07
47.5	–1.65354143e–10	7.61012429e–08	3.10560608e–06	0.95	3.96736808e–07
48.5	–3.12973348e–10	1.39150026e–07	3.17305408e–06	0.95	6.77782659e–07
49.5	–8.48676578e–10	3.82780831e–07	–8.99955570e–06	0.95	1.84750385e–06
50.5	–6.92148698e–10	3.05273387e–07	–2.21022224e–06	0.95	1.42588987e–06
51.5	–3.52451773e–10	1.49567940e–07	–2.77810793e–06	0.95	6.67205223e–07
52.5	–4.88285423e–10	2.06597500e–07	–5.71616451e–06	0.95	9.23676788e–07
53.5	–1.51950475e–10	6.22135728e–08	4.00946070e–06	0.92	3.69972956e–07
54.5	–1.47270077e–10	5.88009296e–08	1.18884773e–06	0.95	2.61720547e–07
55.5	–2.67639507e–10	9.72464276e–08	2.22162082e–05	0.63	1.37799232e–06

56.5	–1.01960607e–10	4.67610258e–08	3.41494514e–06	0.93	2.80937628e–07
57.5	–1.61974440e–10	6.72143036e–08	1.17127082e–06	0.95	3.07827728e–07
58.5	–1.01763203e–09	4.54759489e–07	1.65241671e–05	0.91	3.09599754e–06
59.5	–1.56307209e–10	6.36007172e–08	3.86630485e–06	0.92	3.58530411e–07
60.5	–6.00806861e–10	2.63372194e–07	5.64617215e–07	0.94	1.45080898e–06
61.5	–6.04959878e–10	2.45041951e–07	–1.62883930e–06	0.94	1.21428067e–06
62.5	–6.49554222e–10	2.79301792e–07	1.91126658e–05	0.89	2.08911118e–06
63.5	–4.82850036e–10	1.71382019e–07	2.02470800e–05	0.75	1.67842699e–06
64.5	–1.06653492e–10	4.22914685e–08	1.50553273e–06	0.94	2.03369385e–07
65.5	–8.18714565e–11	3.40516816e–08	1.66550540e–06	0.94	1.76539694e–07
66.5	–9.90389288e–11	4.04518744e–08	1.56394010e–06	0.94	1.96591466e–07
67.5	–9.41472141e–11	3.78395774e–08	8.82049866e–07	0.94	1.80481835e–07
68.5	–8.29145674e–11	3.45290364e–08	5.19960242e–06	0.82	3.44043640e–07
69.5	–1.37956080e–10	5.60239688e–08	1.65024766e–06	0.94	2.65869617e–07
70.5	–1.01440668e–10	4.37751602e–08	9.44754103e–06	0.79	4.90083335e–07
71.5	–8.82187053e–11	3.44490090e–08	2.44945919e–06	0.92	1.89763276e–07
72.5	–1.38052514e–10	5.94292750e–08	4.19292916e–07	0.95	2.87817244e–07
73.5	–4.91176916e–11	2.32864269e–08	1.44437460e–06	0.94	1.39806401e–07
74.5	–6.46953103e–11	2.83325477e–08	2.59377737e–06	0.93	1.66218244e–07
75.5	–7.34309741e–11	3.29461087e–08	4.00460892e–06	0.90	2.45820894e–07
76.5	–3.05657856e–11	2.93068006e–08	1.40723930e–05	0.74	6.32637967e–07
77.5	5.43557600e–11	2.19484499e–08	1.18134495e–05	0.89	5.64382540e–07
78.5	–8.51779066e–11	5.79401798e–08	1.63692915e–05	0.82	8.43951888e–07
79.5	–2.21722606e–10	8.88851417e–08	8.27783879e–06	0.89	6.07167204e–07
80.5	–1.65576278e–10	7.79627572e–08	5.66367756e–06	0.94	4.44114376e–07
81.5	–1.92487027e–10	8.70304770e–08	5.81788594e–06	0.93	5.12896384e–07
82.5	–2.51845067e–10	1.14456368e–07	6.30086163e–06	0.94	6.49515749e–07
83.5	–4.38140196e–10	1.97591643e–07	1.99037756e–05	0.90	1.48395770e–06
84.5	–3.73488547e–10	1.70436208e–07	8.14608828e–06	0.94	9.68131273e–07
85.5	–4.33366783e–10	2.09399580e–07	9.28690005e–06	0.94	1.21724813e–06
86.5	–4.84412766e–10	2.36665683e–07	1.09788284e–05	0.94	1.44126953e–06
87.5	–4.83254202e–10	2.68350608e–07	1.39973835e–05	0.94	1.85920378e–06
88.5	–6.21282703e–10	3.37561898e–07	1.45738166e–05	0.94	2.27765383e–06
89.5	–6.68966301e–10	3.86462205e–07	1.63709915e–05	0.93	2.80715372e–06
90.5	–9.40447671e–10	4.91524881e–07	1.81668436e–05	0.93	3.38519060e–06
91.5	–7.89804624e–10	4.23827993e–07	1.56806295e–05	0.94	2.81369582e–06
92.5	–2.51717440e–10	1.25207391e–07	7.46452895e–06	0.95	7.21226067e–07
93.5	–2.52576412e–10	1.27365730e–07	7.86103295e–06	0.95	7.08295267e–07
94.5	–1.68630601e–10	8.97996451e–08	6.01452925e–06	0.95	5.30470738e–07
95.5	–1.71120327e–10	8.22690427e–08	4.20933726e–06	0.95	4.36420483e–07
96.5	–1.16976002e–10	5.79214134e–08	3.16068207e–06	0.95	3.17857028e–07
97.5	–9.42103907e–10	7.84156346e–07	6.35681772e–05	0.89	9.05302834e–06
98.5	–1.74979936e–10	9.39505851e–08	8.37957920e–06	0.94	6.18586716e–07
99.5	–3.06874683e–10	1.63261897e–07	1.00132945e–05	0.95	9.92576035e–07
100.5	–2.08354284e–10	1.12300476e–07	1.82943275e–06	0.95	6.70876385e–07
101.5	–2.22515562e–10	1.04514427e–07	5.86589870e–06	0.95	5.33557018e–07
102.5	–1.34390246e–09	8.98461854e–07	3.81054263e–05	0.92	7.66619612e–06
103.5	–1.01901721e–09	6.79827099e–07	4.51530159e–05	0.94	5.22679531e–06
104.5	–4.18859821e–10	1.89817197e–07	3.18890523e–06	0.95	9.38122529e–07
105.5	–2.54275033e–10	1.20088332e–07	6.60009868e–06	0.96	5.89125254e–07
106.5	–2.43809593e–10	1.18160635e–07	7.74794070e–06	0.96	5.90449142e–07
107.5	–2.33163874e–10	1.20516330e–07	9.87441885e–06	0.95	6.87291920e–07
108.5	–3.69477413e–10	2.17542411e–07	1.10904940e–05	0.96	1.26819431e–06

109.5	–2.81707873e–10	1.45887138e–07	9.82531461e–06	0.95	7.99552250e–07
110.5	–9.10934796e–11	1.04423228e–07	1.44644224e–05	0.92	1.08652364e–06
111.5	–1.66854605e–10	1.18197160e–07	1.27341149e–05	0.95	8.46551633e–07
112.5	–1.97256040e–10	1.22023811e–07	1.39870362e–05	0.95	8.24895534e–07
113.5	–1.84532308e–10	1.04923564e–07	7.42101884e–06	0.95	6.63927760e–07
114.5	–1.82255068e–10	1.00964734e–07	1.09676338e–05	0.95	5.83301149e–07
115.5	–1.79977830e–10	9.70059057e–08	1.45142487e–05	0.95	5.79507535e–07
116.5	–1.14063699e–10	6.14789756e–08	2.11095772e–05	0.95	3.67271760e–07
117.5	–1.19813939e–09	5.28441463e–07	5.22879409e–05	0.95	2.46827715e–06
118.5	–3.17606335e–10	1.43250820e–07	2.42879319e–05	0.95	6.91404625e–07
119.5	–5.07968379e–10	2.73788903e–07	3.79524397e–05	0.95	1.63559867e–06
120.5	–3.91694650e–09	1.76667070e–06	4.67276673e–05	0.95	8.52689227e–06
121.5	–2.10473407e–08	3.12348452e–05	4.59160841e–03	0.91	3.68717499e–04
122.5	–9.24069369e–10	4.16785440e–07	4.09787537e–05	0.95	2.01162816e–06
123.5	–6.22067015e–10	2.80572523e–07	2.53756139e–05	0.95	1.35419220e–06
124.5	–4.72854326e–10	2.13272731e–07	1.79398692e–05	0.95	1.02936761e–06
125.5	–2.37088928e–10	1.27788104e–07	2.05651276e–05	0.95	7.63398559e–07
126.5	–7.26808556e–10	3.27814376e–07	1.76920985e–05	0.95	1.58220650e–06
127.5	–1.57815999e–10	8.50609426e–08	1.52935833e–05	0.95	5.08149030e–07
128.5	–1.17377545e–10	6.32650980e–08	1.23296767e–05	0.95	3.77941945e–07
129.5	–5.73834119e–11	7.57079693e–08	1.75886126e–05	0.93	7.63296694e–07
130.5	–1.24053248e–09	5.70638506e–07	1.20965081e–04	0.91	4.16222369e–06
131.5	–2.12721218e–10	9.61118248e–08	1.95150657e–05	0.91	6.62435421e–07
132.5	–1.07001857e–10	6.29334120e–08	1.62571838e–05	0.90	5.67873985e–07
133.5	–8.94382834e–10	8.71939234e–07	1.31975911e–04	0.94	7.54203153e–06
134.5	–8.35494200e–11	6.28665121e–08	1.35754292e–05	0.88	7.29144198e–07
135.5	–1.25088026e–10	8.54845405e–08	3.77824430e–05	0.90	8.81264590e–07
136.5	–9.79967900e–11	7.22954986e–08	2.10731394e–05	0.90	7.68205303e–07
137.5	–1.24013546e–10	7.97949440e–08	2.37165611e–05	0.91	7.11357554e–07
138.5	–7.39876006e–11	5.55570063e–08	2.54832371e–05	0.87	6.99090195e–07
139.5	–9.49205508e–10	4.89958571e–07	4.33705249e–05	0.96	2.54613277e–06
140.5	–5.67937224e–10	3.05432744e–07	4.62582464e–05	0.95	1.88073609e–06
141.5	–2.43621952e–10	1.13736869e–07	3.27628394e–05	0.90	8.95784614e–07
142.5	–1.95955912e–10	1.01825495e–07	3.75119030e–05	0.83	1.18926525e–06
143.5	–2.46624207e–10	1.15175318e–07	4.23845795e–05	0.88	1.00877166e–06
144.5	–1.61278923e–10	8.93582633e–08	4.38438448e–05	0.86	9.81989792e–07
145.5	–2.75726953e–10	1.38512452e–07	4.32208222e–05	0.89	1.19372564e–06
146.5	–2.43757781e–10	1.36559581e–07	5.45324615e–05	0.89	1.27366067e–06
147.5	–2.46147842e–10	1.39066818e–07	7.11427892e–05	0.89	1.35250470e–06
148.5	–3.12927956e–10	1.56053330e–07	7.20397030e–05	0.87	1.51332205e–06
149.5	–2.31230729e–10	1.24944106e–07	6.58375866e–05	0.83	1.51364906e–06
150.5	–2.43791216e–10	1.21205065e–07	7.57760769e–05	0.80	1.52268475e–06
151.5	–1.94987017e–10	1.16236962e–07	8.38650446e–05	0.80	1.65675848e–06
152.5	–4.33361801e–10	2.37558655e–07	9.63535070e–05	0.91	2.01495486e–06
153.5	–1.73871412e–10	1.71988954e–07	1.12191003e–04	0.88	2.21903105e–06
154.5	–1.16988909e–09	6.16487236e–07	1.70987119e–04	0.93	4.36900801e–06
155.5	–2.55020760e–10	2.92214578e–07	1.64242591e–04	0.92	3.20494890e–06
156.5	–4.53027932e–10	2.51428725e–07	1.68458783e–04	0.85	2.85808410e–06
157.5	–1.72784194e–10	1.48582781e–07	1.57486859e–04	0.77	2.79008511e–06
158.5	–2.29772147e–10	1.46877406e–07	1.54423418e–04	0.74	2.69140338e–06
159.5	–9.39400590e–11	1.10698536e–07	1.54968996e–04	0.73	2.59598688e–06
160.5	–8.39077851e–11	1.26638098e–07	1.71073746e–04	0.77	2.80522066e–06
161.5	–1.98721268e–10	1.37610016e–07	2.05647262e–04	0.65	3.39322701e–06

162.5	–4.73652596e–10	2.82618134e–07	2.23170447e–04	0.82	3.76275218e–06
163.5	–1.55191039e–10	2.30331717e–07	2.39080251e–04	0.83	4.07902394e–06
164.5	–4.04165128e–10	3.37772150e–07	2.81318936e–04	0.86	4.56771102e–06
165.5	–7.73823055e–12	2.97227900e–07	4.63250839e–04	0.76	7.93202201e–06
166.5	4.07530120e–11	8.57496540e–08	3.29404588e–04	0.51	5.05815432e–06
167.5	–2.04674881e–10	3.39319234e–07	3.67674446e–04	0.81	6.73876290e–06
168.5	–4.43360209e–10	2.79935936e–07	4.04891772e–04	0.66	6.38829474e–06
169.5	1.21153174e–10	2.01744392e–07	5.46199225e–04	0.64	8.70736220e–06
170.5	–5.85190609e–10	4.32779772e–07	6.13206686e–04	0.68	1.01094842e–05
171.5	–5.06522331e–10	4.47020613e–07	6.17992427e–04	0.70	1.06043009e–05
172.5	–3.24768827e–10	3.72615949e–07	6.98235220e–04	0.60	1.23238287e–05
173.5	5.76888817e–11	2.79814116e–07	6.97522794e–04	0.61	1.18627791e–05
174.5	–1.17218795e–10	3.92089797e–07	8.58418577e–04	0.61	1.50705494e–05
175.5	–1.37607193e–10	5.06896902e–07	1.04781557e–03	0.60	1.97468460e–05
176.5	–8.96657609e–10	6.78269058e–07	1.12910891e–03	0.59	2.01888857e–05
177.5	1.32627992e–09	1.79727927e–07	1.42010797e–03	0.47	2.90878237e–05
178.5	1.98167580e–09	8.00937083e–08	1.59925973e–03	0.48	3.18302836e–05
179.5	1.18969584e–09	3.52847586e–07	1.62399680e–03	0.54	3.13644235e–05
180.5	–1.61188575e–09	1.46962414e–06	2.01940644e–03	0.62	4.36405768e–05
181.5	–3.61654690e–09	2.50708549e–06	2.31968020e–03	0.66	5.98817371e–05
182.5	1.44002194e–10	8.58952566e–07	2.34991118e–03	0.46	5.34544458e–05
183.5	–5.43430484e–10	9.53841592e–07	2.52448745e–03	0.45	5.15037308e–05
184.5	–1.30322879e–09	9.76484389e–07	2.20300301e–03	0.47	3.95649715e–05
185.5	–1.62506964e–09	1.13882183e–06	2.50603519e–03	0.44	4.83075423e–05
186.5	–1.89245396e–09	1.37388136e–06	2.88406355e–03	0.44	5.91202561e–05
187.5	6.84720021e–10	6.10050906e–07	3.29718092e–03	0.35	6.56653209e–05
188.5	1.53237630e–09	8.38490308e–07	3.18211645e–03	0.46	7.35219971e–05
189.5	7.23049173e–09	–4.24163156e–07	2.42571457e–03	0.51	6.85476734e–05

Table A2: The Aero-SPAM model describing the photon flux (I, $m^{-2} \cdot s^{-1} \cdot nm^{-1}$) in 37 specified spectral channels depending on the daily $F_{10.7}$ index, $I = P_1 \cdot F_{10.7}^2 + P_2 \cdot F_{10.7} + P_3$. P_1, P_2 and P_3 are the regression coefficients for the 37 EUV spectral intervals (λ) including 17 lines and 20 bands. R is a correlation coefficient between $F_{10.7}$ and photon flux. RMSE is the root-mean-square error for the measured and simulated I values.

№	**λ_{min}, nm**	**λ_{max}, nm**	**P_1**	**P_2**	**P_3**	**R**	**RMSE**
1	5	10	–7.22814128e+06	4.34844365e+09	–1.63154083e+11	0.96	2.49833157e+10
2	10	15	–1.72793713e+08	1.06538527e+11	–2.83695953e+12	0.96	6.38391466e+11
3	15	20	–1.79873111e+09	1.05716281e+12	–2.74337230e+13	0.96	6.09484906e+12
4	20	25	–1.67014302e+09	9.88384185e+11	–3.90160466e+13	0.96	5.65031654e+12
5	25.6		–2.42136993e+08	1.44676220e+11	–7.27167455e+12	0.96	8.22340432e+11
6	28.4		–2.15749026e+08	1.47186233e+11	–5.25550336e+12	0.92	1.36257538e+12
7	25	30	–8.49047253e+08	4.39836923e+11	–1.07767192e+13	0.96	2.37564549e+12
8	30.3		–1.05374887e+09	6.15749059e+11	2.21870265e+13	0.94	4.36129879e+12
9	30	35	–5.78821182e+08	4.09300016e+11	–7.39277758e+12	0.93	3.67860958e+12
10	36.8		–3.67641064e+08	2.23500665e+11	–3.44107714e+12	0.93	1.76712865e+12
11	35	40	–5.27393084e+08	2.60815376e+11	–4.81963679e+12	0.94	1.61468490e+12
12	40	45	–1.76485806e+08	9.43602417e+10	1.20746026e+12	0.95	5.78446944e+11
13	46.5		–9.16428947e+06	1.10576870e+10	3.46127070e+12	0.84	1.99324850e+11
14	45	50	–3.28417068e+08	1.54464379e+11	2.70338559e+11	0.96	7.65976697e+11
15	50	55	–4.35029980e+08	1.94267789e+11	–9.12633707e+11	0.96	9.17807984e+11
16	55.4		–7.45540942e+07	2.70143268e+10	6.20498828e+12	0.60	4.21493552e+11
17	58.4		–2.67242090e+08	1.26513904e+11	5.22846617e+12	0.91	9.60988214e+11
18	55	60	–1.11331394e+08	4.91943896e+10	2.59480808e+12	0.94	2.86378660e+11

19	60.9		–1.75317009e+08	7.84311521e+10	2.56019089e+11	0.94	4.50958343e+11
20	62.9		–1.95380036e+08	8.57116193e+10	6.10932407e+12	0.89	6.88675932e+11
21	60	65	–3.18739604e+08	1.31380748e+11	7.10288562e+12	0.90	8.93006924e+11
22	65	70	–1.54464890e+08	6.57942854e+10	3.90335230e+12	0.93	3.82370215e+11
23	70.3		–3.92892316e+07	1.62255869e+10	3.31133072e+12	0.78	1.84543928e+11
24	70	75	–1.17284653e+08	5.16415922e+10	2.62008424e+12	0.94	2.82746960e+11
25	76.5		–2.80655392e+07	1.48549365e+10	5.22726113e+12	0.72	2.63413854e+11
26	77.0		–1.42682444e+07	1.64116032e+10	4.19804672e+12	0.88	2.42046487e+11
27	78.9		–5.13752841e+07	2.67845754e+10	6.25669926e+12	0.81	3.56475663e+11
28	75	80	–1.09163517e+08	4.63578518e+10	4.91238247e+12	0.89	3.39676578e+11
29	80	85	–5.71385988e+08	2.65288858e+11	1.93295978e+13	0.94	1.62478581e+12
30	85	90	–1.26716263e+09	6.53242857e+11	2.77927431e+13	0.94	4.18839876e+12
31	90	95	–1.14503862e+09	5.87977430e+11	2.50221903e+13	0.95	3.62200988e+12
32	97.8		–4.60750790e+08	3.84479195e+11	3.11115764e+13	0.90	4.64901797e+12
33	95	100	–3.84402107e+08	1.97008185e+11	1.26370475e+13	0.95	1.14344491e+12
34	102.6		–7.45028477e+08	4.75205812e+11	1.89621526e+13	0.93	4.08952635e+12
35	103.2		–6.18608147e+08	3.73585739e+11	2.24459796e+13	0.94	2.81357100e+12
36	100	105	–4.16550795e+08	2.04940624e+11	5.82827246e+12	0.96	1.07697392e+12
37	121.6		–2.81408845e+10	2.25475006e+13	2.62203706e+15	0.92	2.35540620e+14

Data Availability Statement

The authors are grateful for the provided data used in this work. F10.7 solar activity index is available at OMNIweb Plus database (https://omniweb.gsfc.nasa.gov/ow.html). TIMED SEE data are available at LASP Interactive Solar Irradiance Data Center (https://lasp.colorado.edu/home/see/data/). F10.7 forecast is provided by IZMIRAN Space Weather prediction Center (http://spaceweather.izmiran.ru/eng/forecasts.html).

The SPAM model scripts are available on Zenodo (https://zenodo.org/record/6985548, DOI:10.5281/zenodo.6985548).

References

Banks, P.M., & Kockarts, G., 2013. Aeronomy. Elsevier.

Brasseur, G.P., & Solomon, S., 2005. Aeronomy of the Middle Atmosphere: Chemistry and Physics of the Stratosphere and Mesosphere. Springer Dordrecht. doi:10.1007/1-4020-3824-0.

Bruevich, E., & Yakunina, G., 2019. Flux variations in lines of solar euv radiation beyond flares in cycle 24. *Geomagnetism and Aeronomy 59*, 155–161. doi:10.1134/S0016793219020038.

Byram, E., Chubb, T., & Friedman, H., 1956. The solar X-ray spectrum and the density of the upper atmosphere. *Journal of Geophysical Research 61*,251–263. doi:10.1029/JZ061i002p00251.

Cervera, M.A., Harris, T.J., Holdsworth, D.A., & Netherway, D.J., 2021. Ionospheric effects on HF radio wave propagation. *Ionosphere Dynamics and Applications,* 439–492. doi:10.1002/9781119815617.ch19.

Chamberlin, P.C., Eparvier, F.G., Knoer, V., Leise, H., Pankratz, A., Snow, M., Templeman, B., Thiemann, E.M.B., Woodraska, D.L., & Woods, T.N., 2020. The flare irradiance spectral model-version 2 (FISM2). *Space Weather 18,* e2020SW002588. doi:10.1029/2020SW002588.

Chamberlin, P.C., Woods, T.N., & Eparvier, F.G., 2007. Flare irradiance spectral model (FISM): Daily component algorithms and results. *Space Weather5*(7). doi:10.1029/2007SW000316.

Chamberlin, P.C., Woods, T.N., & Eparvier, F.G., 2008. Flare irradiance spectral model (FISM): Flare component algorithms and results. *Space Weather 6*(5). doi:10.1029/2007SW000372.

Chapman, S., 1931. The absorption and dissociative or ionizing effect of monochromatic radiation in an atmosphere on a rotating earth. *Proceedings of the Physical Society* (1926-1948) 43, 26. doi:10.1088/0959- 5309/43/1/305.

Del Zanna, G., & Mason, H.E., 2018. Solar UV and X-ray spectral diagnostics. Living *Reviews in Solar Physics 15*, 1–278. doi:10.1007/s41116-018-0015-3.

Didkovsky, L., Judge, D., Wieman, S., Woods, T., & Jones, A., 2009. EUV spectrophotometer (ESP) in extreme ultraviolet variability experiment (EVE): algorithms and calibrations, in: The solar dynamics observatory. *Springer*, pp. 179–205. doi:10.1007/s11207-009-9485-8.

Dudok de Wit, T., 2022. Detecting undocumented trends in solar irradiance observations. *Journal of Space Weather and Space Climate 12*, 10. doi:10.1051/swsc/2021041.

Fuller-Rowell, T., Solomon, S., Roble, R., & Viereck, R., 2004. Impact of solar EUV, XUV, and X-ray variations on earth's atmosphere. *Geophysical monograph 141*, 341–354. doi:10.1029/141GM23.

Gaidash, S., Belov, A., Abunina, M., & Abunin, A., 2017. Space weather forecasting at IZMIRAN. *Geomagnetism and Aeronomy 57*, 869–876. doi:10.1134/S0016793217070088.

Gao, H., Li, G., Li, Y., Yang, Z., & Wu, X., 2006. Ionospheric effect of HF surface wave over-the-horizon radar. *Radio science 41*, 1–10. doi:10.1029/2005RS003323.

Girazian, Z., & Withers, P., 2015. An empirical model of the extreme ultravioletsolar spectrum as a function of F10. 7. *Journal of Geophysical Research: Space Physics 120*, 6779–6794. doi:10.1002/ 2015JA021436.

Gray, L.J., Beer, J., Geller, M., Haigh, J.D., Lockwood, M., Matthes, K., Cubasch, U., Fleitmann, D., Harrison, G., Hood, L., Luterbacher J., Meehl G. A., Shindell D., van Geel B., & White W., 2010. Solar influences on climate. *Reviews of Geophysics 48*. doi:10.1029/2009RG000282.

Henney, C., Toussaint, W., White, S., & Arge, C., 2012. Forecasting F10.7 with solar magnetic flux transport modeling. *Space Weather 10*. doi:10.1029/2011SW000748.

Huang, C., Liu, D.D., & Wang, J.S., 2009. Forecast daily indices of solar activity, f10. 7, using support vector regression method. *Research in Astronomyand Astrophysics 9*, 694. doi:10.1088/1674-4527/9/6/008.

Kaufmann, P., & Paes de Barros, M., 1969. Some relationships between solar X-ray bursts and SPA's produced on VLF propagation in the lower ionosphere. *Solar Physics 9*, 478–486. doi:10.1007/BF02391673.

Klimov, P., Sigaeva, K., & Sharakin, S., 2021. Flight calibration of the photodetector in the TUS detector. *Instruments and Experimental Techniques 64*, 450–455. doi:10.1134/S0020441221030192.

Kretzschmar, M., Dudok de Wit, T., Lilensten, J., Hochedez, J.F., Aboudarham, J., Amblard, P.O., Auchère, F., & Moussaoui, S., 2009. Solar EUV/FUV irradiance variations: analysis and observational strategy. *Acta Geophysica 57*, 42–51. doi:10.2478/s11600-008-0066-2.

Lanchester, B., Rees, M., Lummerzheim, D., Otto, A., Sedgemore-Schulthess, K., Zhu, H., & McCrea, I., 2001. Ohmic heating as evidence for strong field-aligned currents in filamentary aurora. *Journal of GeophysicalResearch: Space Physics 106*, 1785–1794. doi:10.1029/1999JA000292.

LASP Interactive Solar Irradiance Data Center, a. FISM-P Earth Solar Spectral Irradiance, Time Series. https://lasp.colorado.edu/lisird/data/fism_p_ssi_earth/. Online; accessed 4 August 2022.

LASP Interactive Solar Irradiance Data Center, b. TIMED SEE Database. http://lasp.colorado.edu/home/see/data. Online; accessed 4 August 2022.

LASP Interactive Solar Irradiance Data Center, c. TIMED SEE Level 3A Data Products description. http://lasp.colorado.edu/data/timed_see/level3a/README_SEE_L3A_012.TXT. Online; accessed 4 August 2022.

LASP Interactive Solar Irradiance Data Center, d. TIMED SEE Version 12 Data Product Release Notes. http://lasp.colorado.edu/data/timed_see/SEE_v12_releasenotes.txt. Online; accessed 4 August 2022.

Lean, J., 1987. Solar ultraviolet irradiance variations: A review. *Journal of Geophysical Research: Atmospheres 92*, 839–868. doi:10.1029/JD092iD01p00839.

Lean, J., 1990. A comparison of models of the sun's extreme ultraviolet irradiance variations. *Journal of Geophysical Research: Space Physics 95*, 11933–11944. doi:10.1029/JA095iA08p11933.

Lean, J., White, O., Livingston, W., & Picone, J., 2001. Variability of a composite chromospheric irradiance index during the 11-year activity cycle and over longer time periods. *Journal of Geophysical Research: Space Physics 106*, 10645–10658. doi:10.1029/2000JA000340.

Lean, J., Woods, T., Eparvier, F., Meier, R., Strickland, D., Correira, J., & Evans, J., 2011. Solar extreme ultraviolet irradiance: Present, past, and future. Journal of *Geophysical Research: Space Physics 116*. doi:10.1029/2010JA015901.

Lei, L., Zhong, Q., Wang, J., Shi, L., & Liu, S., 2019. The mid-term forecast method of f10. 7 based on extreme ultraviolet images. *Advances in Astronomy 2019*. doi:10.1155/2019/5604092.

Lilensten, J., Dudok de Wit, T., Kretzschmar, M., Amblard, P.O., Moussaoui, S., Aboudarham, J., & Auchère, F., 2008. Review on the solar spectral variability in the EUV for space weather purposes, in: Annales Geophysicae, *Copernicus GmbH*. pp. 269–279. doi:10.1002/2017SW001725.

Mauceri, S., Richard, E., Pilewskie, P., Harber, D., Coddington, O., Béland, S., Chambliss, M., & Carson, S., 2020. Degradation correction of TSIS SIM. *Solar Physics 295*, 1–21. doi:10.1007/s11207-020-01707-y.

Nikolaeva, V., Gordeev, E., Nikolaev, A., Rogov, D., & Troshichev, O., 2022a. Auroral ionosphere model with PC index as an input. *Atmosphere 13*, 402. doi:10.3390/atmos13030402.

Nikolaeva, V., Gordeev, E., Rogov, D., & Nikolaev, A., 2021a. Auroral ionosphere model (AIM-E) adjustment for the regular E layer. *Solar-TerrestrialPhysics 7*, 41–46. doi:10.12737/szf-71202106.

Nikolaeva, V., Gordeev, E., Rogov, D., & Novikov, S., 2022b. Calibration of empirical EUV spectra for the regular e-region modeling. *Bulletin of the Russian Academy of Sciences: Physics 86*, 329–334. doi:10.3103/S1062873822030194.

Nikolaeva, V., Gordeev, E., Sergienko, T., Makarova, L., & Kotikov, A., 2021b. AIM-E: E-region auroral ionosphere model. *Atmosphere 12*, 748. doi:10.3390/atmos12060748.

Nusinov, A., Antonova, L., Kazachevskaya, T., Katyushina, V., & Svidsky,P., 2000. 11-year solar cycle extreme ultraviolet and soft X-ray variations according to the ionospheric e-region data and results of direct measurements. *Advances in Space Research 25*, 73–78. doi:10.1016/S0273- 1177(99)00900-X.

Nusinov, A.A., Kazachevskaya, T.V., & Katyushina, V.V., 2021. Solar extreme and far ultraviolet radiation modeling for aeronomic calculations. *RemoteSensing 13,* 1454. doi:10.3390/rs13081454.

Ohshio, M., Maeda, R., & Sakagami, H., 1966. Height distribution of local photoionization efficiency. *J. Radio Res. Lab 13*, 245.

Pacini, A.A., & Raulin, J.P., 2006. Solar X-ray flares and ionospheric sudden phase anomalies relationship: A solar cycle phase dependence. *Journal ofGeophysical Research: Space Physics 111*. doi:10.1029/2006JA011613.

Picone, J., Hedin, A., Drob, D.P., & Aikin, A., 2002. NRLMSISE-00 empirical model of the atmosphere: Statistical comparisons and scientific issues. *Journal of Geophysical Research: Space Physics 107,* SIA–15. doi:10.1029/2002JA009430.

Qian, L., & Solomon, S.C., 2012. Thermospheric density: An overview of temporal and spatial variations. *Space science reviews 168*, 147–173. doi:10.1007/s11214-011-9810-z.

Richards, P., Fennelly, J., & Torr, D., 1994. EUVAC: A solar EUV flux model for aeronomic calculations. *Journal of Geophysical Research: Space Physics 99*, 8981–8992. doi:10.1029 / 94JA00518.

Richards, P.G., Woods, T.N., & Peterson, W.K., 2006. HEUVAC: A new high resolution solar EUV proxy model. *Advances in Space Research 37*, 315–322. doi:10.1016/j.asr.2005.06.031.

Rozanov, E., Egorova, T., Schmutz, W., & Peter, T., 2006. Simulation of the stratospheric ozone and temperature response to the solar irradiance variability during sun rotation cycle.

Journal of Atmospheric and Solar-Terrestrial Physics 68, 2203–2213. doi:10.1016/j.jastp.2006.09.004.

Schmidtke, G., 2015. Extreme ultraviolet spectral irradiance measurements since 1946. *History of Geo-and Space Sciences 6*, 3–22. doi:10.5194/hgss-6-3-2015.

Schunk, R., & Nagy, A., 1980. Ionospheres of the terrestrial planets. *Reviews of Geophysics 18*, 813–852. doi:10.1029/RG018i004p00813.

Smith III, F., & Smith, C., 1972. Numerical evaluation of Chapman's grazing incidence integral ch(x, χ). *Journal of Geophysical Research 77*, 3592– 3597. doi:10.1029/JA077i019p03592.

Snow, M., McClintock, W., & Woods, T., 2010. Solar spectral irradiance variability in the ultraviolet from SORCE and UARS SOLSTICE. *Advances in Space Research 46*, 296–302. doi:10.1016/j.asr.2010.03.027.

Space Weather Prediction Center (IZMIRAN). Review and forecast of solar and geomagnetic activity (IZMIRAN). http://spaceweather.izmiran.ru/eng/forecasts.html. Online; accessed 4 August 2022.

Space Weather Prediction Center of National Oceanic and Atmospheric Administration, a. NOAA 20-years Sunspot Numberand 10.7 cm Radio Flux and Geomagnetic Indices Prediction.https://www.swpc.noaa.gov/products/usaf-45-day-ap-and-f107cm-flux-forecast. Online; accessed 4 August 2022.

Space Weather Prediction Center of National Oceanic and Atmospheric Administration, b. NOAA 27-Day Outlook of 10.7 cm Radio Flux and Geomagnetic Indices. https://www.swpc.noaa.gov/products/27-day-outlook-107-cm-radio-flux-and-geomagnetic-indices. Online; accessed 4 August 2022.

Space Weather Prediction Center of National Oceanic and Atmospheric Administration, c. NOAA 45-Day Outlook of 10.7 cm Radio Flux and Geomagnetic Indices. https://www.swpc.noaa.gov/products/usaf-45-day-ap-and-f107cm-flux-forecast. Online; accessed 4 August 2022.

SPDF Goddard Space Flight Center. OMNIWeb Database. https://omniweb.gsfc.nasa.gov/ow.html. Online; accessed 4 August 2022.

Svalgaard, L., 2013. Solar activity – past, present, future. *Journal of SpaceWeather and Space Climate 3*, A24. doi:10.1051/swsc/2013046/.

Tapping, K., 2013. The 10.7 cm solar radio flux (f10. 7). *Space weather 11*, 394–406. doi:10.1002/swe.20064.

Tobiska, W., 1996. Current status of solar EUV measurements and modeling.*Advances in Space Research 18*, 3–10. doi:10.1016/0273-1177(95)00827-2.

Tobiska, W.K., & Eparvier, F., 1998. EUV97: Improvements to EUV irradiance modeling in the soft X-rays and FUV. *Solar Physics 177*, 147–159. doi:10.1023/A:1004931416167.

Torr, D., & Torr, M.R., 1979. Chemistry of the thermosphere and ionosphere. *Journal of Atmospheric and Terrestrial Physics 41*, 797–839. doi:10.1016/0021-9169(79)90126-0.

Vaishnav, R., Jacobi, C., Berdermann, J., Schmölter, E., & Codrescu, M., 2018. Ionospheric response to solar euv variations: Preliminary results. *Advances in Radio Science 16*, 157–165. doi:10.5194/ars-16-157-2018.

Verronen, P., Andersson, M., Marsh, D., Kovács, T., & Plane, J., 2016. WACCM-D — Whole Atmosphere Community Climate Model with D-region ion chemistry. *Journal of Advances in Modeling Earth Systems 8*, 954–975. doi:10.1002/2015MS000592.

Vourlidas, A., & Bruinsma, S., 2018. EUV irradiance inputs to thermospheric density models: Open issues and path forward. *Space Weather 16*, 5–15. doi:10.1002/2017SW001725.

Ward W., Seppälä A., Yiğit E., Nakamura T., Stolle C., Laštovička J., Woods T.N., Tomikawa Y., Lübken F.-J., Solomon S.C., Marsh D.R., Funke B. & Pallamraju D., 2021. Role of the sun and the middle atmosphere/thermosphere/ionosphere inclimate (ROSMIC): a retrospective and prospective view. *Progress in Earth and Planetary Science 8*, 1–38. doi:10.1186/s40645-021-00433-8.

Woodraska, D.L., Woods, T.N., & Eparvier, F.G., 2004. In-flight calibration and performance of the solar extreme ultraviolet experiment (SEE) aboard the timed satellite, in: *Instruments, Science, and Methods for Geospace and Planetary Remote Sensing, SPIE.* pp. 36–47. doi:10.1117/12.579034.

Woods, T.N., 2008. Recent advances in observations and modeling of the solar ultraviolet and X-ray spectral irradiance. *Advances in Space Research 42,* 895–902. doi:10.1016/j.asr.2007.09.026.

Woods, T.N., Rottman, G.J., Harder, J.W., Lawrence, G.M., McClintock, W.E., Kopp, G.A., & Pankratz, C., 2000. *Overview of the EOS SORCE mission, in: Earth Observing Systems V, SPIE*. pp. 192–203. doi:10.1117/12.494229.

Zhang, W., Zhao, X., Feng, X., Liu, C., Xiang, N., Li, Z., & Lu, W., 2022. Predicting the daily 10.7-cm solar radio flux using the long short-term memory method. *Universe 8*, 30. doi:10.3390/universe8010030.

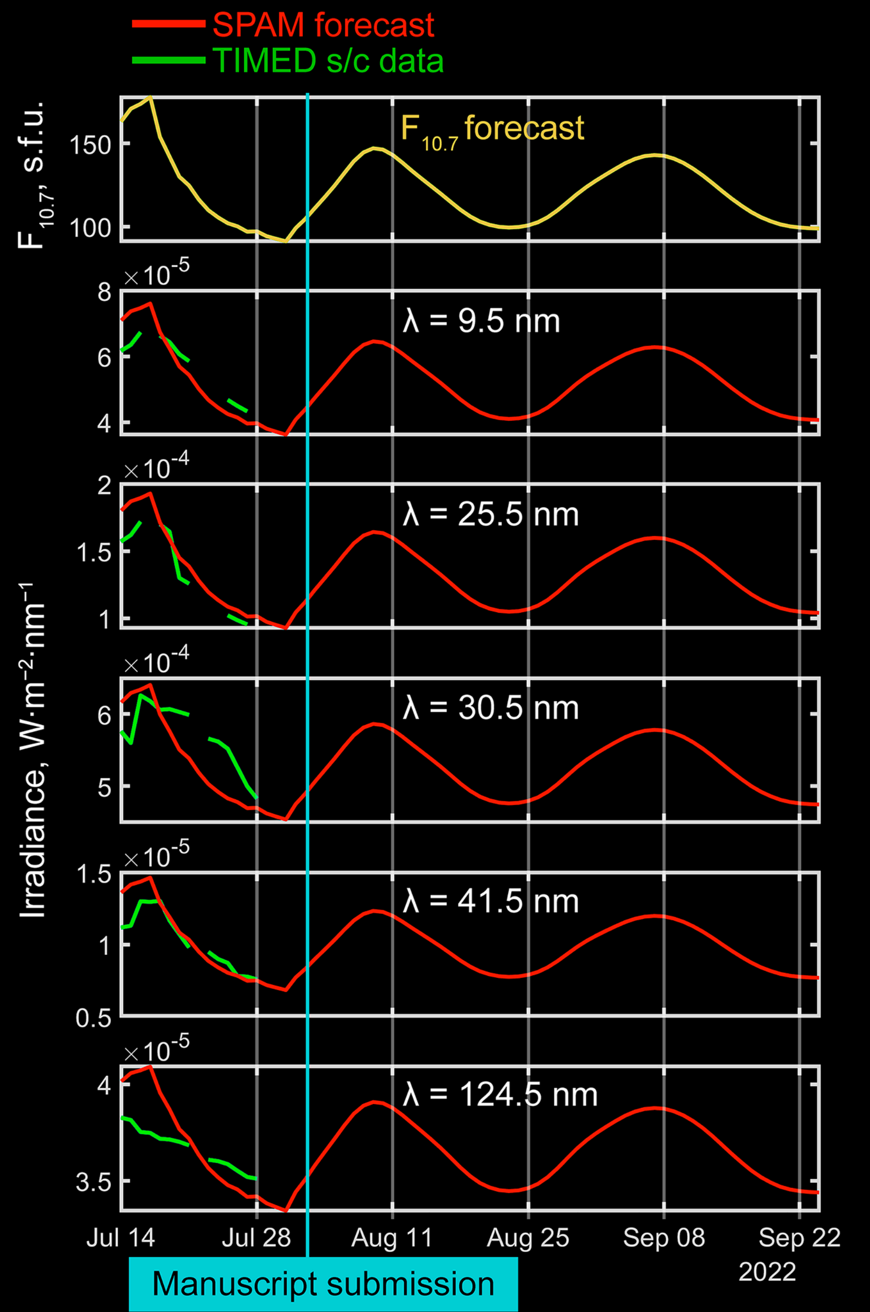

$F_{10.7}$ forecast is provided by IZMIRAN Space Weather Prediction Center
http://spaceweather.izmiran.ru/eng/forecasts.html

AGU PUBLICATIONS

Space Weather

Supporting Information for

SPAM: Solar Spectrum Prediction for Applications and Modeling

Vera Nikolaeva[1,2] and Evgeny Gordeev[3]

[1]Arctic and Antarctic Research Institute, St. Petersburg, 199397 Russia.

[2]Pushkov Institute of Terrestrial Magnetism, Ionosphere, and Radio Wave Propagation, Russian Academy of Sciences, Moscow, 142191 Russia.

[3]Saint Petersburg State University, St. Petersburg, 199034 Russia.

Corresponding authors: Vera Nikolaeva (nikolaeva.vera@gmail.com) and Evgeny Gordeev (evgeny.i.gordeev@spbu.ru)

Contents of this file

Introduction

Figures in this Supplementary file show the time series of solar irradiance for each spectral channel of the TIMED SEE instrument, covering the spectral interval from 0 to 190 nm with 1-nm resolution.

The panels on the left demonstrate the TIMED SEE measurements (red and green) for the entire period of spacecraft operation from 2002 to 2022 years. The vertical blue line denotes the date of the last calibration flight of a suborbital rocket on June 1, 2016. Half a year after the last calibration, artificial trends emerged in different spectral lines, which are easy to recognize by the sharp step-like change in the measured values (e.g. 43.5 nm, 46.5 nm, 55.5 nm and others). The data obtained before the sensor degradation is shown in red, and after – in green. The black curve denotes the Solar-SPAM model calculations based on the TIMED SEE Level 3 data shown in red and parameterized by daily F10.7 solar activity index.

The panels on the right show the scatterplots of the TIMED SEE solar irradiance versus the F10.7 solar activity index.

Figures capture. Left panels: time series of solar radiation obtained by the TIMED SEE instrument in each spectral channel from 0 to 190 nm with a resolution of 1 nm. The TIMED SEE measurements shown in red (before) and green (after sensor degradation); black curve is the Solar-SPAM model calculations. Blue vertical line denotes the date of the last absolute detector calibration on June 1, 2016. Right panels show the scatterplots of the radiation flux versus the F10.7 index and the quadratic interpolation line.

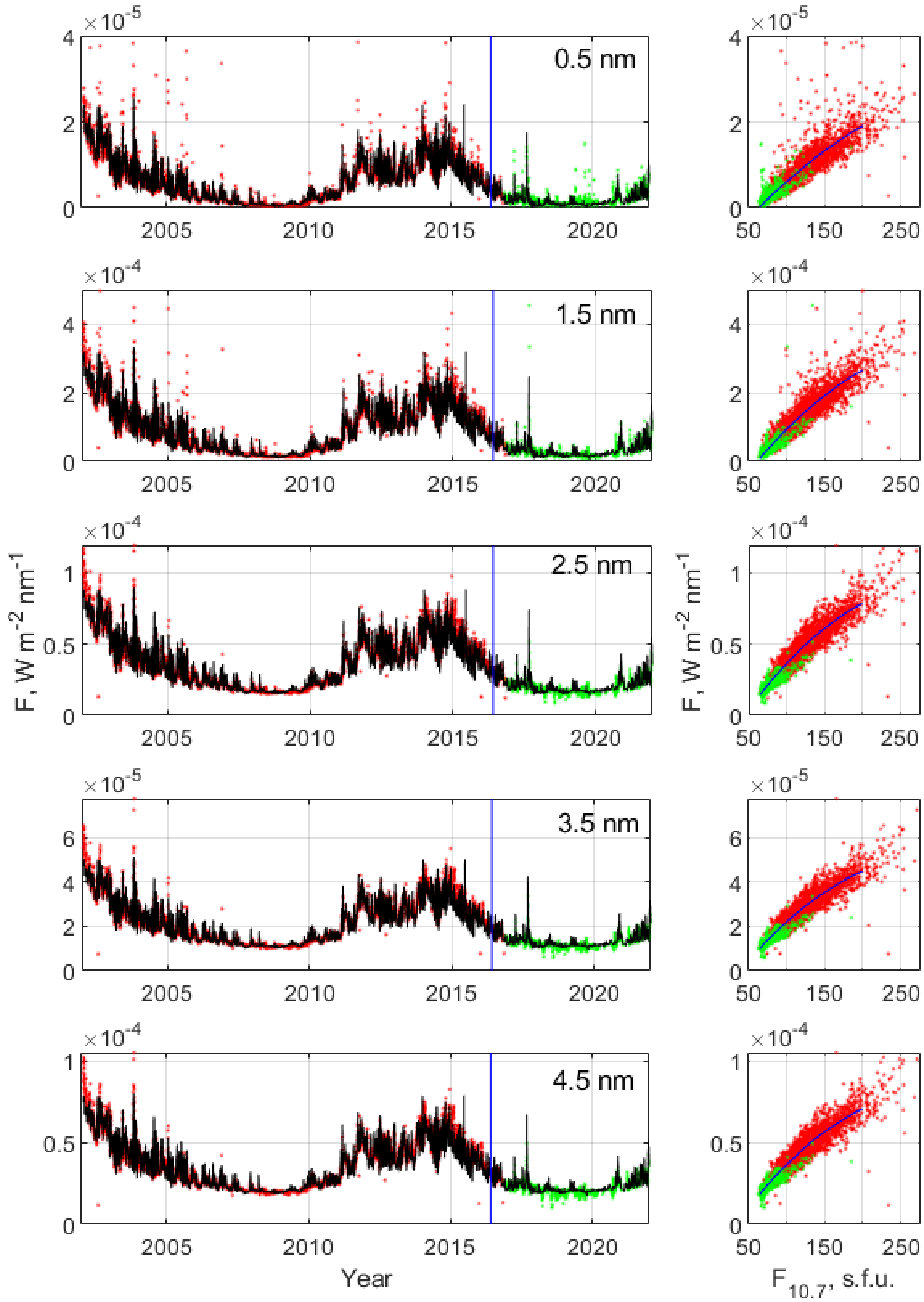
0.5 nm
1.5 nm
2.5 nm
3.5 nm
4.5 nm
Year
F, W m^{-2} nm^{-1}
$F_{10.7}$, s.f.u.

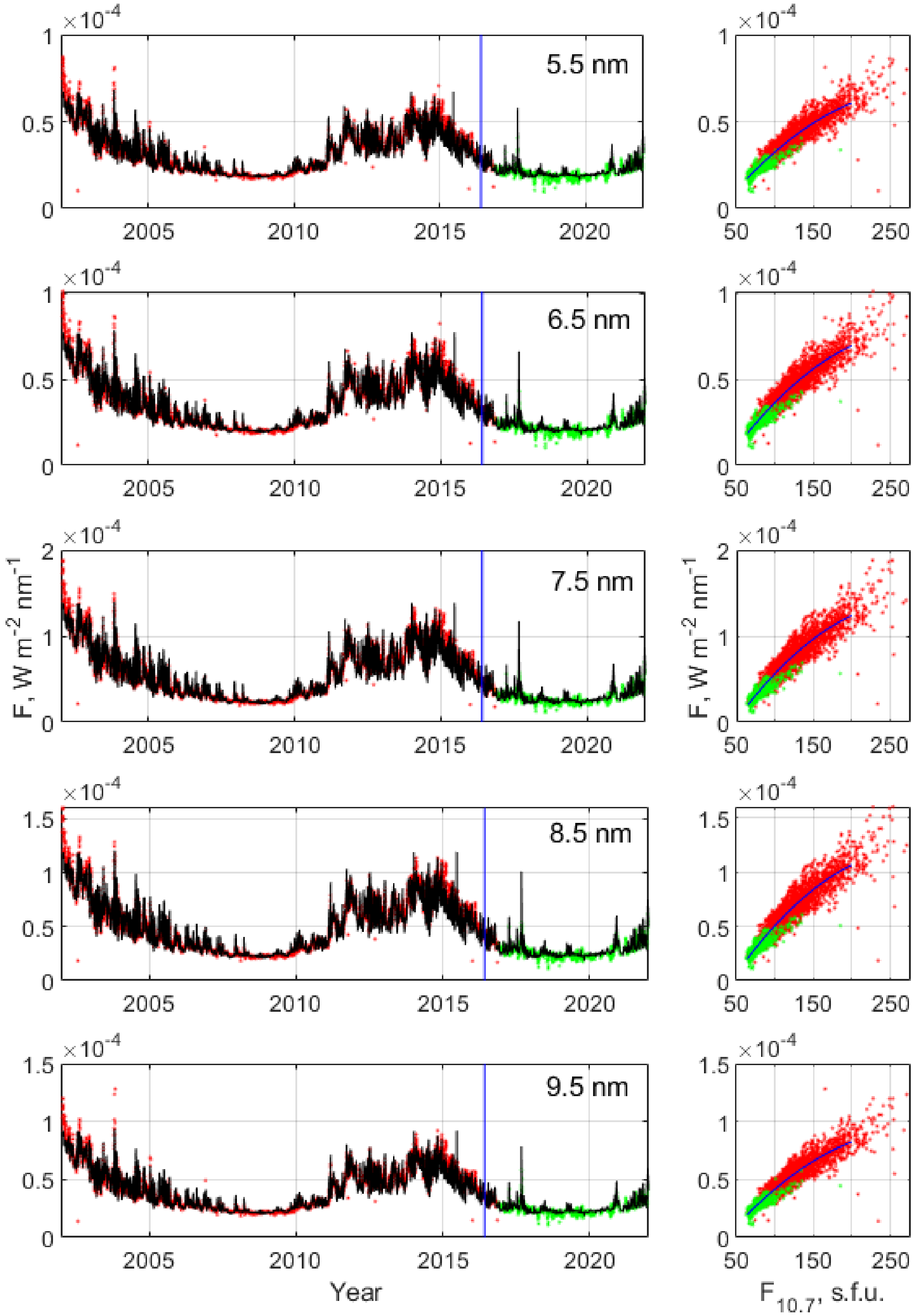
5.5 nm
6.5 nm
7.5 nm
8.5 nm
9.5 nm
F, W m^{-2} nm^{-1}
Year
$F_{10.7}$, s.f.u.

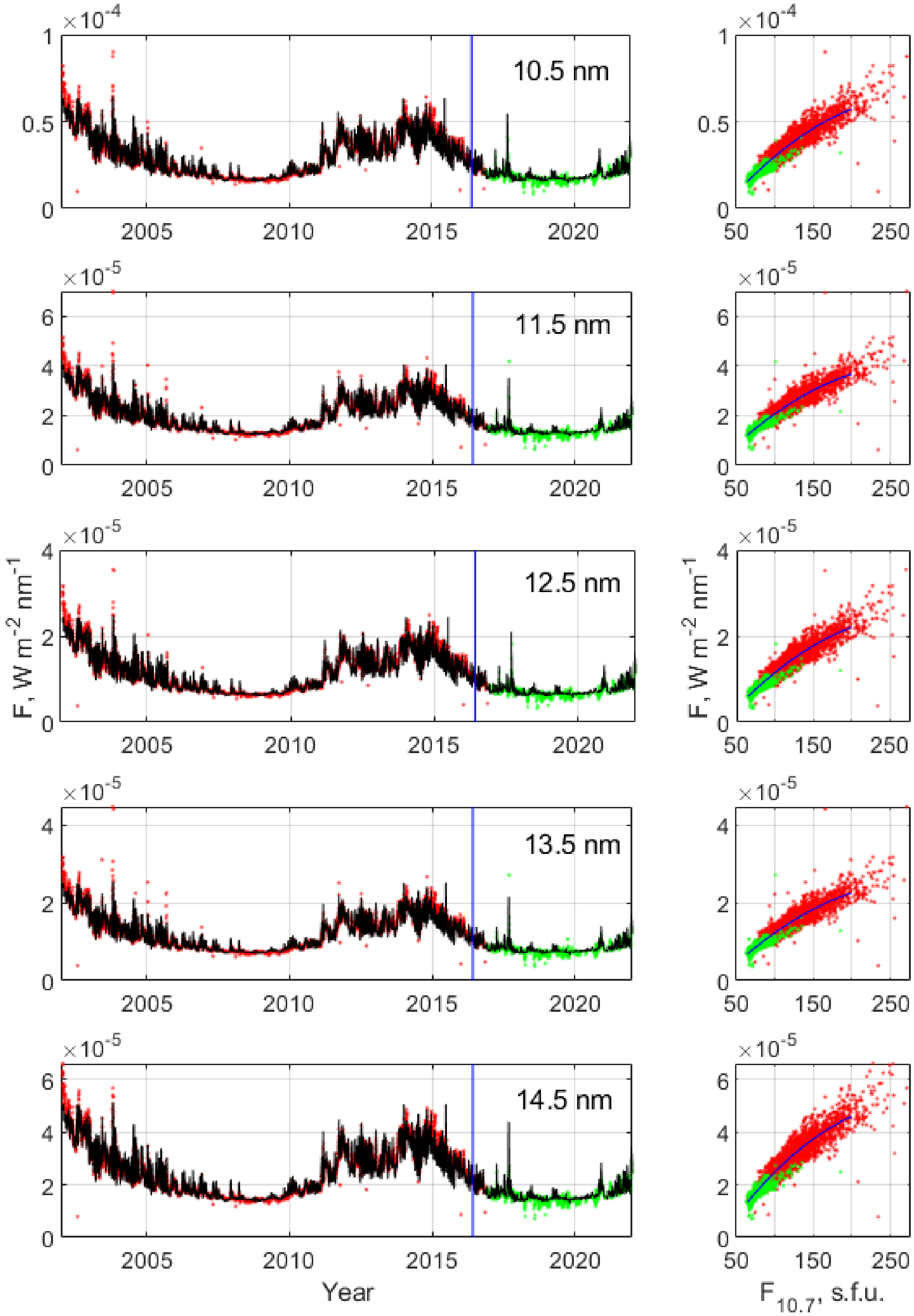

10.5 nm
11.5 nm
12.5 nm
13.5 nm
14.5 nm
F, W m^{-2} nm^{-1}
Year
$F_{10.7}$, s.f.u.

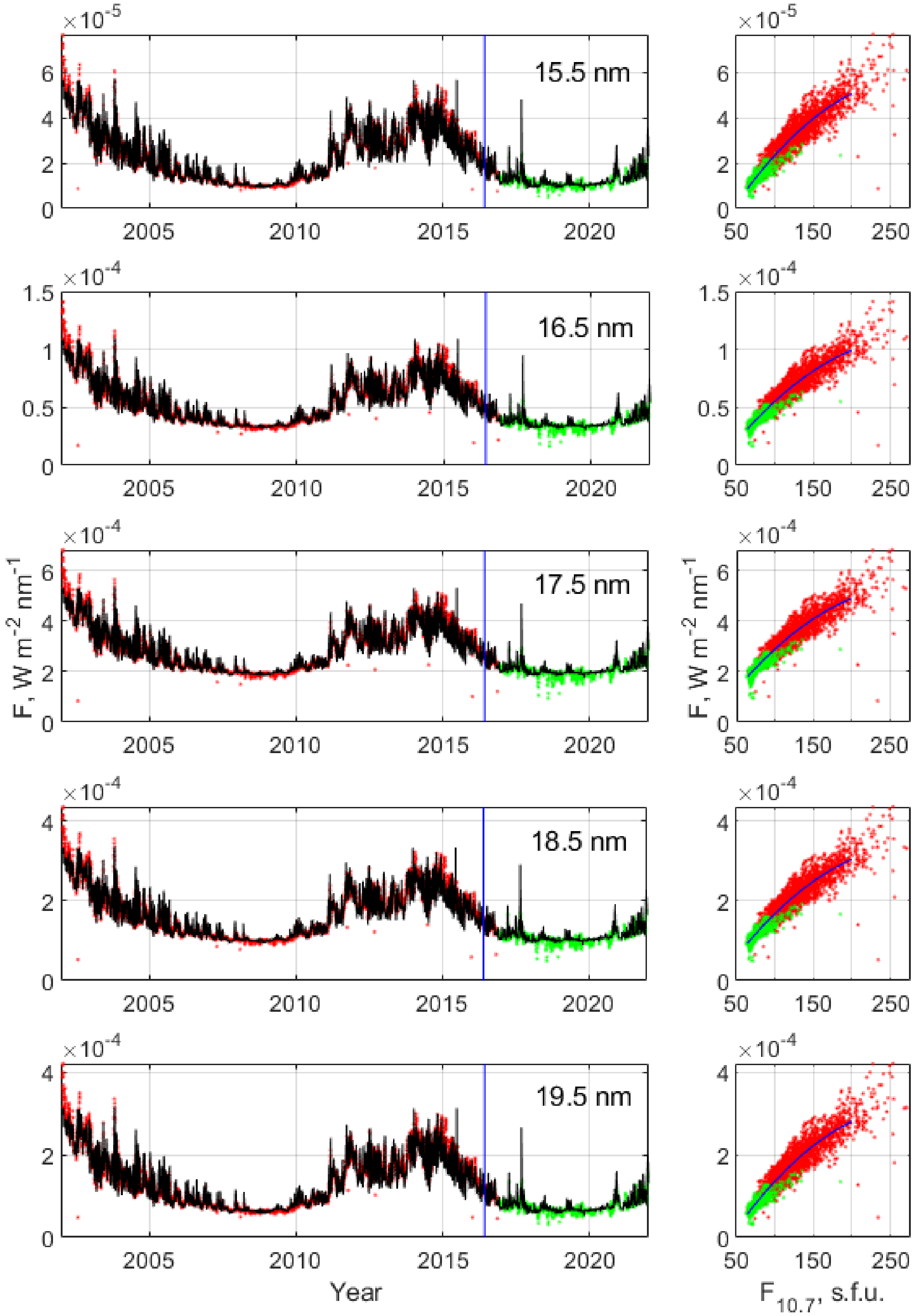
15.5 nm
16.5 nm
17.5 nm
18.5 nm
19.5 nm
×10^-5
×10^-4
F, W m^-2 nm^-1
Year
F10.7, s.f.u.
2005
2010
2015
2020
50
150
250

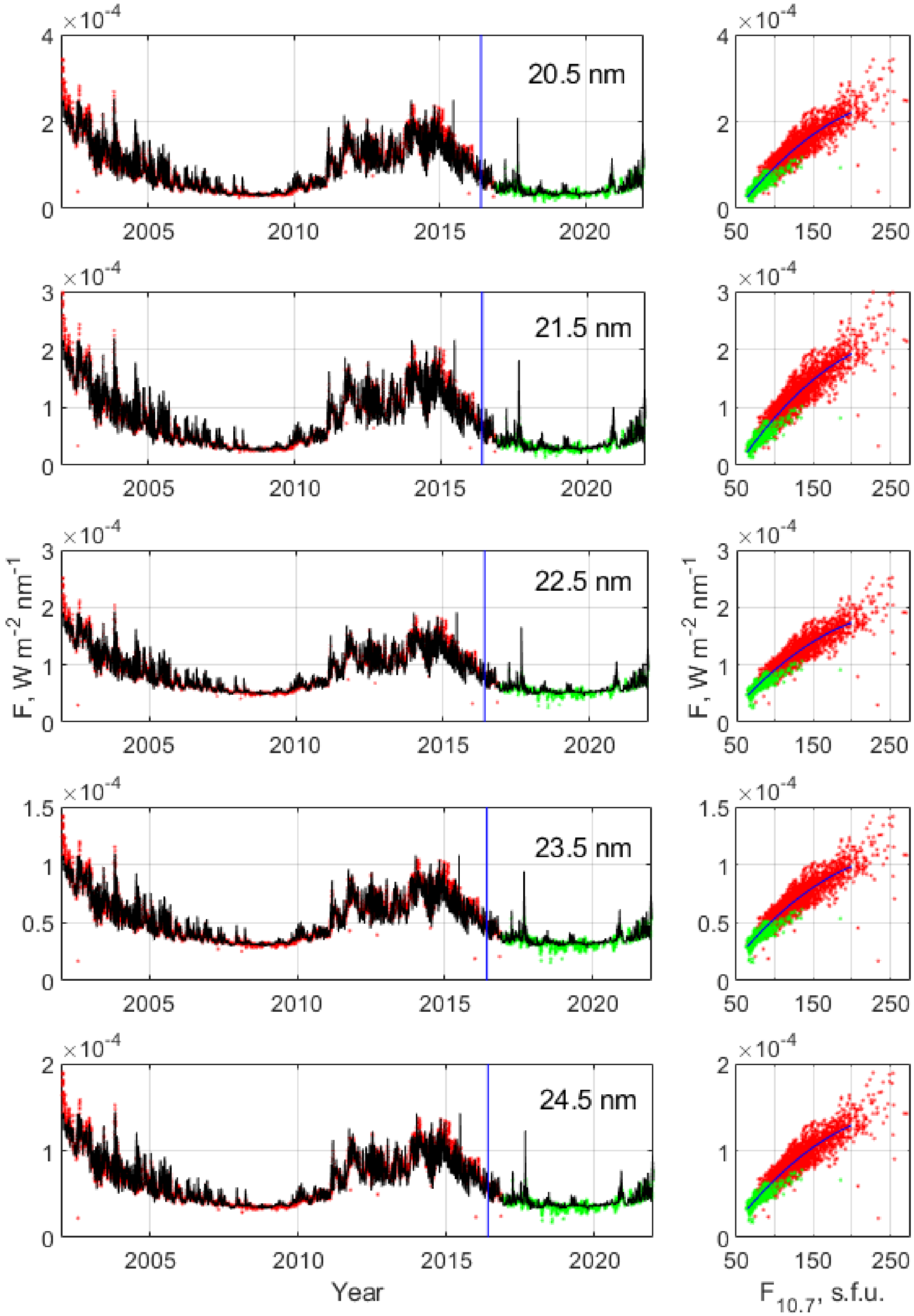

20.5 nm
21.5 nm
22.5 nm
23.5 nm
24.5 nm
$\times 10^{-4}$
F, W m^{-2} nm^{-1}
Year
$F_{10.7}$, s.f.u.
2005
2010
2015
2020
50
150
250

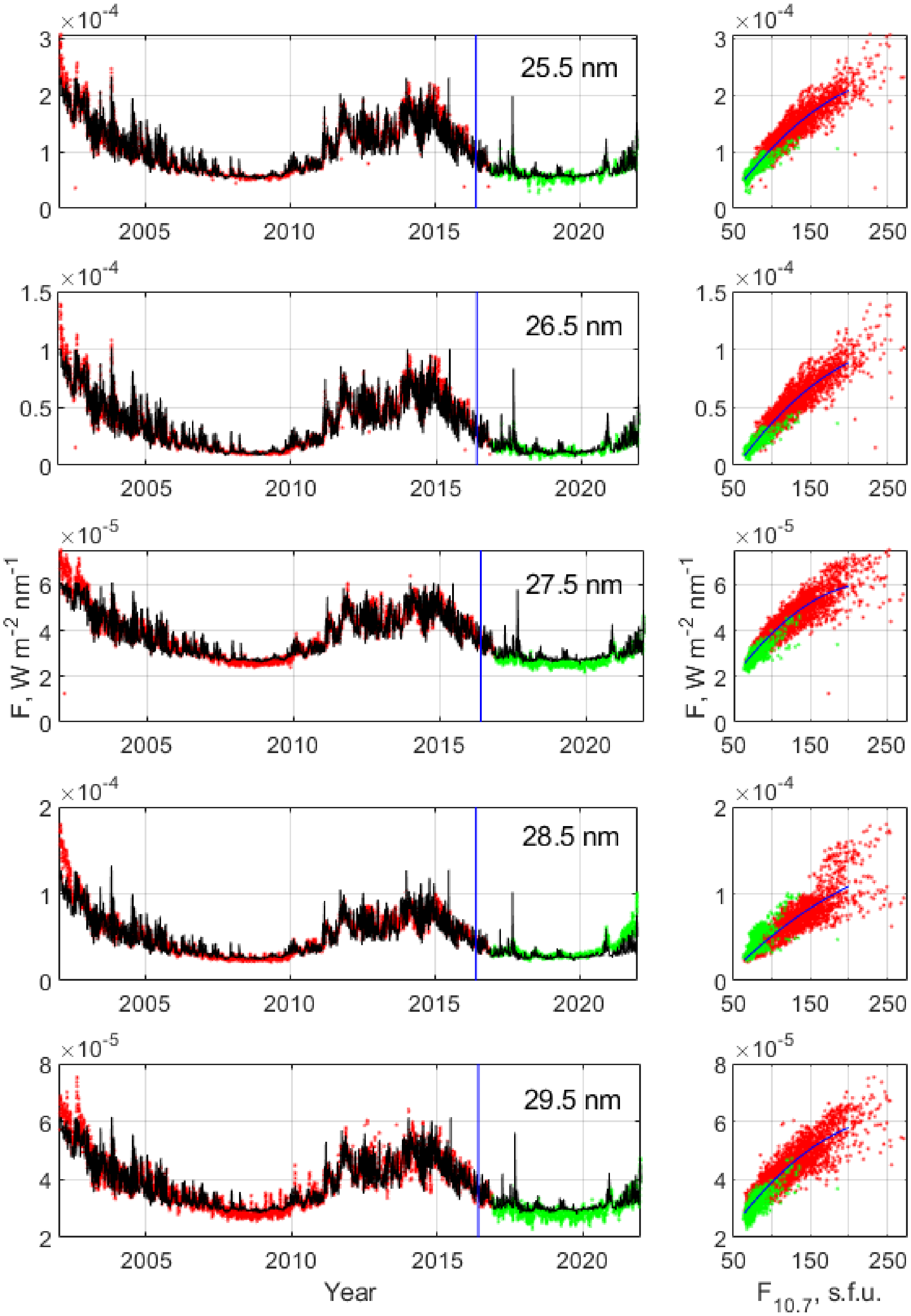
25.5 nm
26.5 nm
27.5 nm
28.5 nm
29.5 nm
F, W m^{-2} nm^{-1}
Year
$F_{10.7}$, s.f.u.

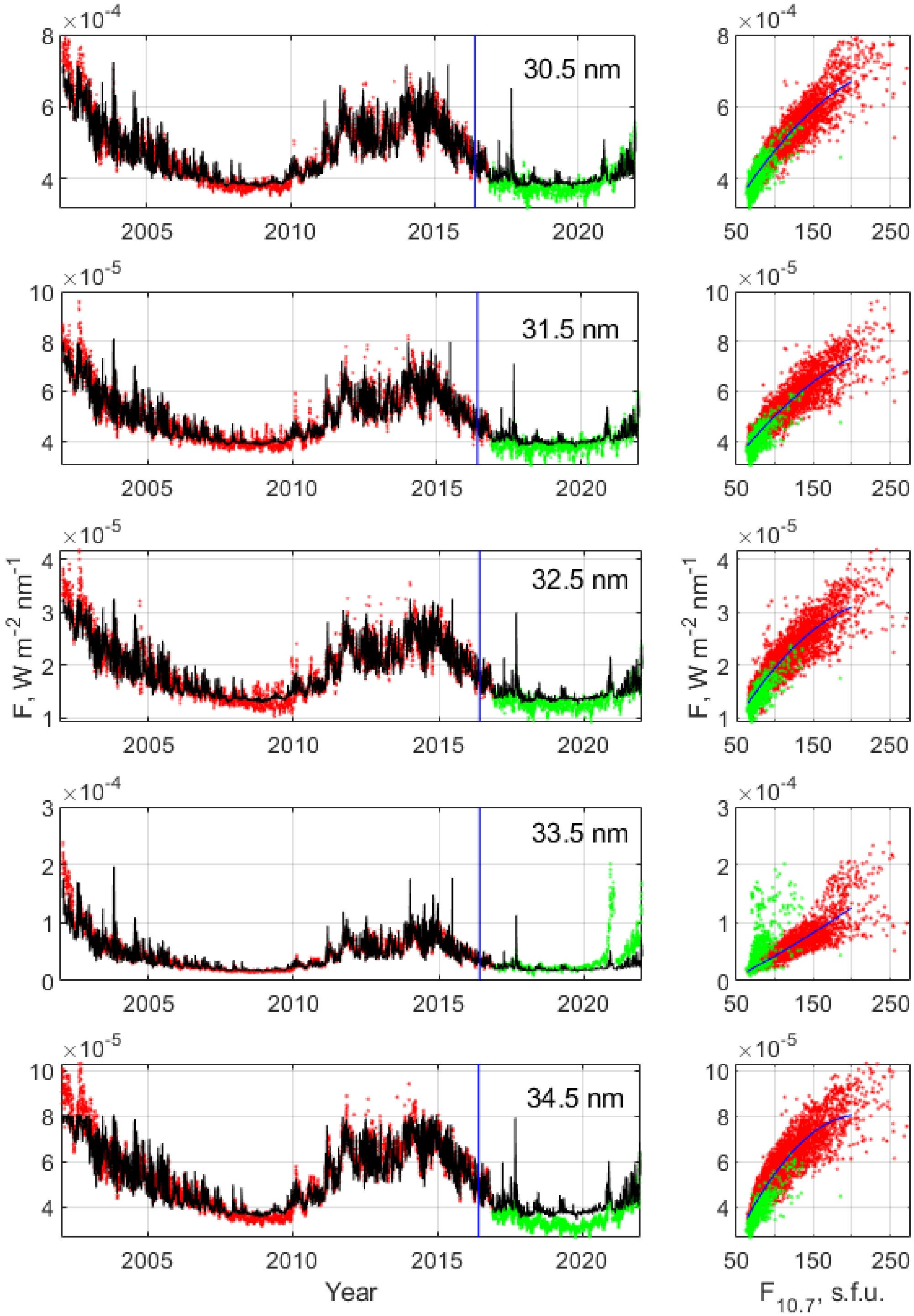

30.5 nm
31.5 nm
32.5 nm
33.5 nm
34.5 nm
×10^-4
×10^-5
F, W m^-2 nm^-1
Year
F10.7, s.f.u.
2005
2010
2015
2020
50
150
250

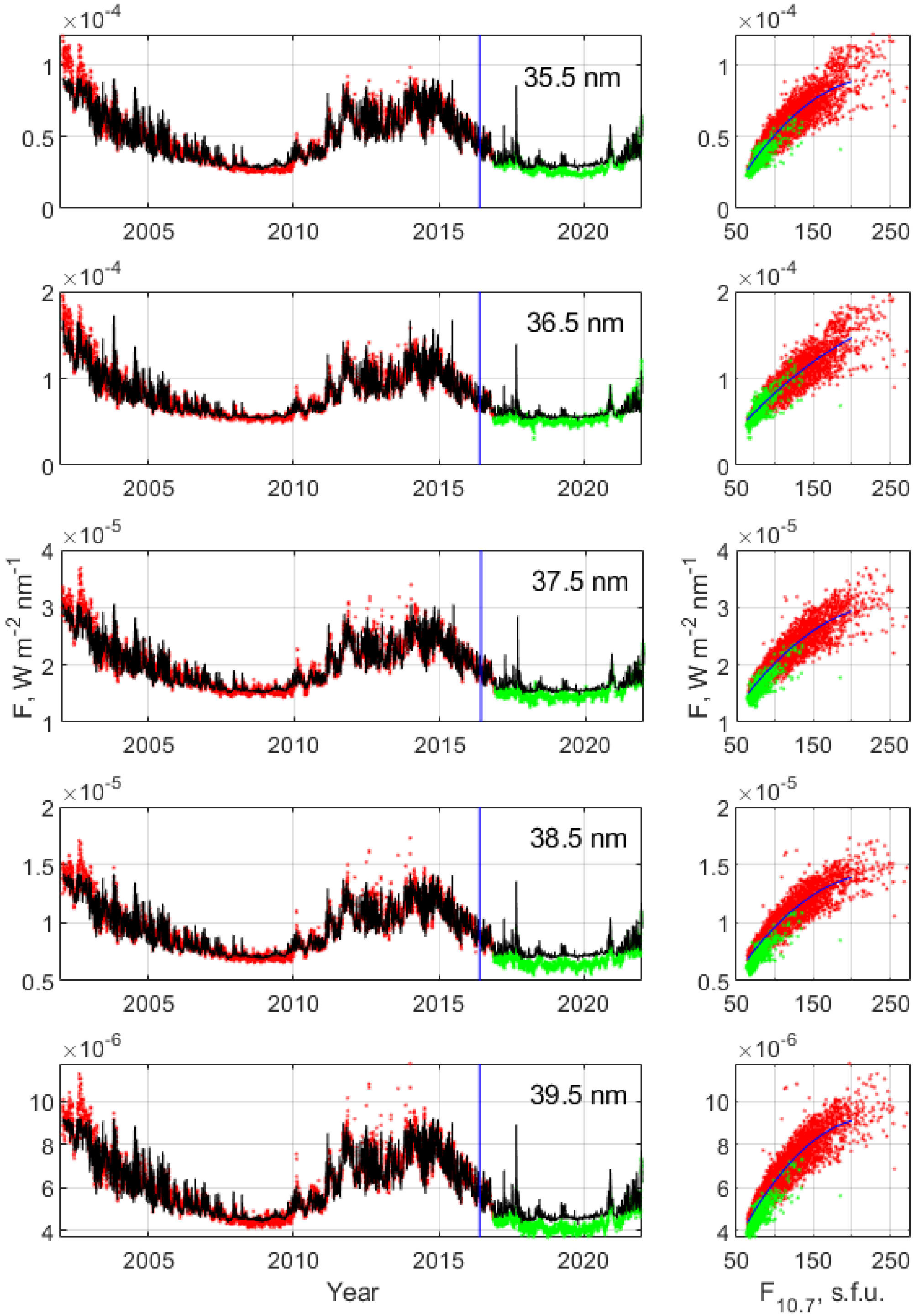
35.5 nm
36.5 nm
37.5 nm
38.5 nm
39.5 nm
F, W m^{-2} nm^{-1}
Year
$F_{10.7}$, s.f.u.

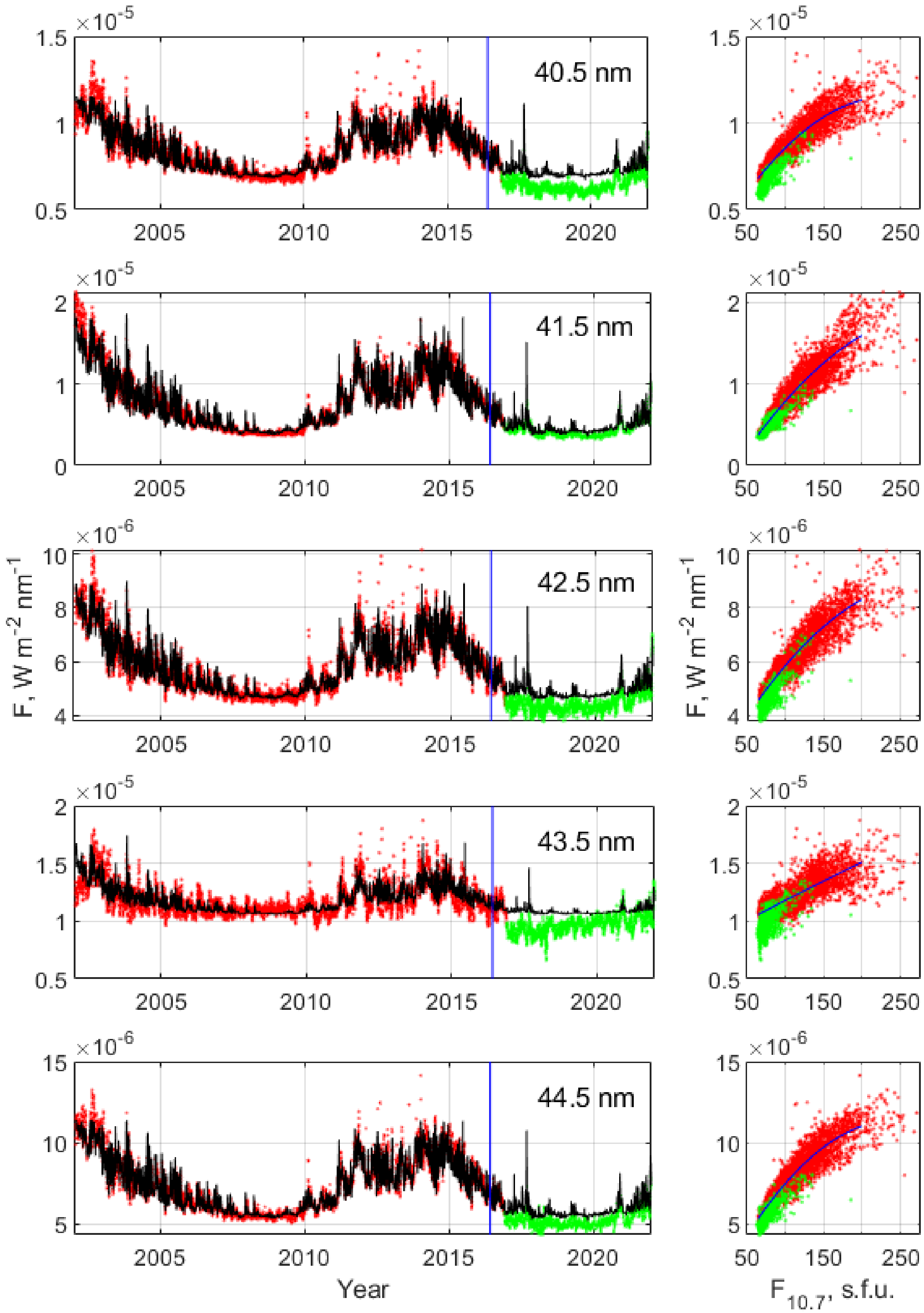
40.5 nm
41.5 nm
42.5 nm
43.5 nm
44.5 nm
F, W m-2 nm-1
Year
F10.7, s.f.u.
2005
2010
2015
2020
50
150
250

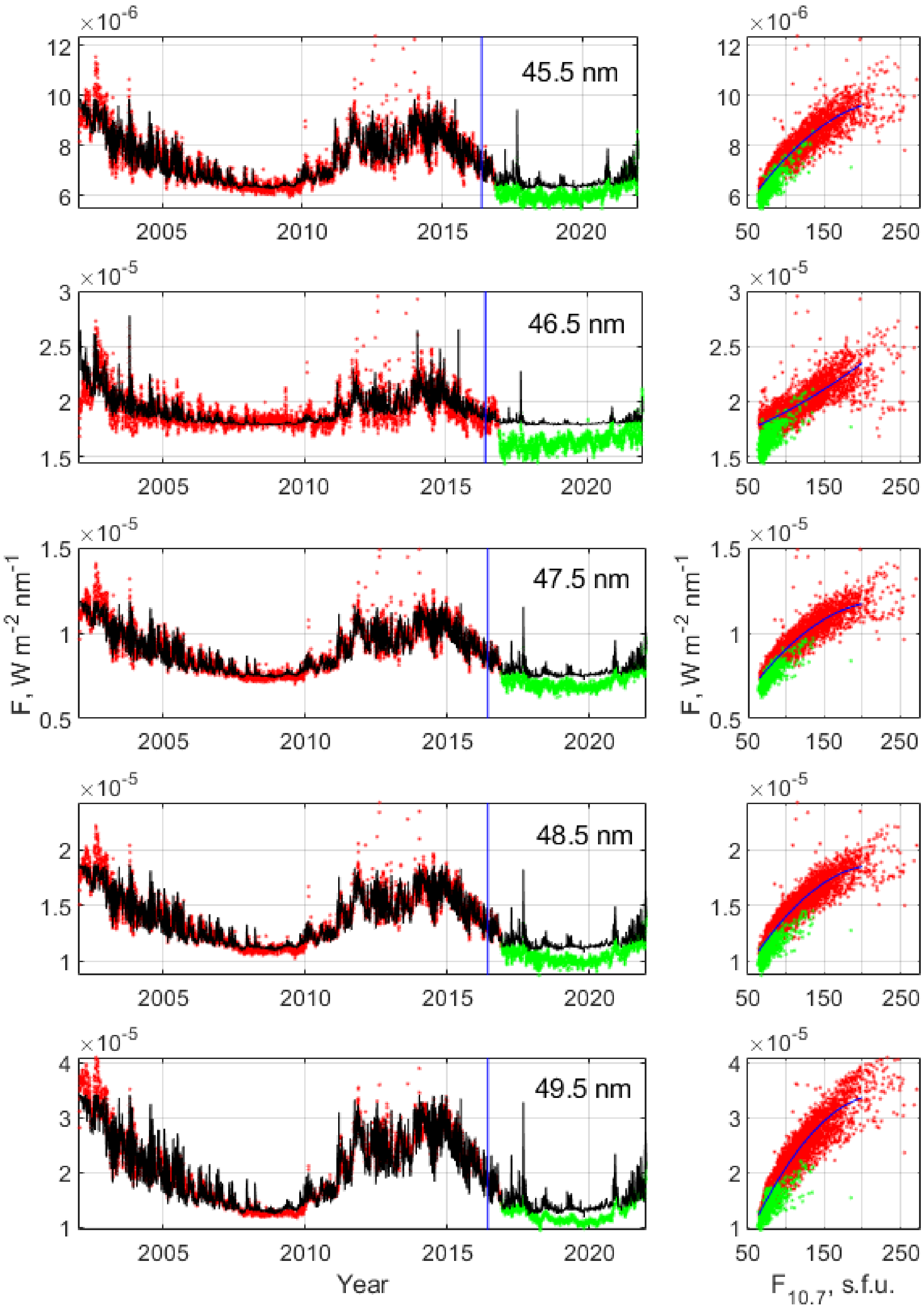

45.5 nm
46.5 nm
47.5 nm
48.5 nm
49.5 nm
F, W m^{-2} nm^{-1}
Year
$F_{10.7}$, s.f.u.

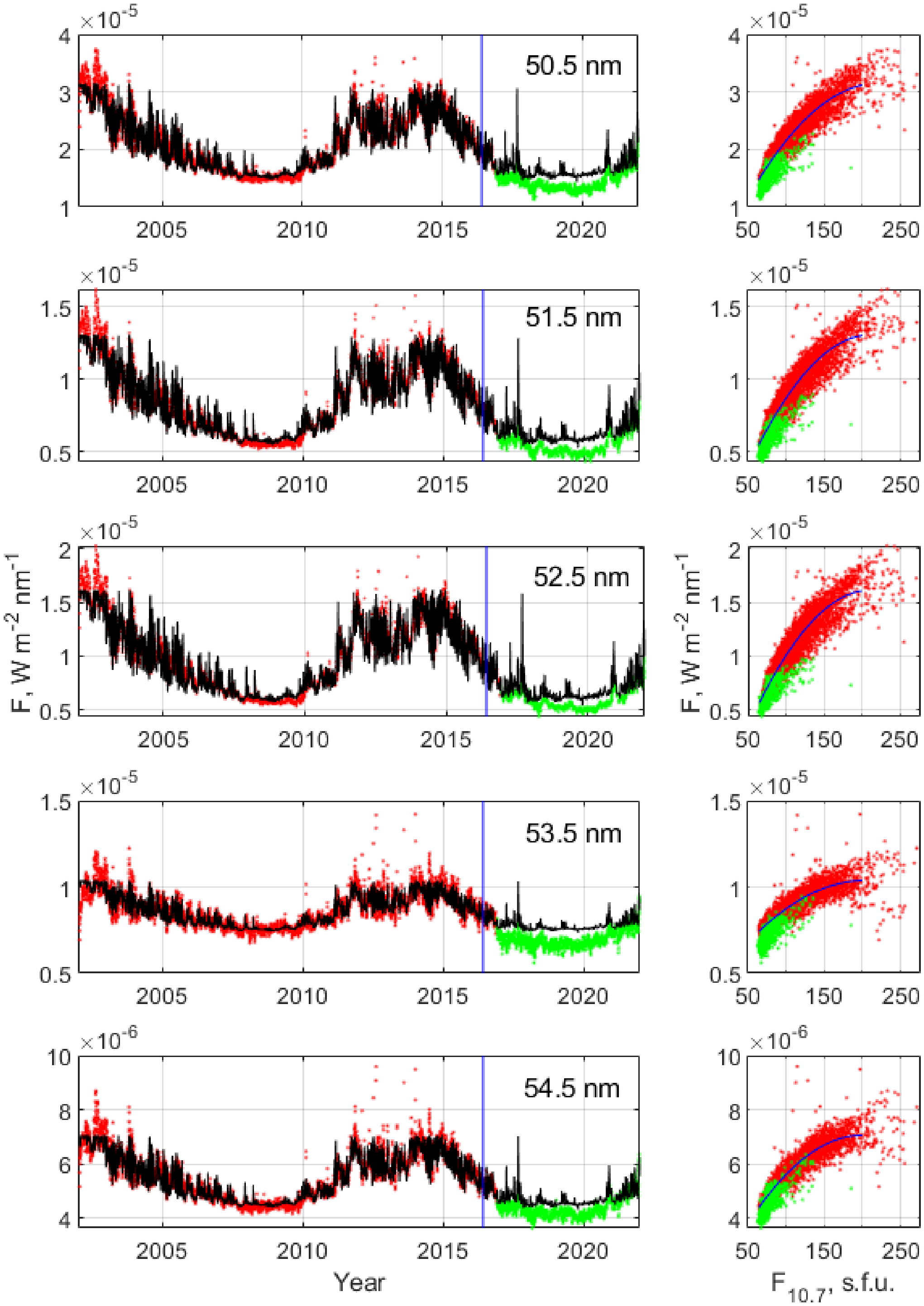
50.5 nm
51.5 nm
52.5 nm
53.5 nm
54.5 nm
F, W m^{-2} nm^{-1}
Year
$F_{10.7}$, s.f.u.

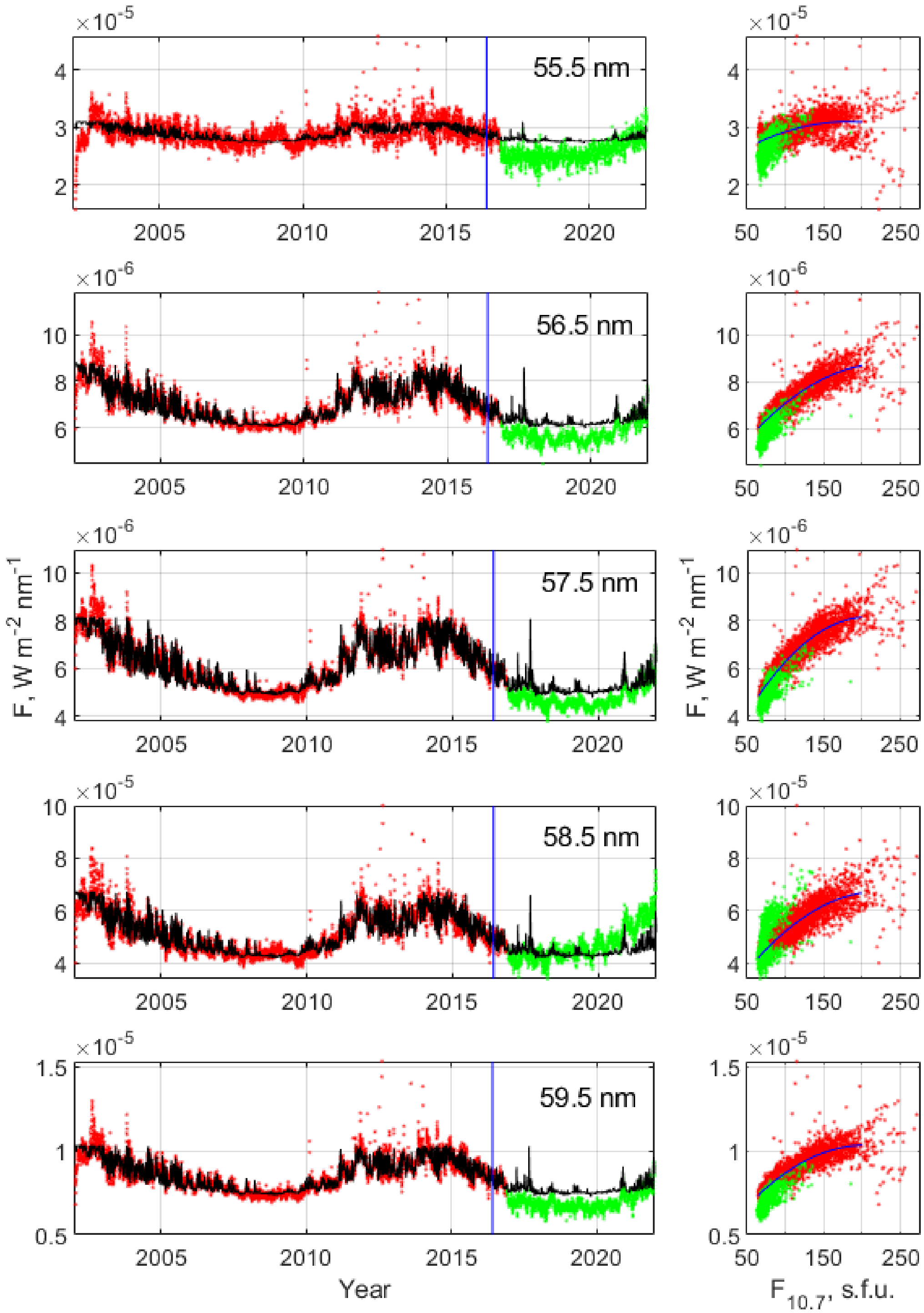

55.5 nm
56.5 nm
57.5 nm
58.5 nm
59.5 nm
F, W m^{-2} nm^{-1}
Year
$F_{10.7}$, s.f.u.

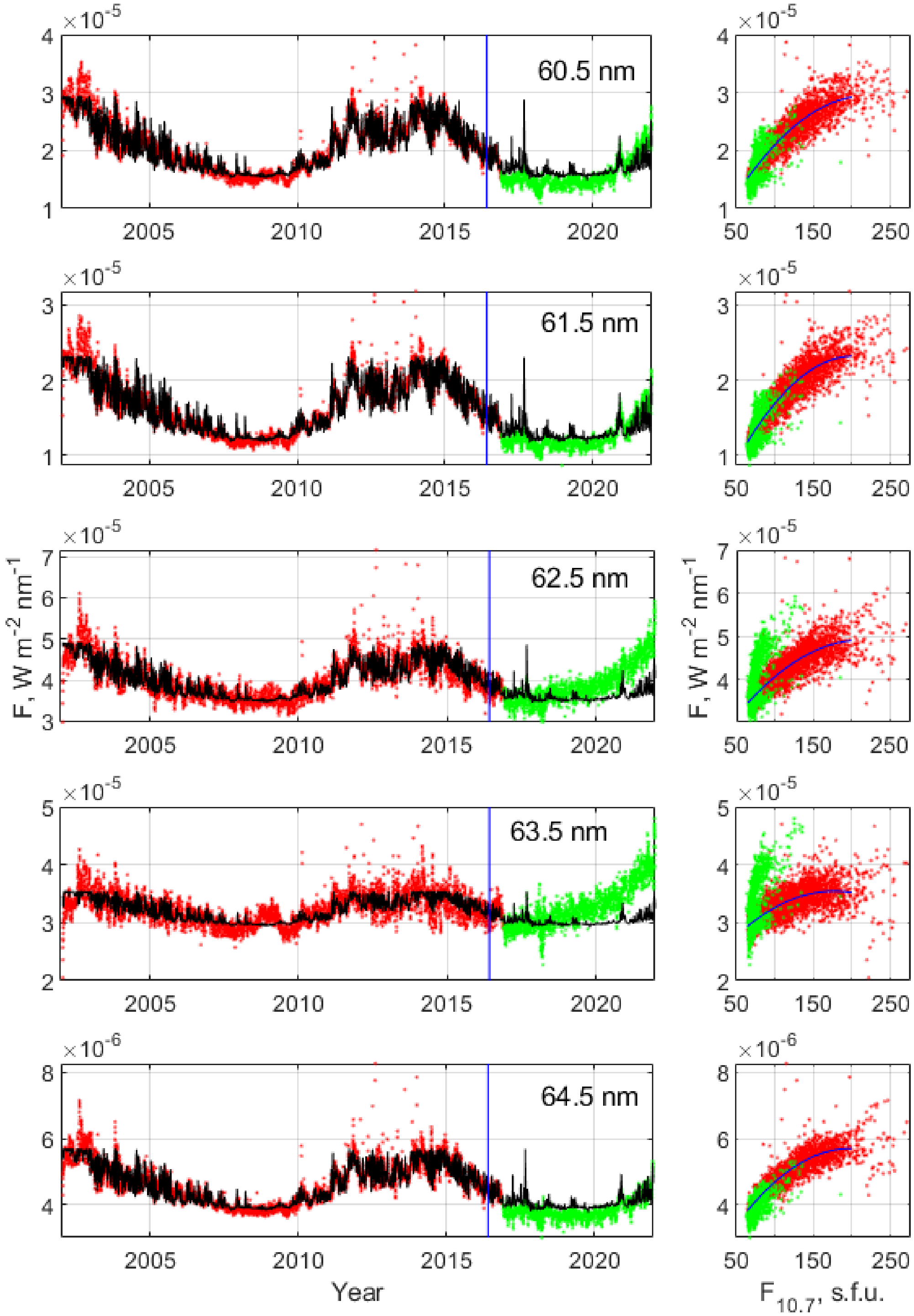

60.5 nm
61.5 nm
62.5 nm
63.5 nm
64.5 nm
F, W m-2 nm-1
Year
F10.7, s.f.u.

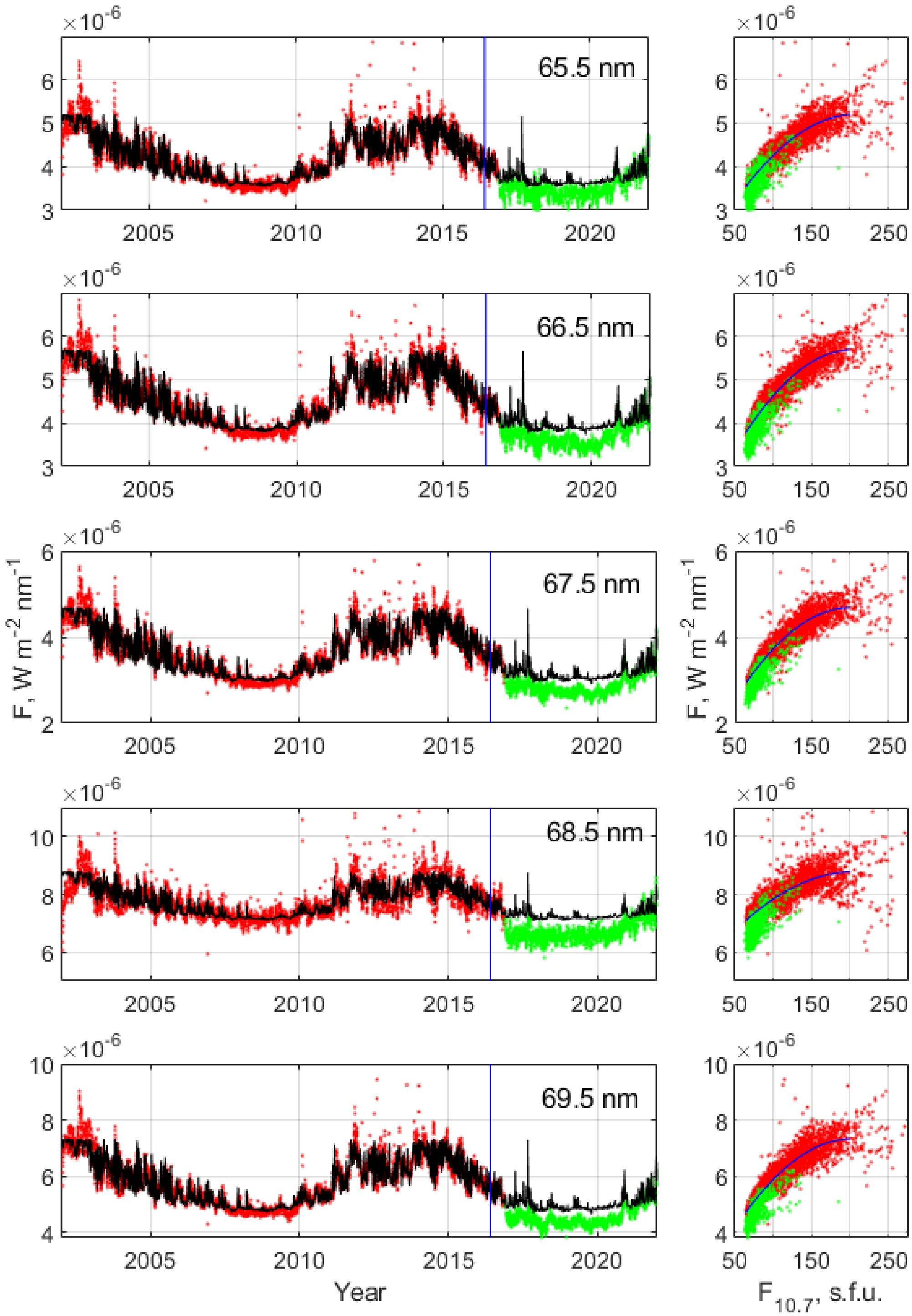

65.5 nm
66.5 nm
67.5 nm
68.5 nm
69.5 nm
F, W m^{-2} nm^{-1}
Year
$F_{10.7}$, s.f.u.

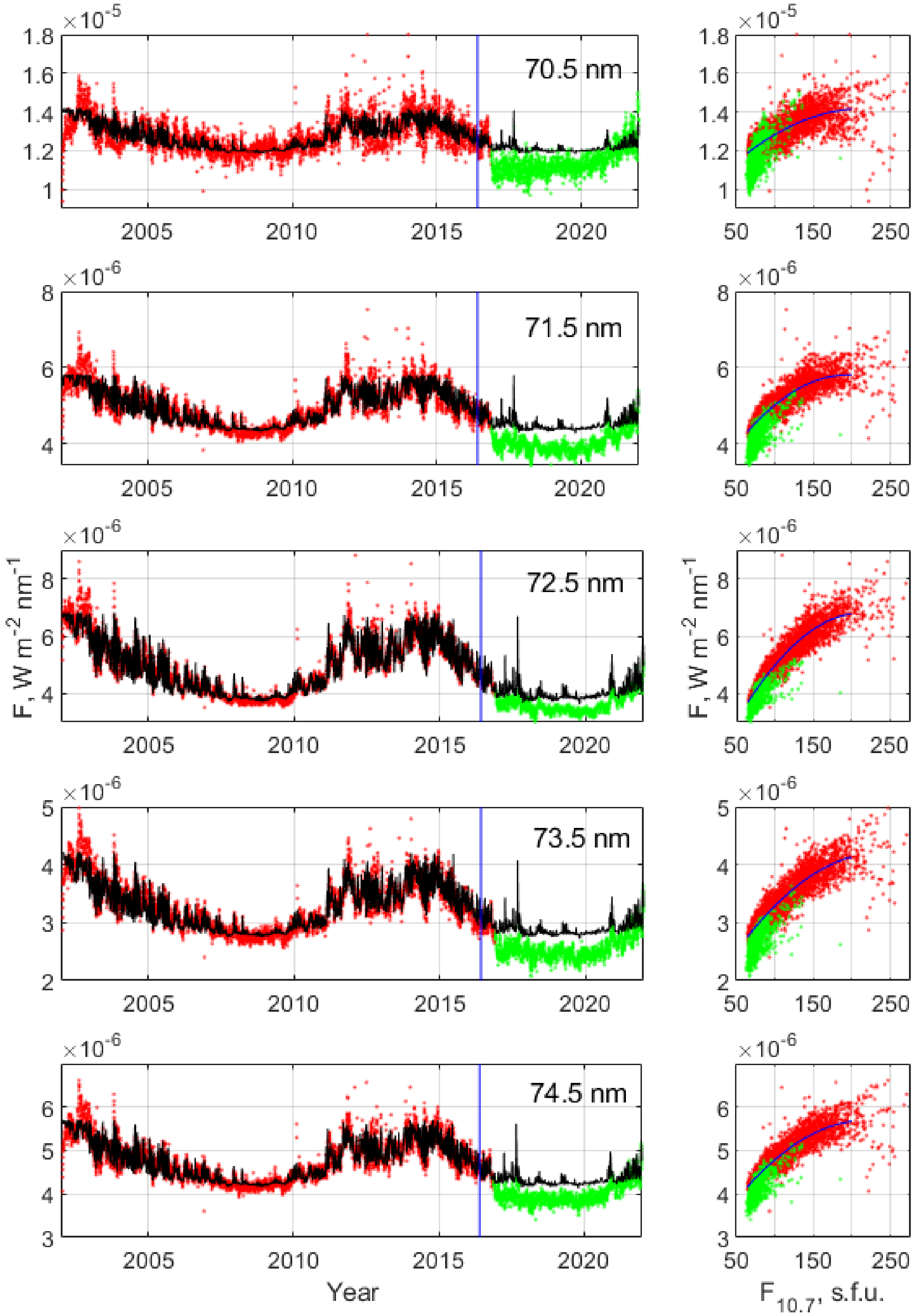

70.5 nm
71.5 nm
72.5 nm
73.5 nm
74.5 nm
F, W m-2 nm-1
Year
F10.7, s.f.u.

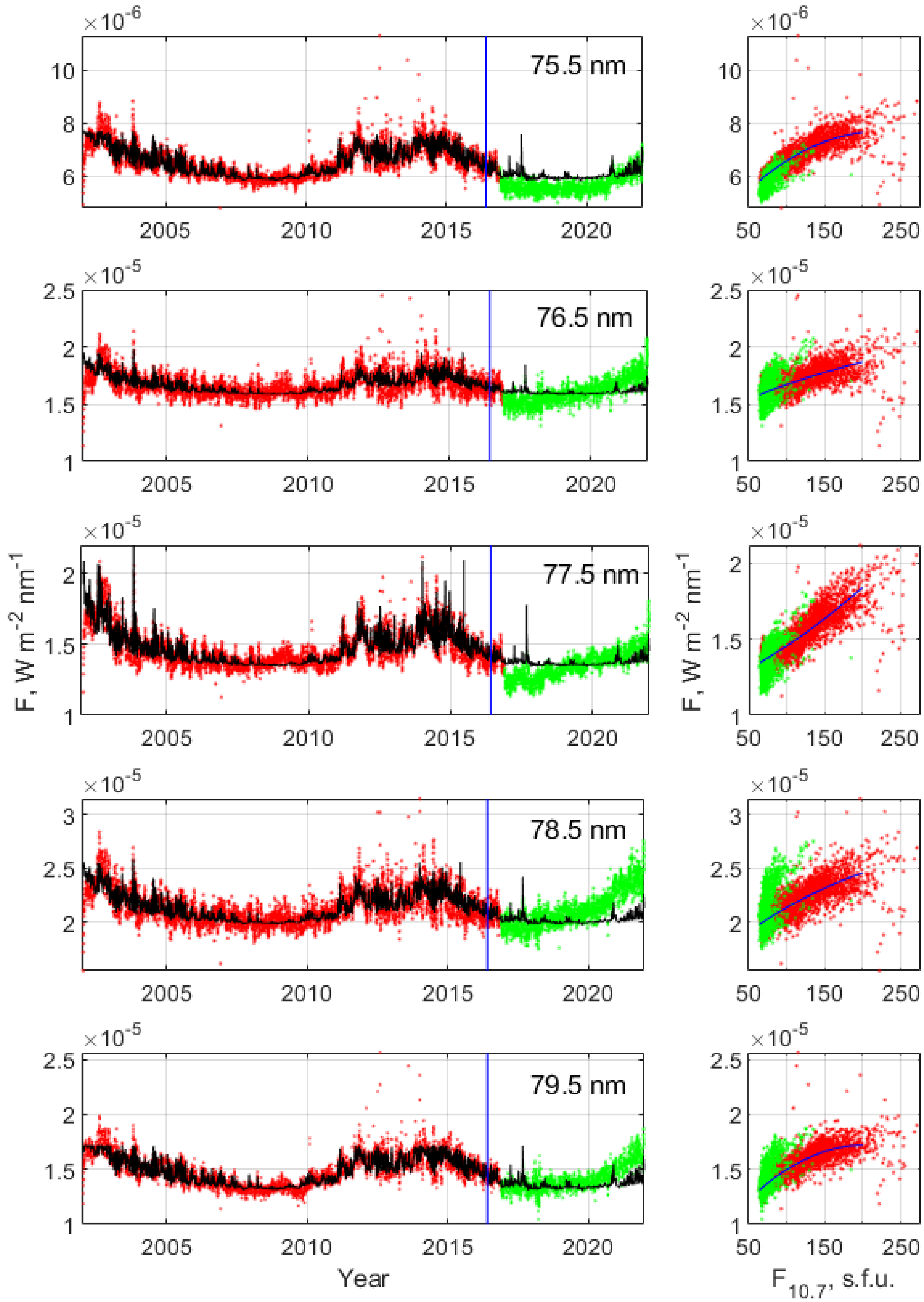

75.5 nm
76.5 nm
77.5 nm
78.5 nm
79.5 nm
F, W m^{-2} nm^{-1}
Year
$F_{10.7}$, s.f.u.

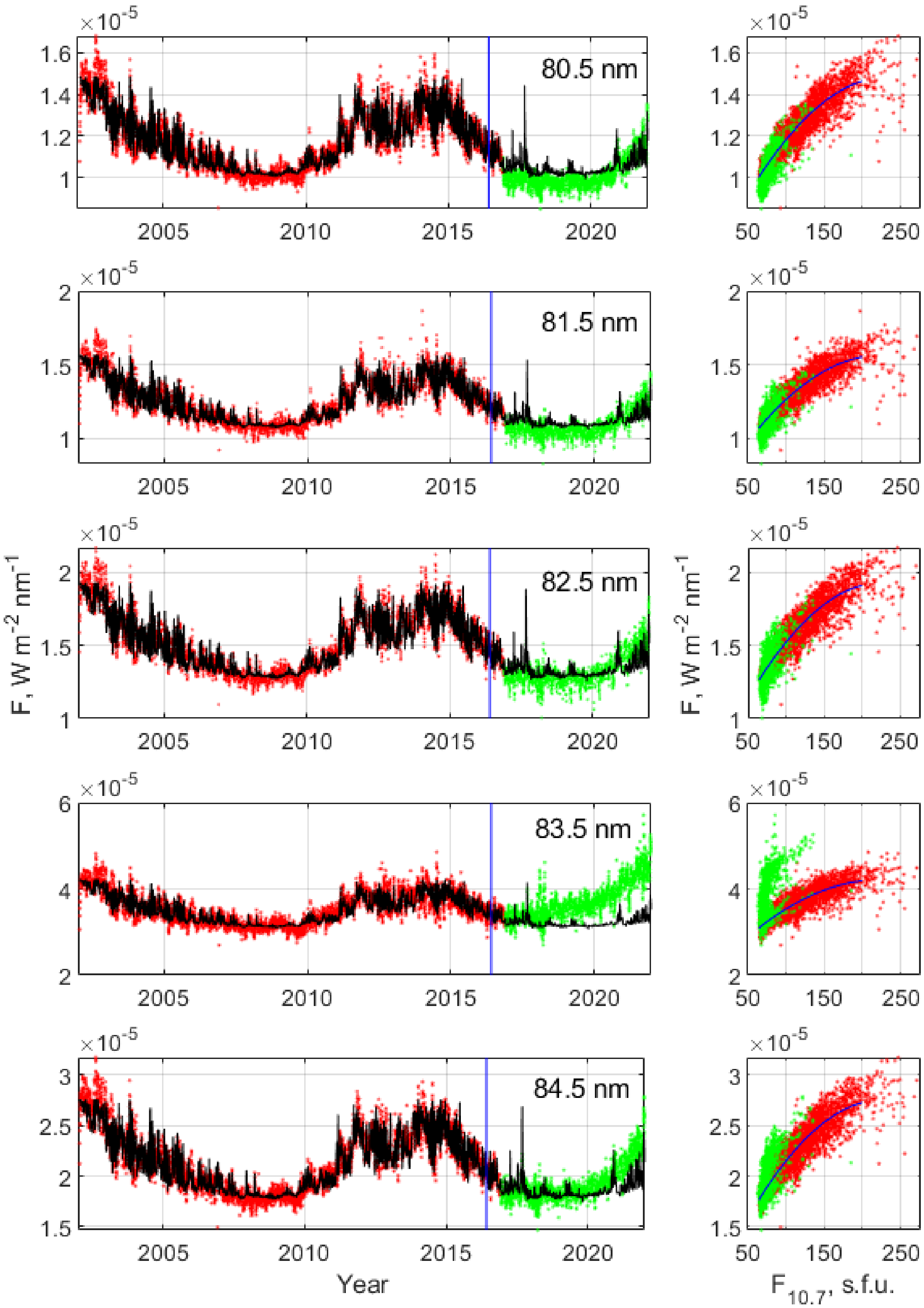
×10^-5
80.5 nm
81.5 nm
82.5 nm
83.5 nm
84.5 nm
F, W m^-2 nm^-1
Year
F10.7, s.f.u.
2005
2010
2015
2020
50
150
250

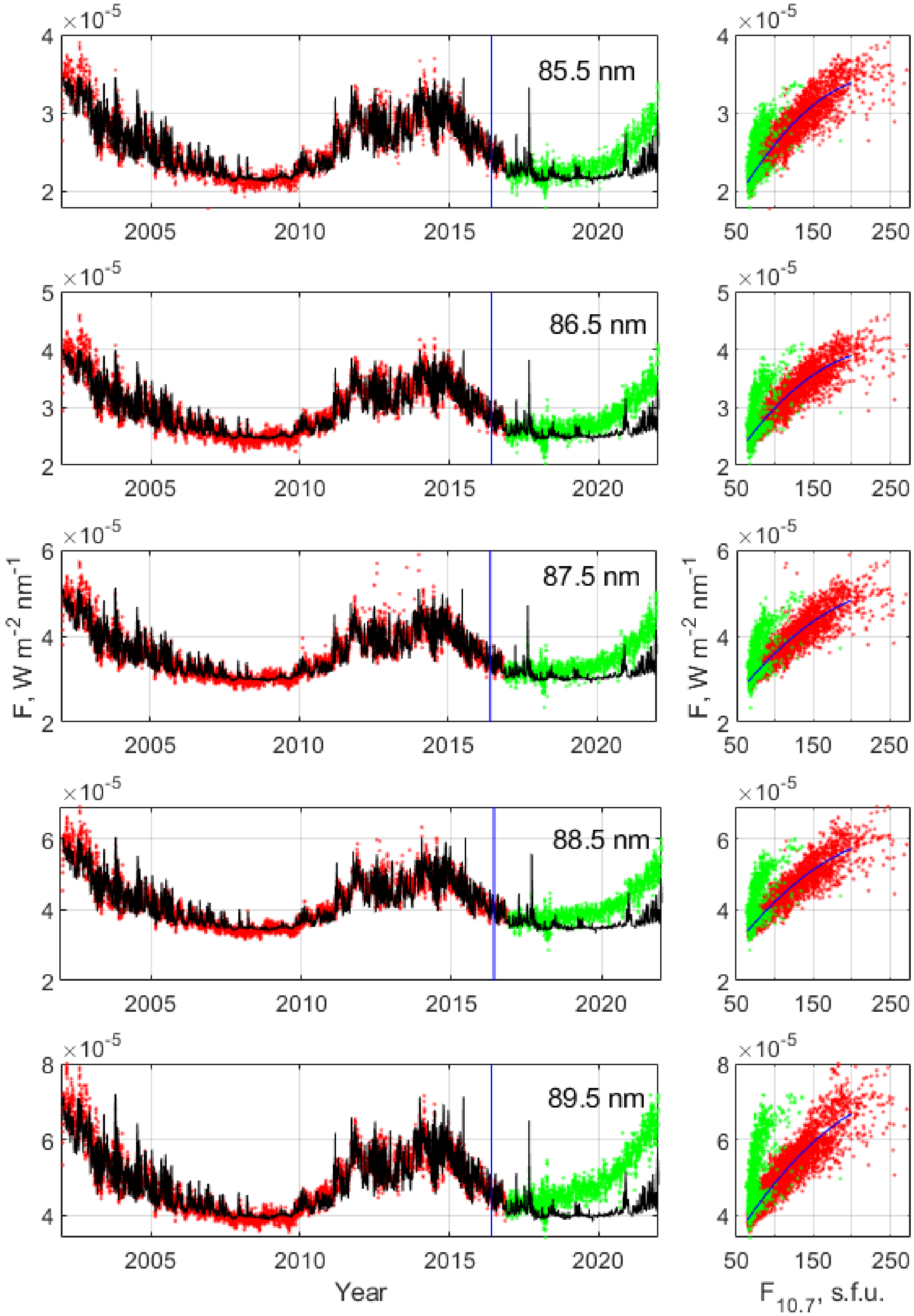

85.5 nm
86.5 nm
87.5 nm
88.5 nm
89.5 nm
Year
F, W m^-2 nm^-1
F_10.7, s.f.u.
×10^-5

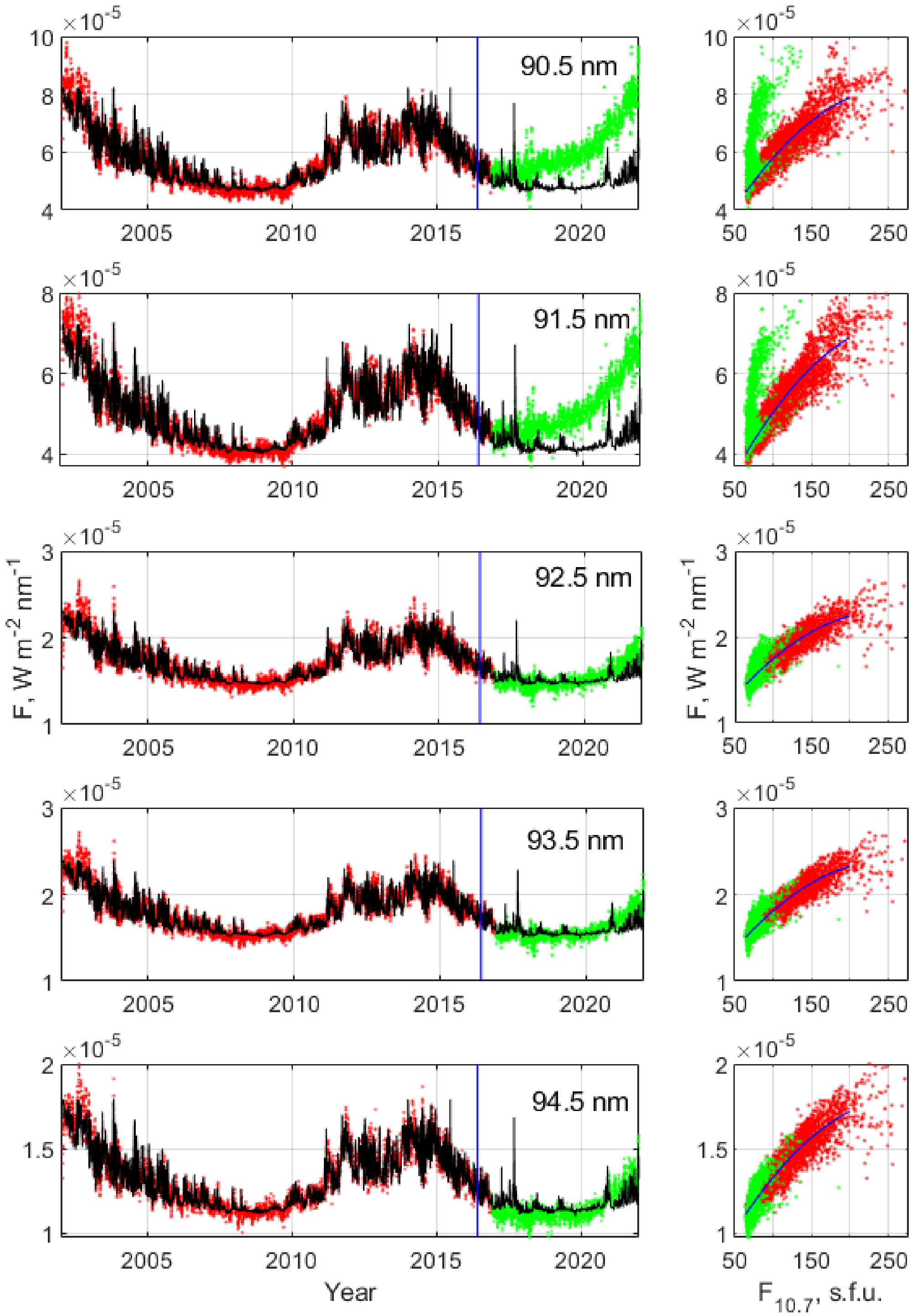
90.5 nm
91.5 nm
92.5 nm
93.5 nm
94.5 nm
×10^-5
F, W m^-2 nm^-1
2005
2010
2015
2020
Year
50
150
250
F_10.7, s.f.u.

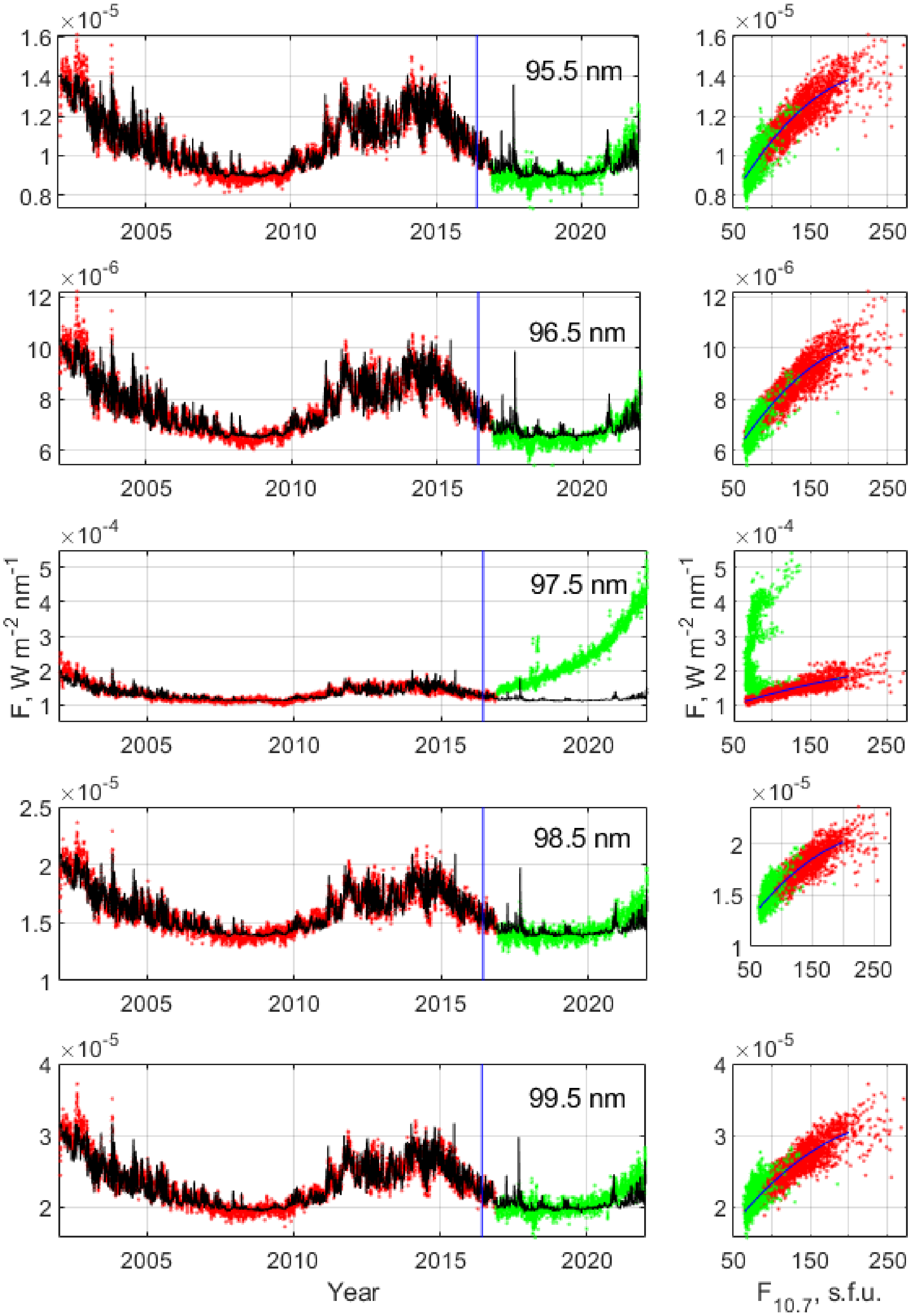

95.5 nm
96.5 nm
97.5 nm
98.5 nm
99.5 nm
F, W m^{-2} nm^{-1}
Year
F$_{10.7}$, s.f.u.

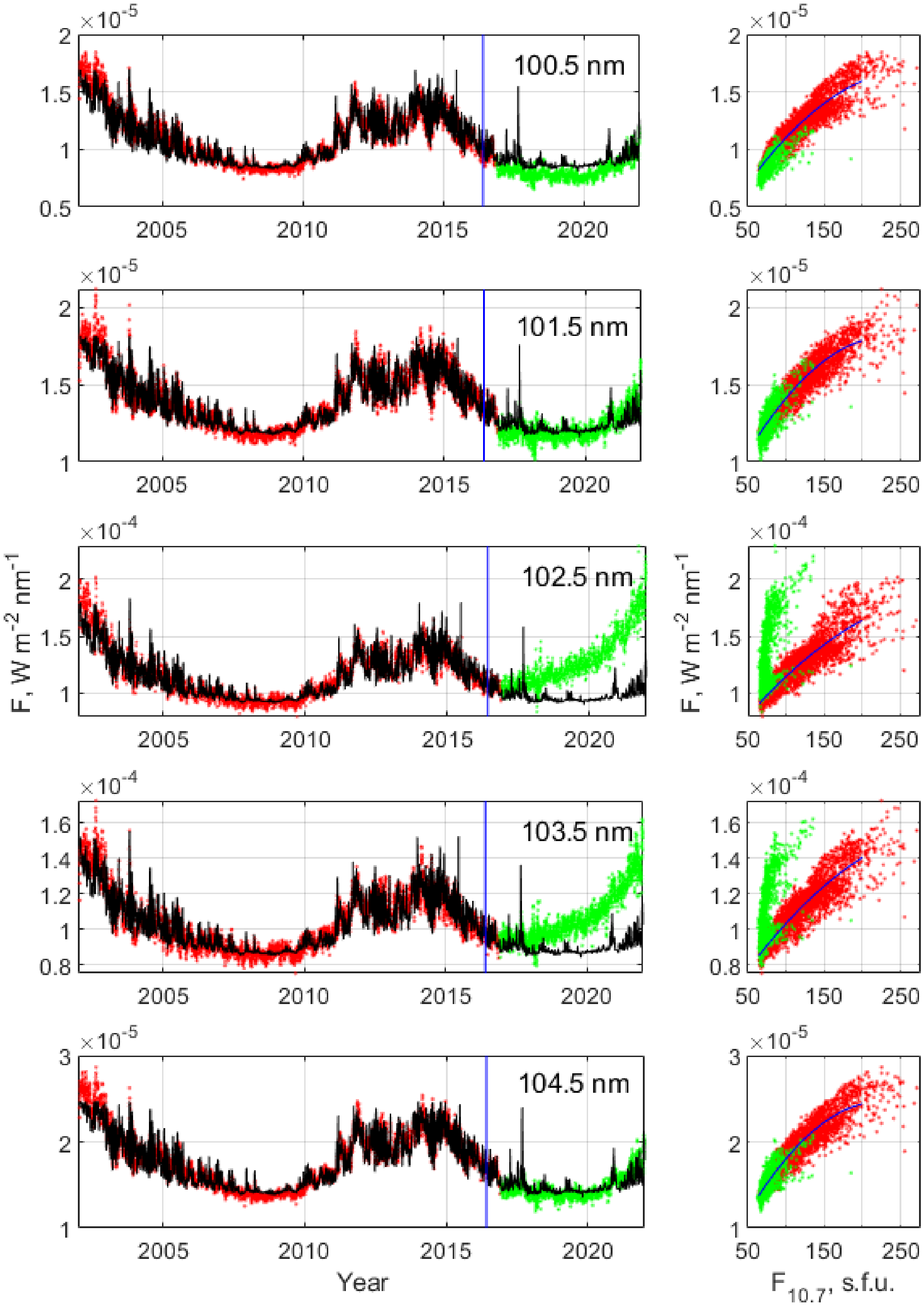

100.5 nm
101.5 nm
102.5 nm
103.5 nm
104.5 nm
×10^-5
×10^-4
F, W m^-2 nm^-1
Year
F10.7, s.f.u.

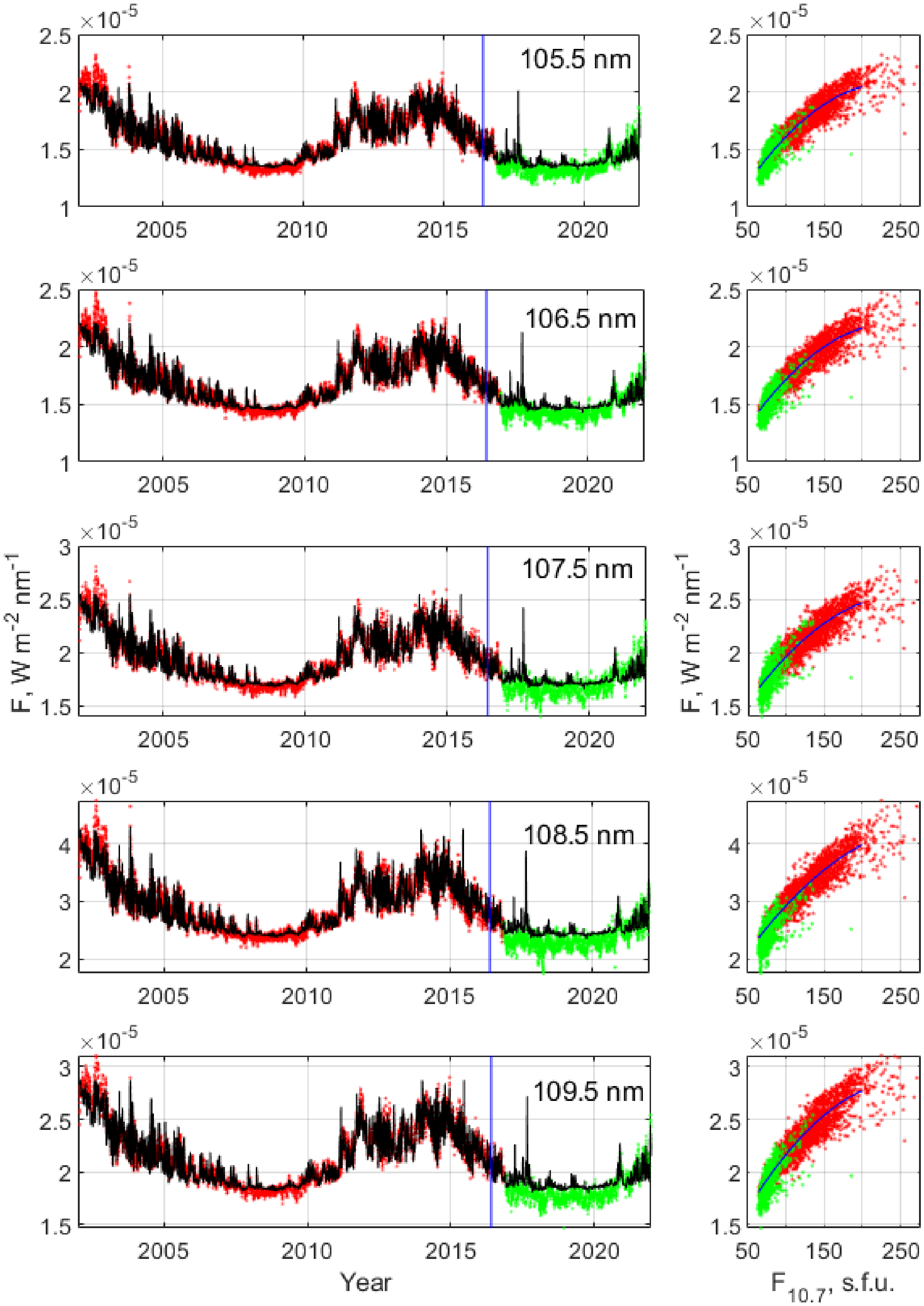

105.5 nm
106.5 nm
107.5 nm
108.5 nm
109.5 nm
F, W m^{-2} nm^{-1}
Year
$F_{10.7}$, s.f.u.

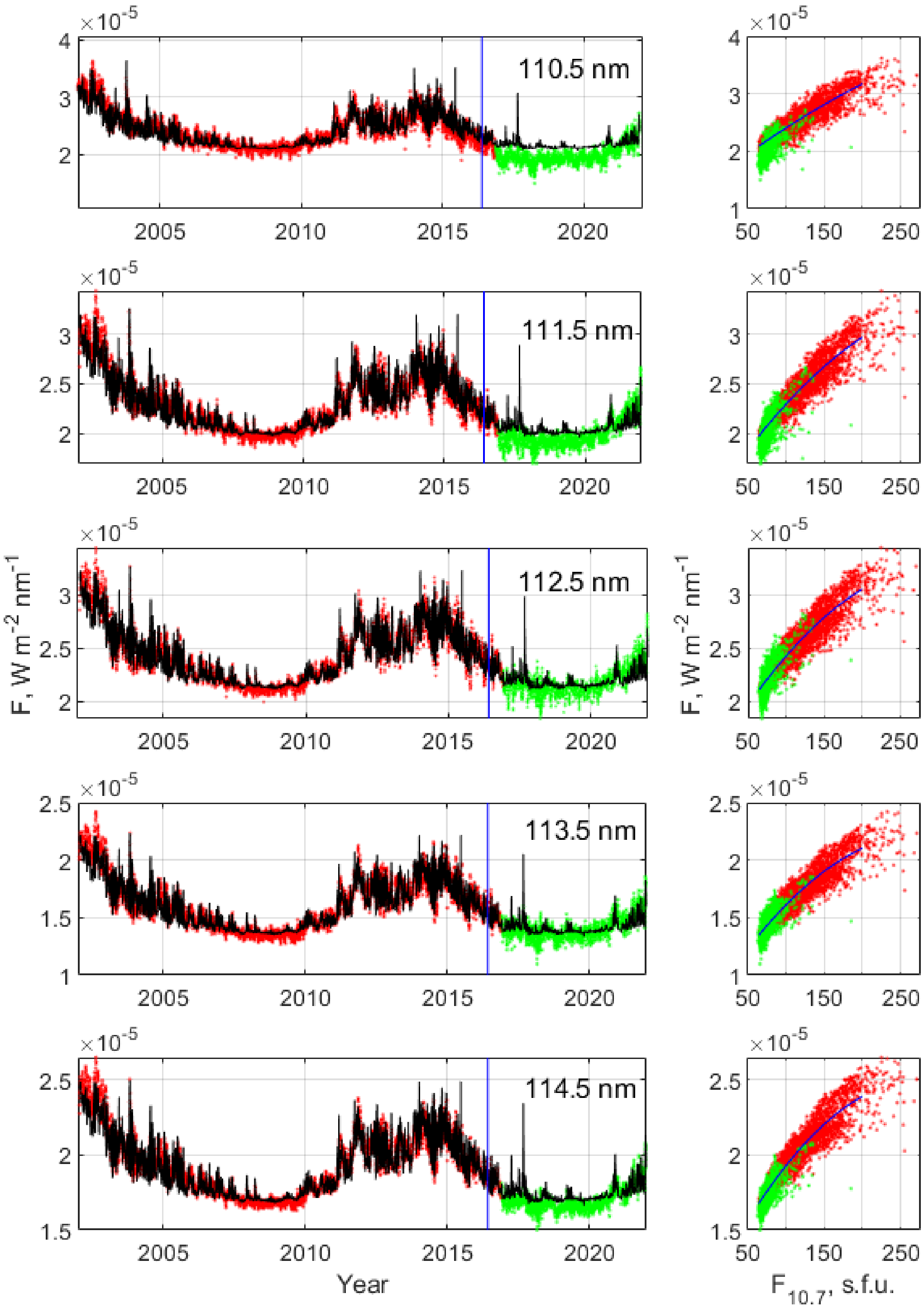
110.5 nm
111.5 nm
112.5 nm
113.5 nm
114.5 nm
F, W m^{-2} nm^{-1}
Year
$F_{10.7}$, s.f.u.

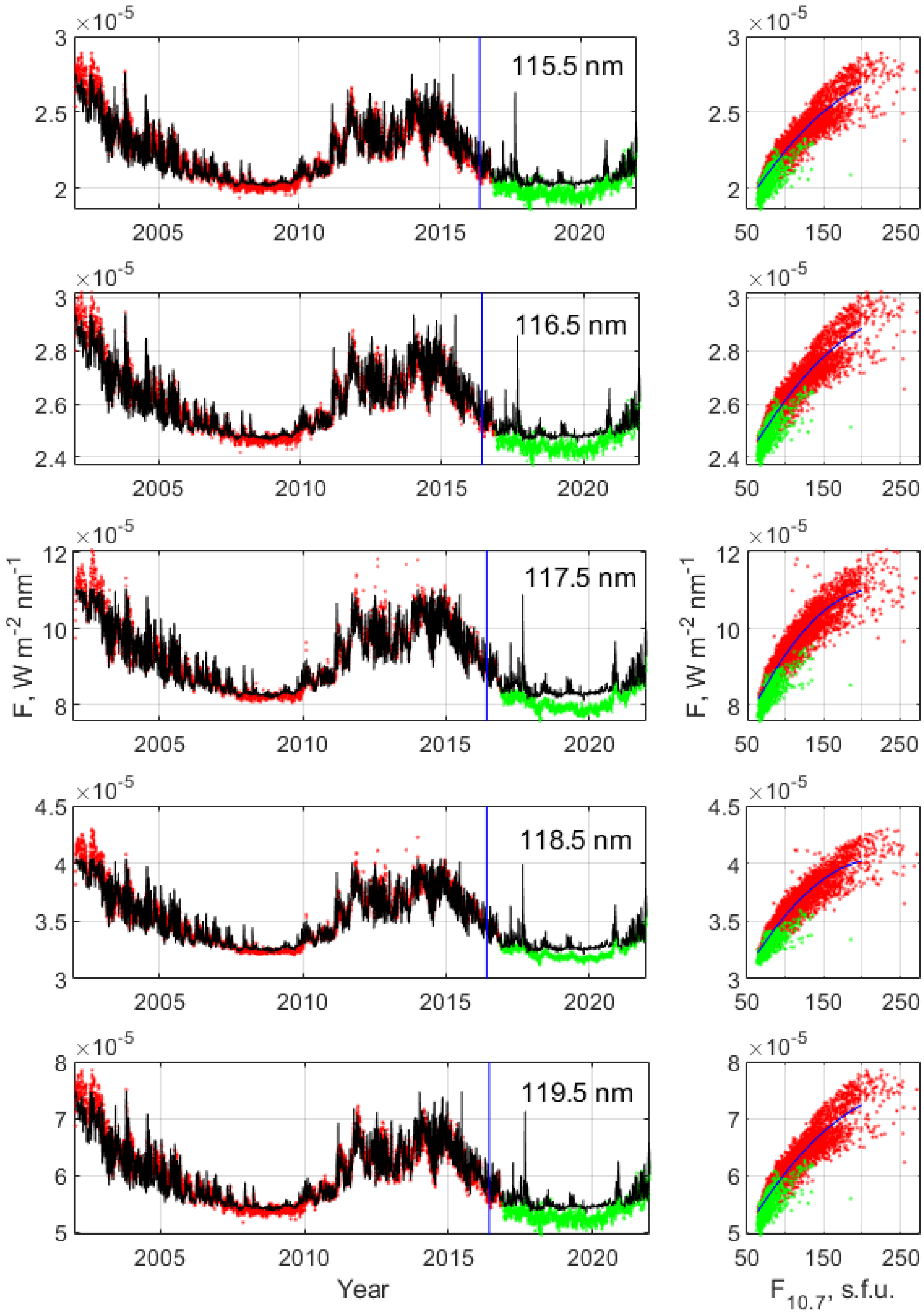
×10^-5
115.5 nm
116.5 nm
117.5 nm
118.5 nm
119.5 nm
F, W m^-2 nm^-1
Year
F10.7, s.f.u.

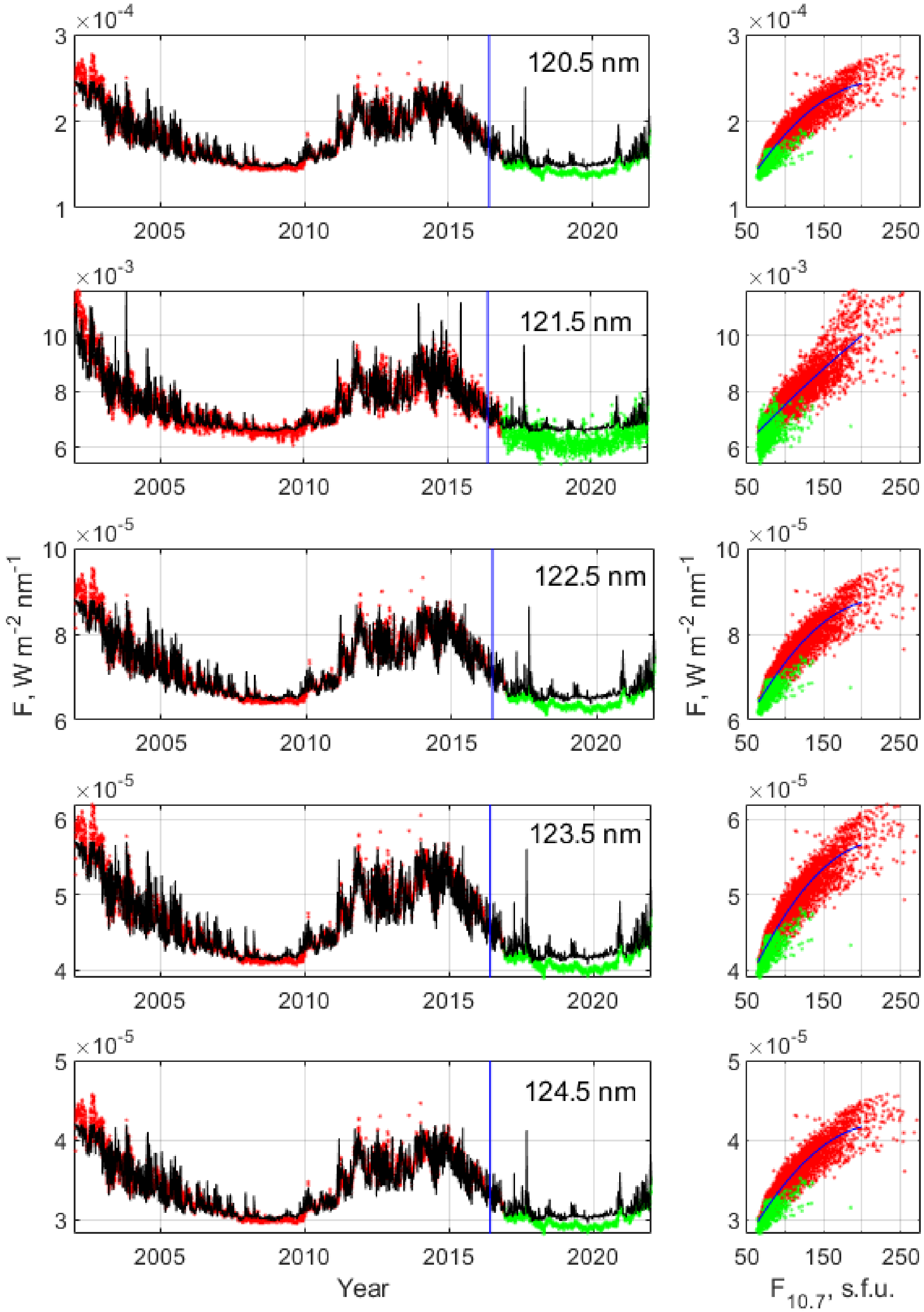

120.5 nm
121.5 nm
122.5 nm
123.5 nm
124.5 nm
F, W m-2 nm-1
Year
F10.7, s.f.u.

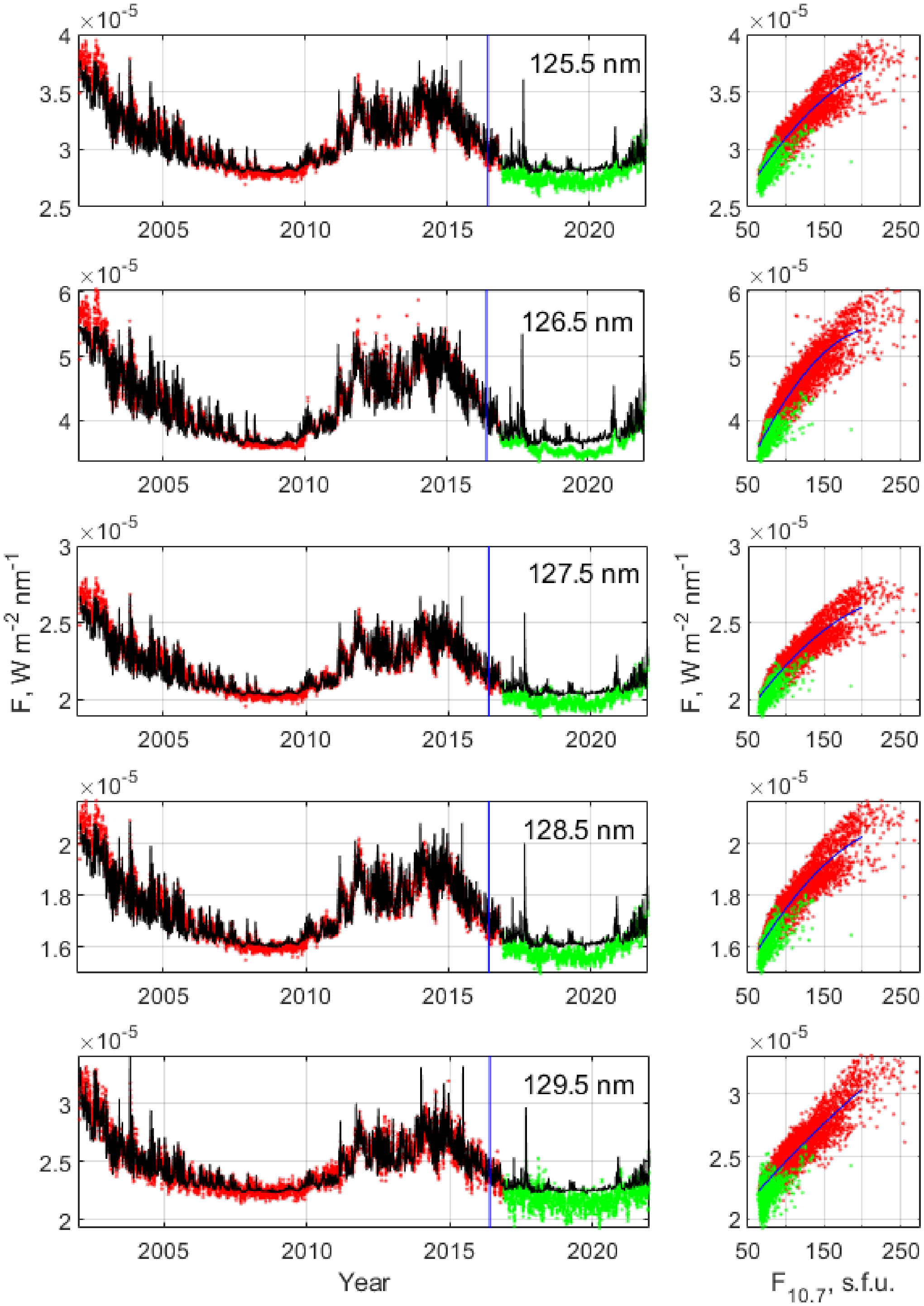

125.5 nm
126.5 nm
127.5 nm
128.5 nm
129.5 nm
F, W m-2 nm-1
Year
F10.7, s.f.u.

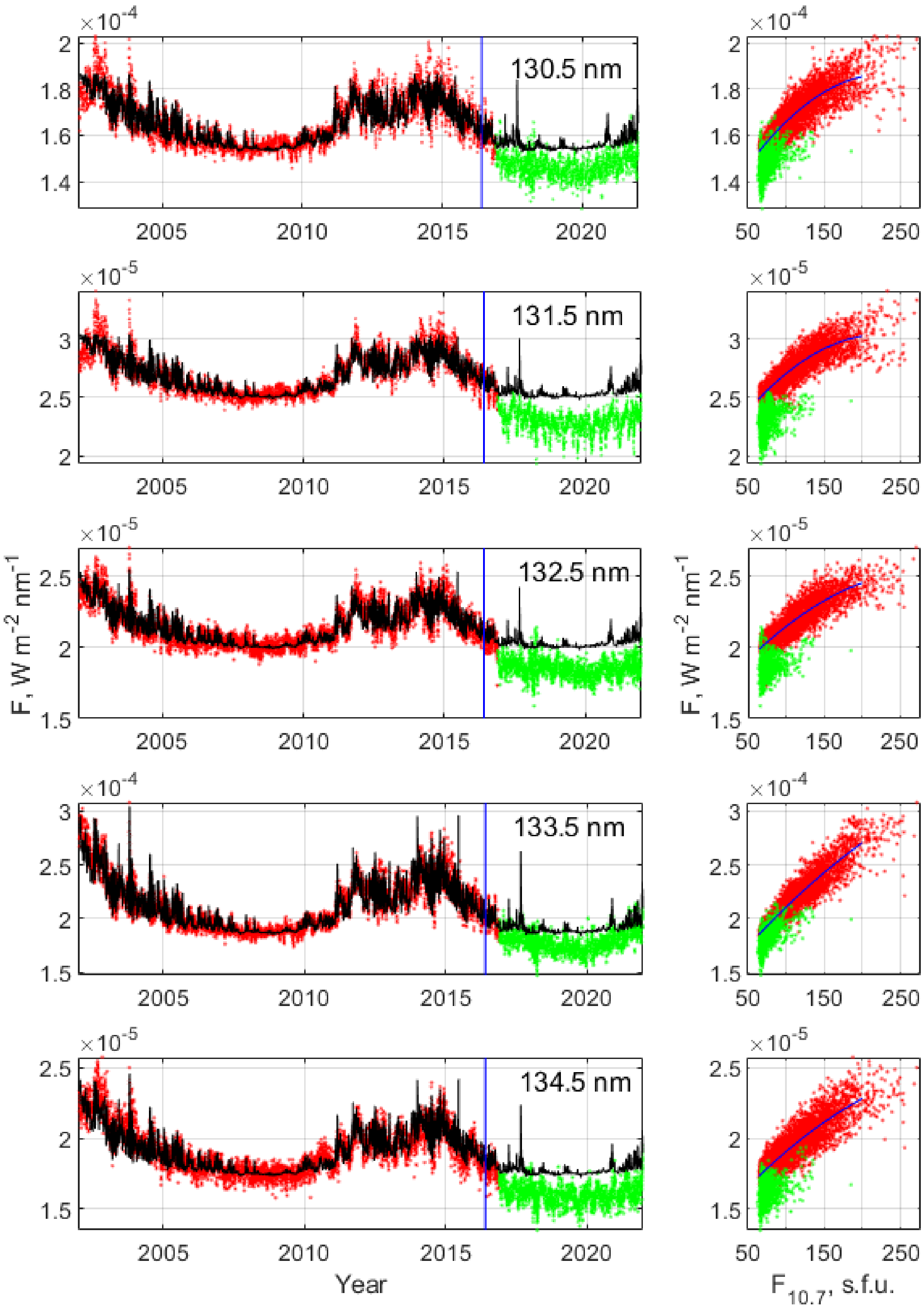

130.5 nm
131.5 nm
132.5 nm
133.5 nm
134.5 nm
F, W m^{-2} nm^{-1}
Year
$F_{10.7}$, s.f.u.

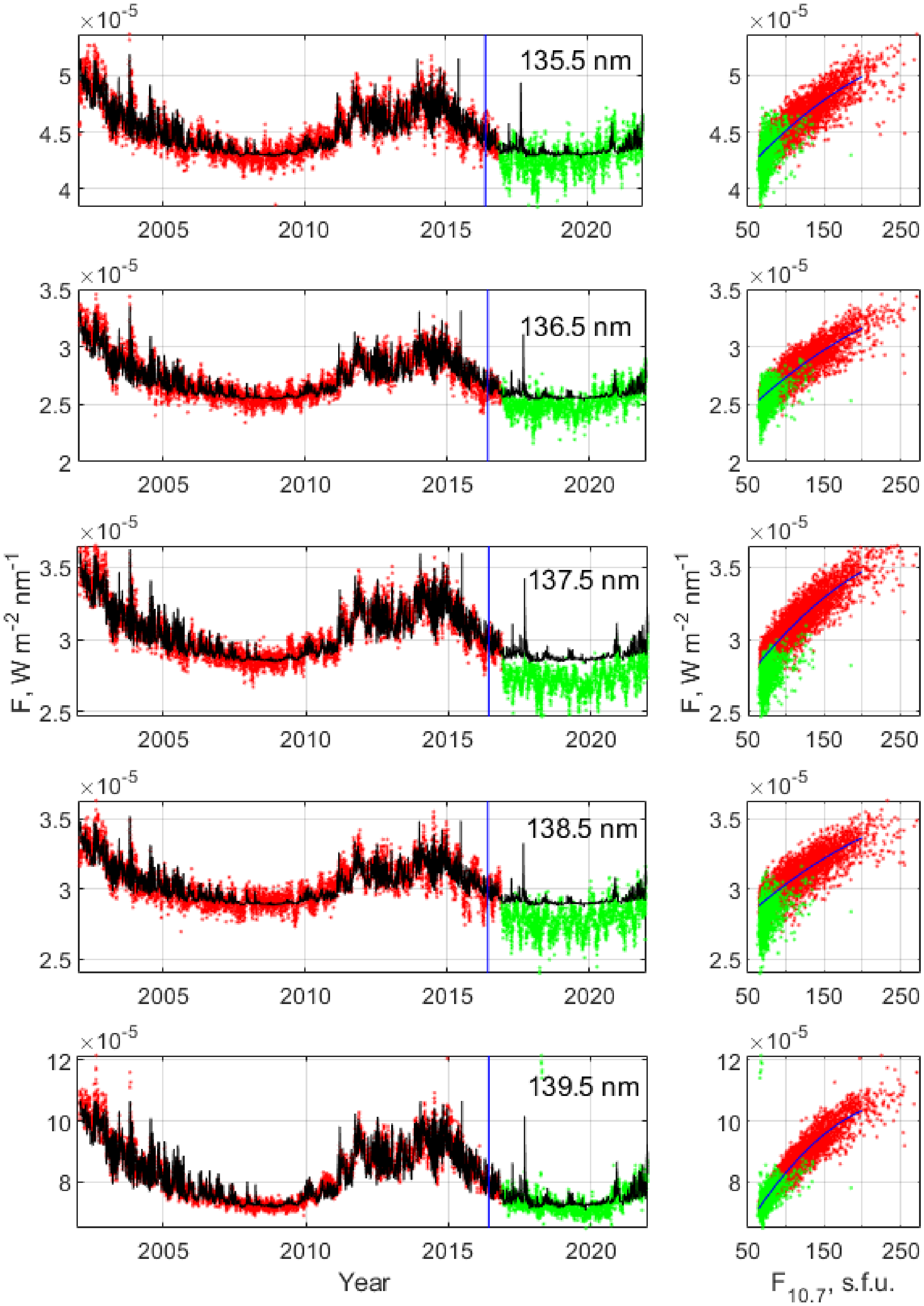
135.5 nm
136.5 nm
137.5 nm
138.5 nm
139.5 nm
F, W m^{-2} nm^{-1}
Year
$F_{10.7}$, s.f.u.

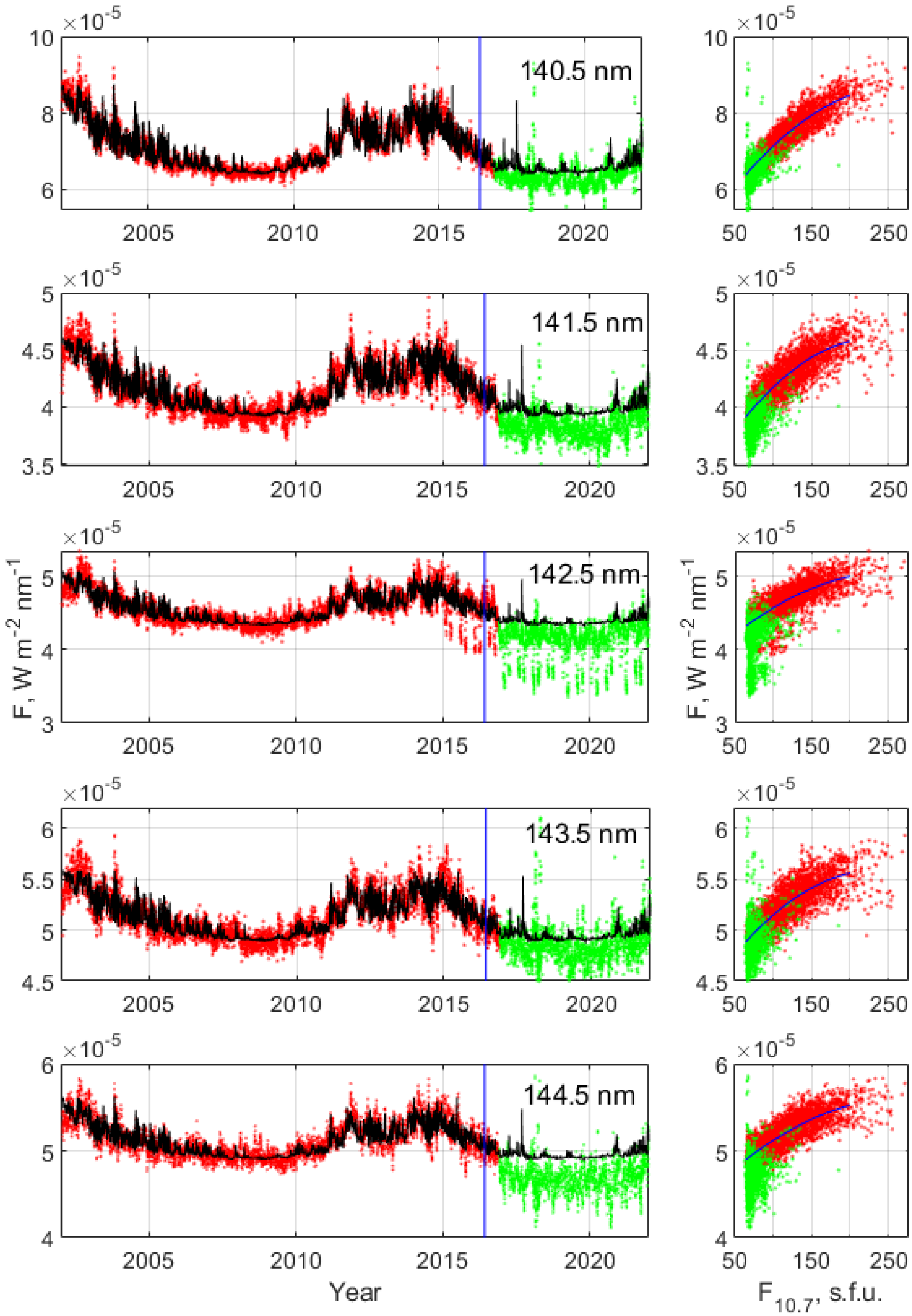

140.5 nm
141.5 nm
142.5 nm
143.5 nm
144.5 nm
F, W m^{-2} nm^{-1}
Year
$F_{10.7}$, s.f.u.

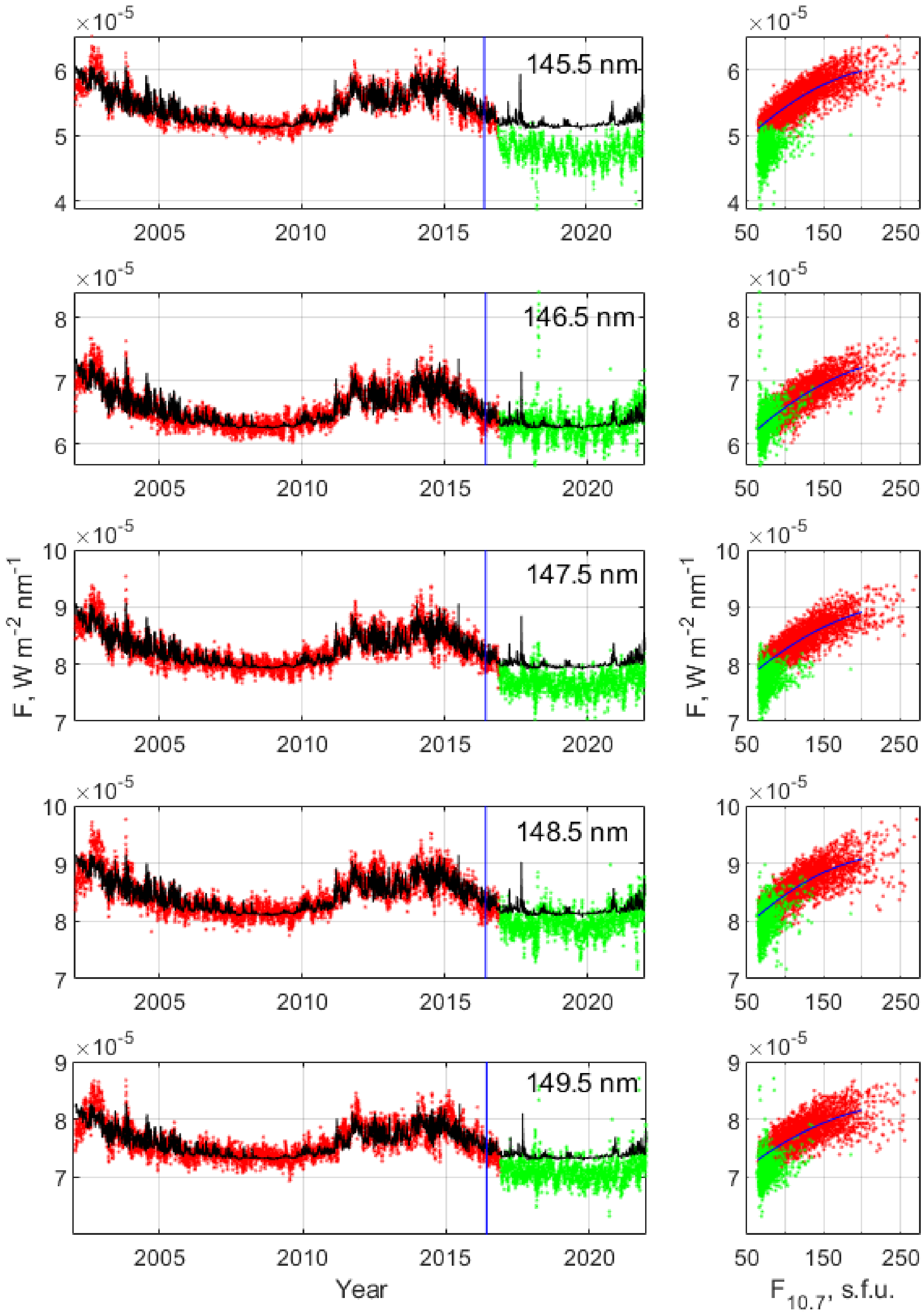
145.5 nm
146.5 nm
147.5 nm
148.5 nm
149.5 nm
×10^-5
F, W m^-2 nm^-1
Year
F10.7, s.f.u.
2005
2010
2015
2020
50
150
250

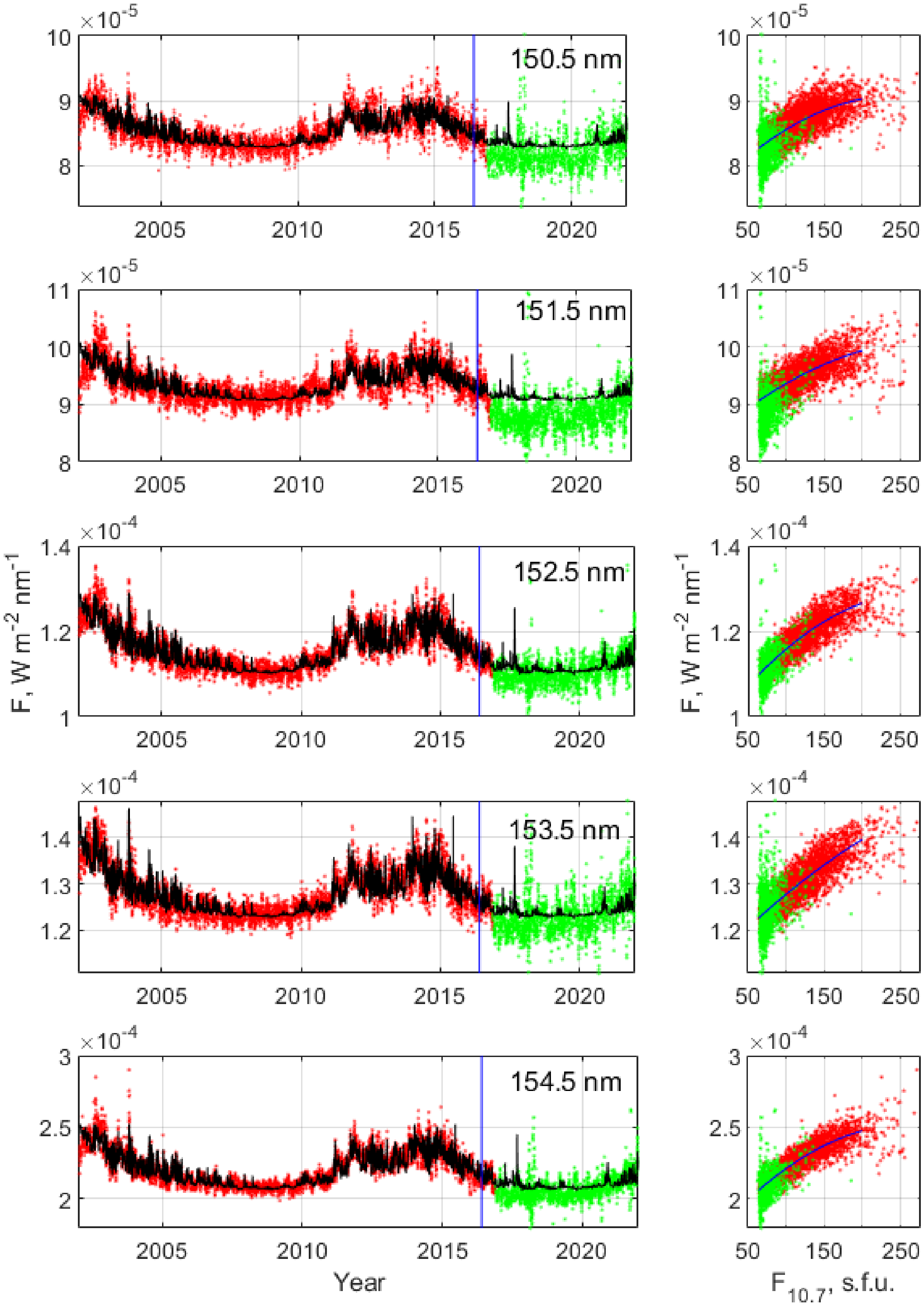

×10⁻⁵
150.5 nm
151.5 nm
×10⁻⁴
152.5 nm
153.5 nm
154.5 nm
F, W m⁻² nm⁻¹
Year
F10.7, s.f.u.
2005
2010
2015
2020
50
150
250

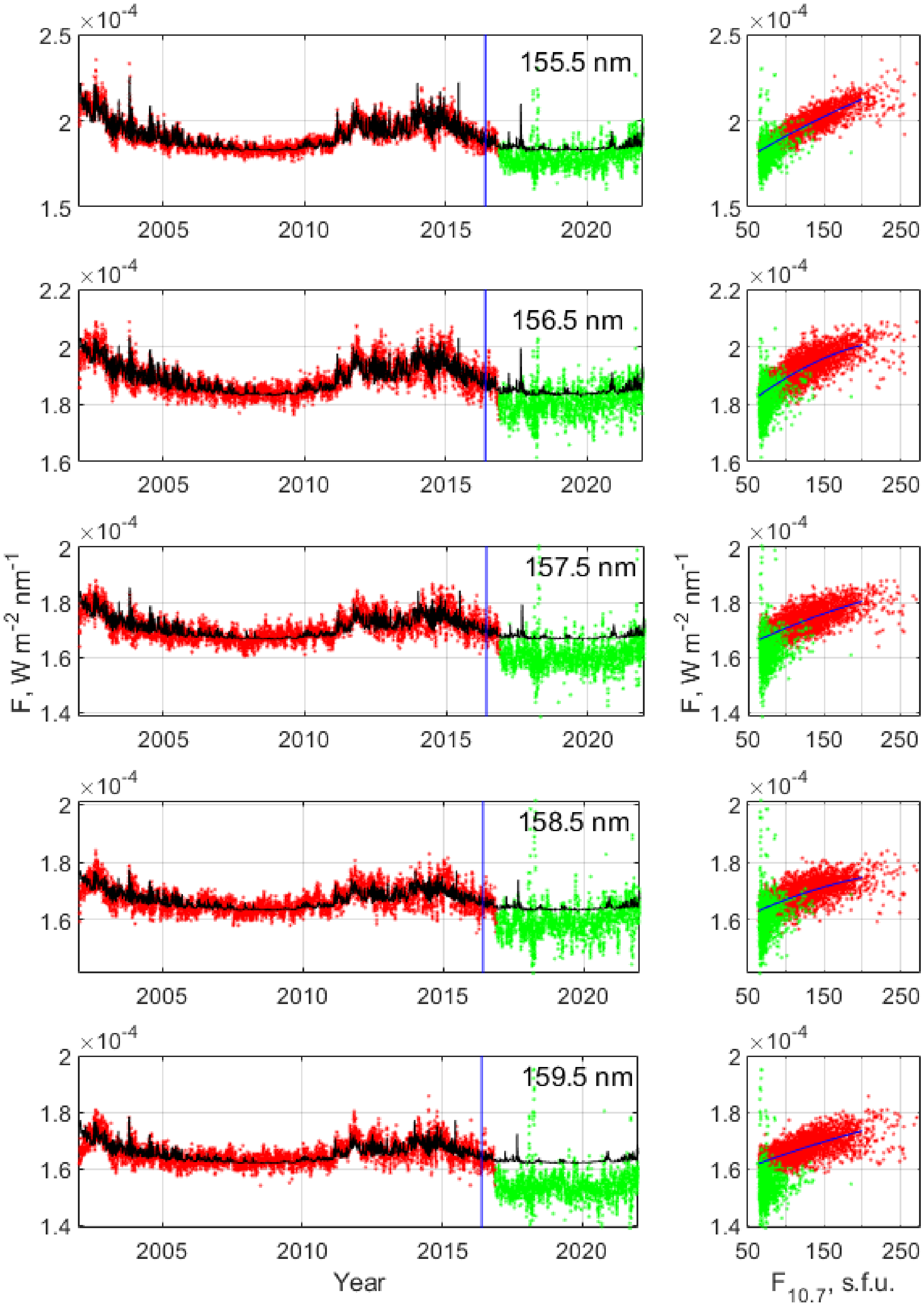

155.5 nm
156.5 nm
157.5 nm
158.5 nm
159.5 nm
F, W m-2 nm-1
Year
F10.7, s.f.u.

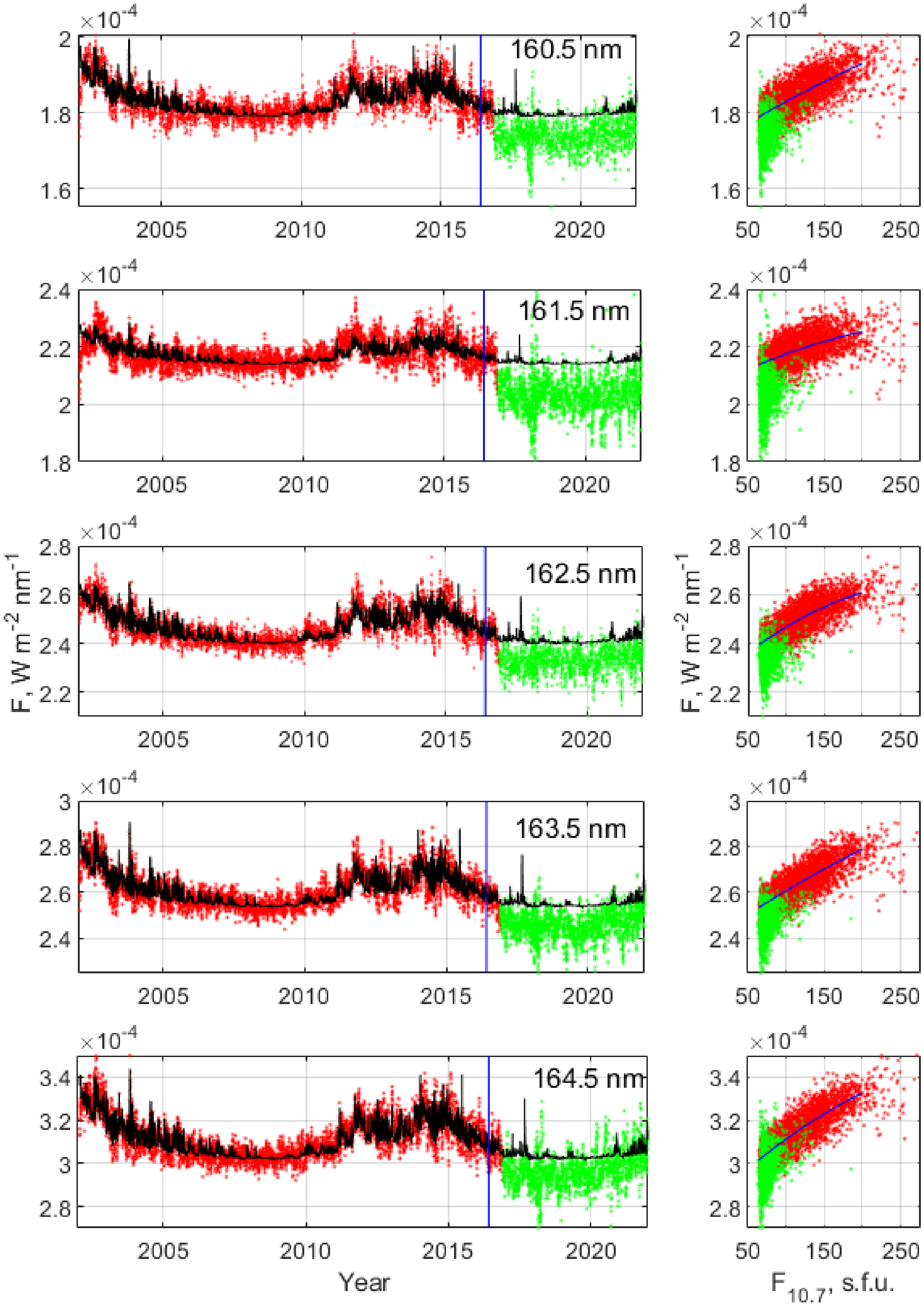
160.5 nm
161.5 nm
162.5 nm
163.5 nm
164.5 nm
Year
F, W m^{-2} nm^{-1}
$F_{10.7}$, s.f.u.

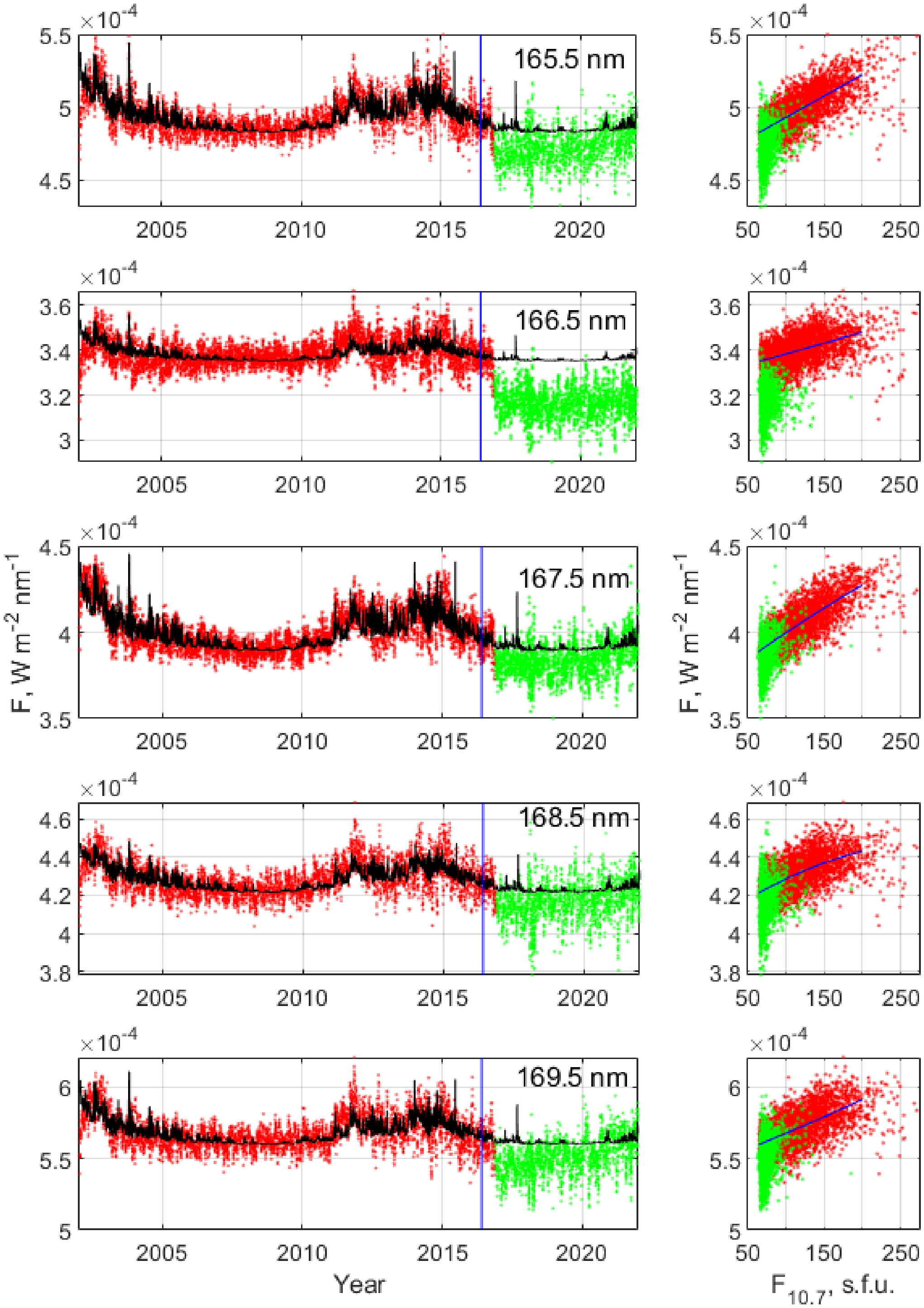
165.5 nm
166.5 nm
167.5 nm
168.5 nm
169.5 nm
×10^-4
F, W m^-2 nm^-1
Year
F_10.7, s.f.u.
2005
2010
2015
2020
50
150
250

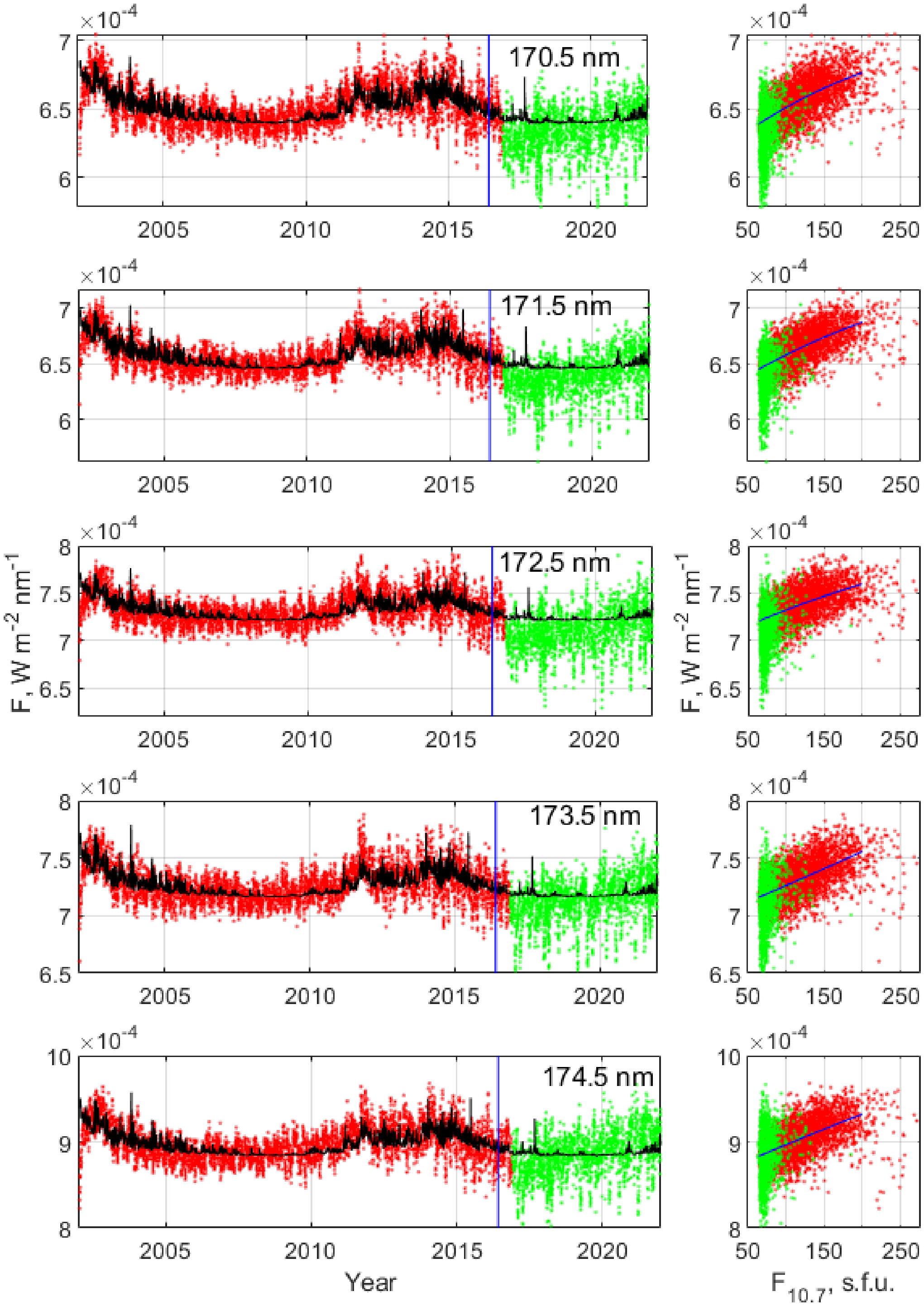
170.5 nm
171.5 nm
172.5 nm
173.5 nm
174.5 nm
F, W m^-2 nm^-1
Year
F10.7, s.f.u.

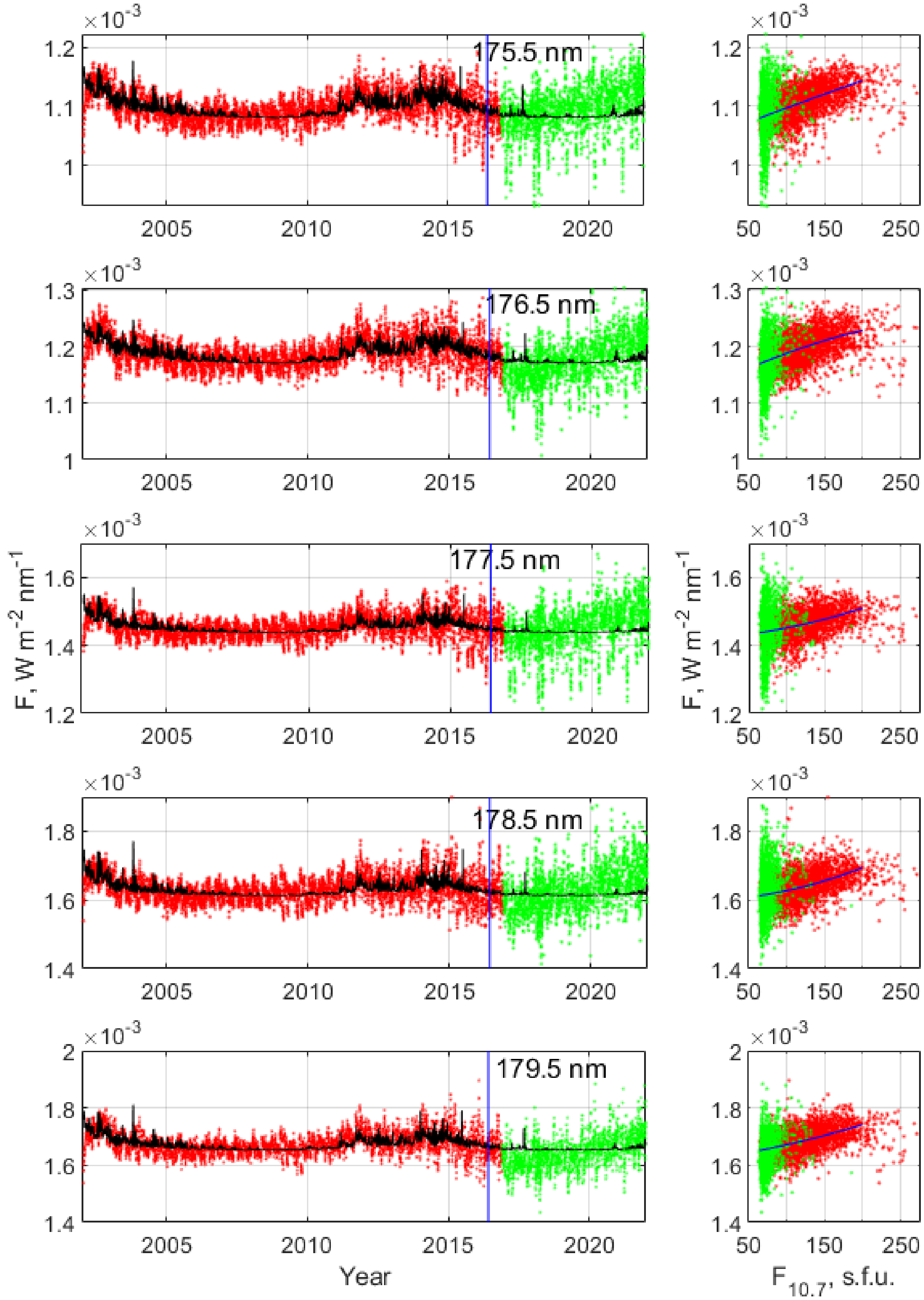

175.5 nm
176.5 nm
177.5 nm
178.5 nm
179.5 nm
F, W m^{-2} nm^{-1}
Year
F$_{10.7}$, s.f.u.

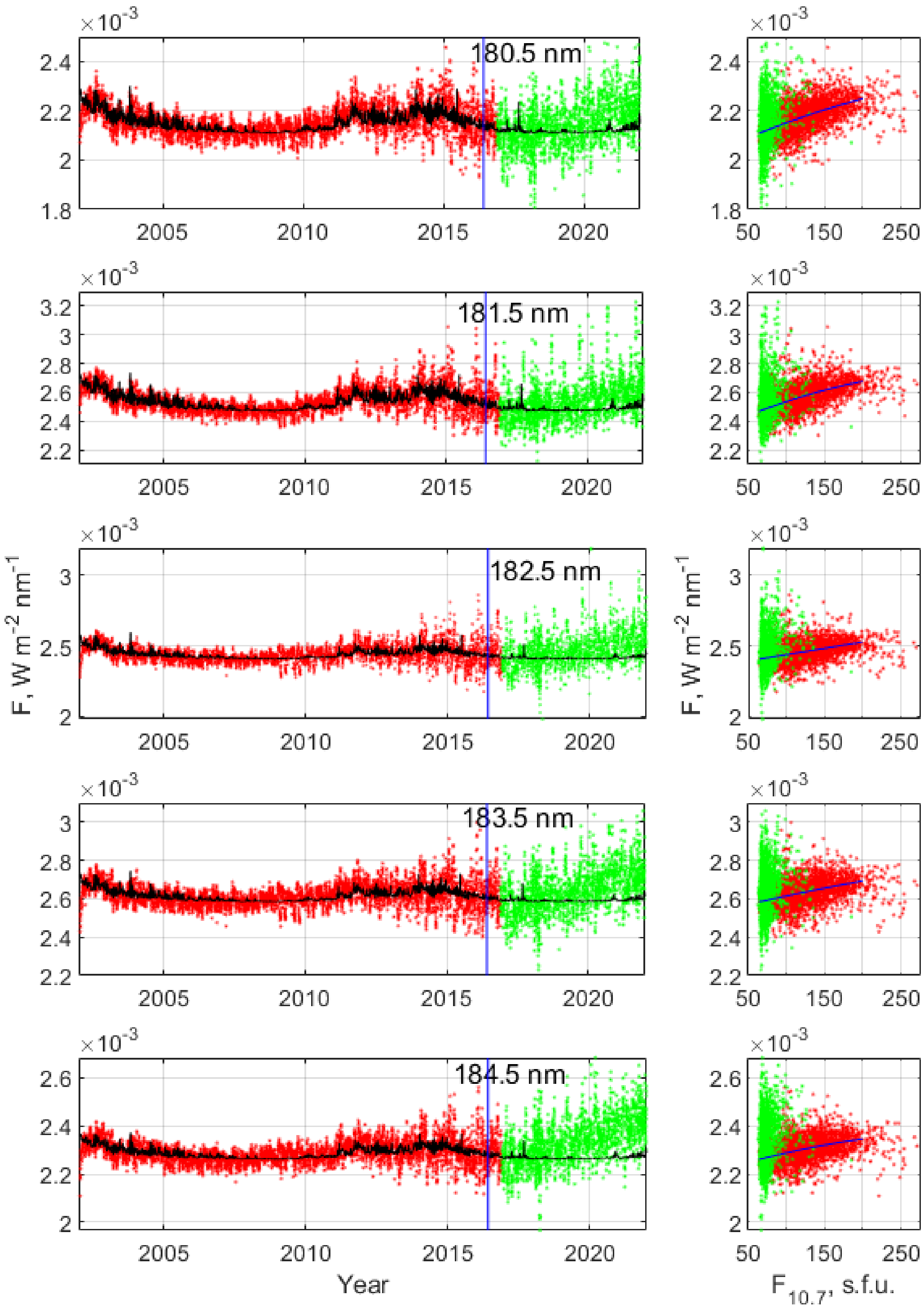

×10^-3
180.5 nm
181.5 nm
182.5 nm
183.5 nm
184.5 nm
F, W m^-2 nm^-1
Year
F10.7, s.f.u.
2005
2010
2015
2020
50
150
250

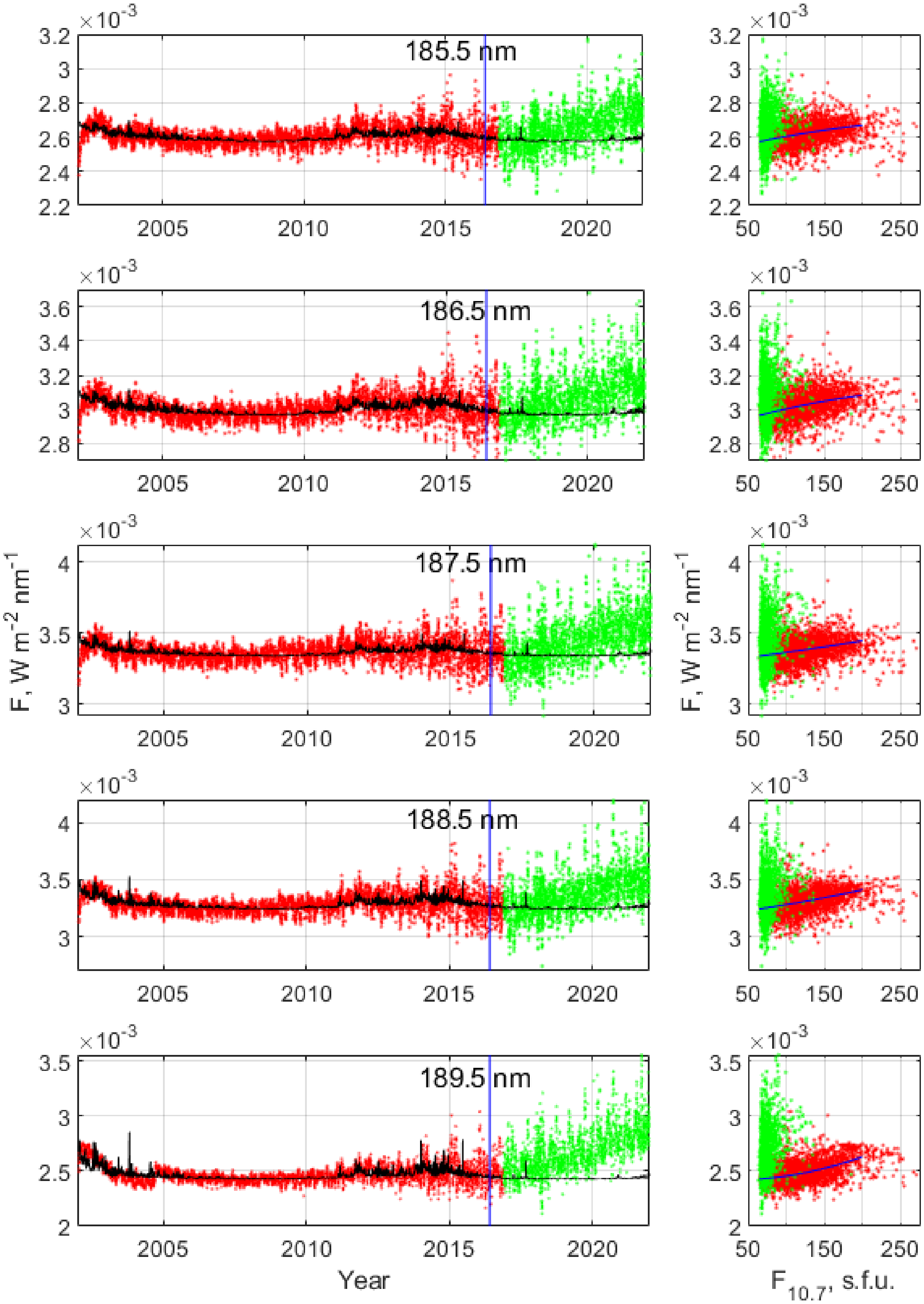
185.5 nm
186.5 nm
187.5 nm
188.5 nm
189.5 nm
F, W m^{-2} nm^{-1}
Year
$F_{10.7}$, s.f.u.
×10^{-3}